Abstract

This thesis comprises three parts. The first part proposes an optimal design and retrofit method for complex refrigeration systems using pure refrigerants. This kind of refrigeration systems has significant economic importance, since it applies to all low temperature processes where refrigeration is needed. The second part introduces a systematic synthesis method to deal with complex refrigeration systems using mixtures as refrigerants. Because it features simpler machinery and lower maintenance problems, this kind of refrigeration systems gains more and more importance in many applications, especially in LNG. Due to the lack of systematic design method, conventional approaches are largely trial-and-error and therefore operations can be far away from the optimal conditions. The systematic synthesis method proposed in this thesis opens more possibilities and greatly improves operating efficiency for mixed-refrigerant systems. In the third part, a graphical exergy analysis method, called the Ω-H diagram, is introduced. Exergy analysis helps engineers obtain understanding and insights into the problems they are dealing with, and make rational comparisons among many possible design options. Although many graphical analysis methods already have been proposed, they cannot cope with all types of unit operations in processes. The Ω-H diagram uses a generic definition for the Ω, and consequently can represent exergy loss due to thermal, mechanical and composition changes in processes. Area on the Ω-H diagram represents exergy, therefore exergy balances and exergy loss calculations can be carried out directly on the diagram. The Ω-H diagram can be integrated with optimisation methods and acts as a platform to display pros and cons due to process design changes.

Table of Contents

Part 1. Optimal Design of Pure-Refrigerant Systems

Part 1.

Optimal Design of Pure-Refrigerant Systems

1 INTRODUCTION AND LITERATURE REVIEW

1.1 Introduction

In the chemical process industry (CPI), there are many processes that operate below ambient temperature. These processes often require heat removal from processes and heat rejection to external agents, such as cooling water or air. Refrigeration systems are employed to supply low temperature cooling. Usually refrigeration systems are much more expensive than other normal utilities, due to high operating cost and capital-intensive compression trains. The operating costs for refrigeration systems are often dominated by the cost of shaftwork to drive the compressors. In subambient processes, such as ethylene plants and natural gas liquefaction plants, design of refrigeration systems is the major concern for energy consumption and capital investment.

A subambient process usually comprises of three major parts, namely: the process, the heat exchanger network and the refrigeration system, as shown in Figure 1-1.

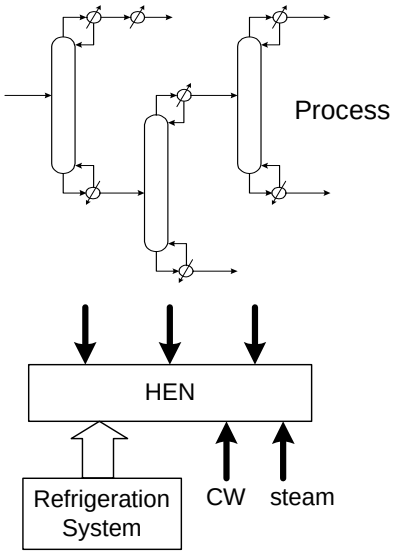

Figure 1-1. The interaction between process, HEN and refrigeration system

These systems are all highly interactive and interlinked to each other. Changes in any one of them will cause changes in the other two parts. Any modifications in the process or in the HEN will have a downstream impact on the shaftwork requirement of the refrigeration system. The interactions make the design of refrigeration systems very complex. All design considerations incur trade-offs between energy saving and extra capital investment. Figure 1-2 shows a typical grand composite curve (GCC) of subambient processes. It gives the whole heat source and sink profile of the process. Further energy saving can be achieved by better heat integration with processes (Linnhoff, 1991) Therefore, optimal synthesis of refrigeration systems can not be accomplished without considering the overall context of processes.

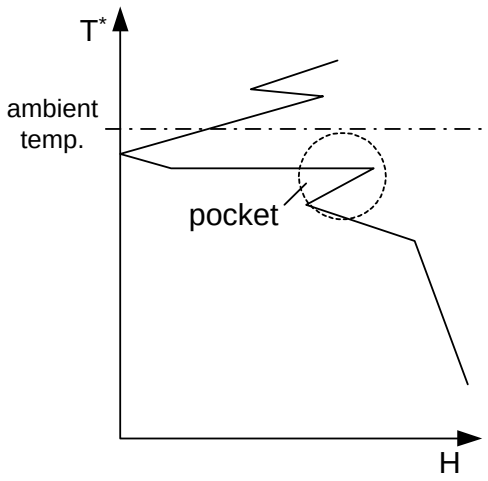

Figure 1-2. A typical GCC of subambient processes.

1.1.1 Refrigeration Systems

There are four basic types of refrigeration systems: vapour recompression cycle, adsorption cycle, absorption cycle and steam jet cycle. The majority of industrial applications use the vapour recompression cycle, in which several types of compressors, namely centrifugal reciprocating and screw compressors, may be employed. This thesis will focus on the application and design of vapour recompression cycle. A basic vapour recompression cycle, as shown in Figure 1-3, consists of four parts: a compressor, a condenser, an evaporator, and an expansion valve.

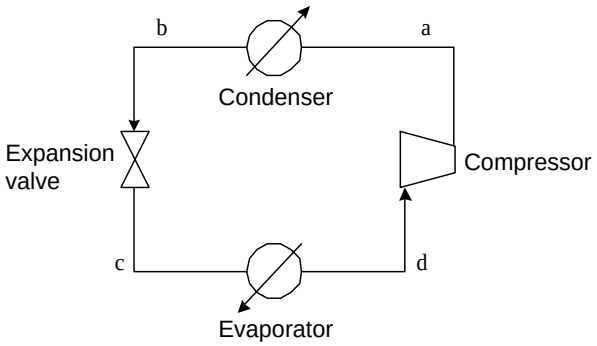

(a)

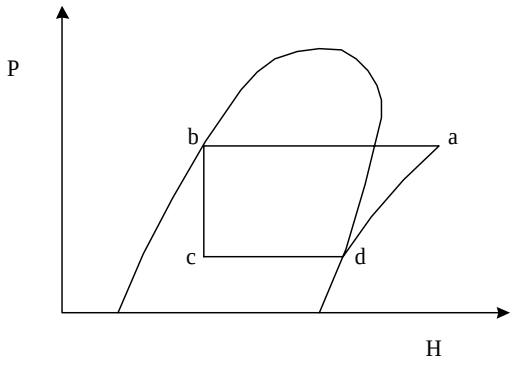

(b)

Figure 1-3. A simple vapour-compression cycle: a) Flow diagram; b) Pressure-enthalpy diagram

The saturated refrigerant vapour at point *d* goes through the compressor after absorbing heat in the evaporator, where the shaftwork is consumed and the pressure of the vapour is lifted. The outlet superheated vapour is at point *a*. The vapour is cooled down in the condenser at constant pressure until it reaches the dew point temperature. Then the saturated vapour is condensed at constant temperature and at point *b* the vapour is totally converted to saturated liquid. To reach its evaporating temperature at point *c*, the saturated liquid goes through an expansion valve under an isenthalpic process. From point *c* to point *d*, the refrigerant absorbs heat and is evaporated. Note that the vapour refrigerant formed in the expansion process does not provide any refrigeration duty.

When refrigeration is required at very low temperatures, a cascade refrigeration system is often used, which consists of two or more cycles and each cycle operates by a

different refrigerant. A simple cascade refrigeration system is shown in Figure 1-4. The lower cycle absorbs heat at temperature level 1-2 and rejects condensation heat to the upper cycle at temperature level 3-4. The upper cycle absorbs rejected heat from the lower cycle by operating an evaporation level at 5-6, which is colder than level 3-4. Finally, the heat in the upper cycle is rejected at level 7-8 to external heat sinks.

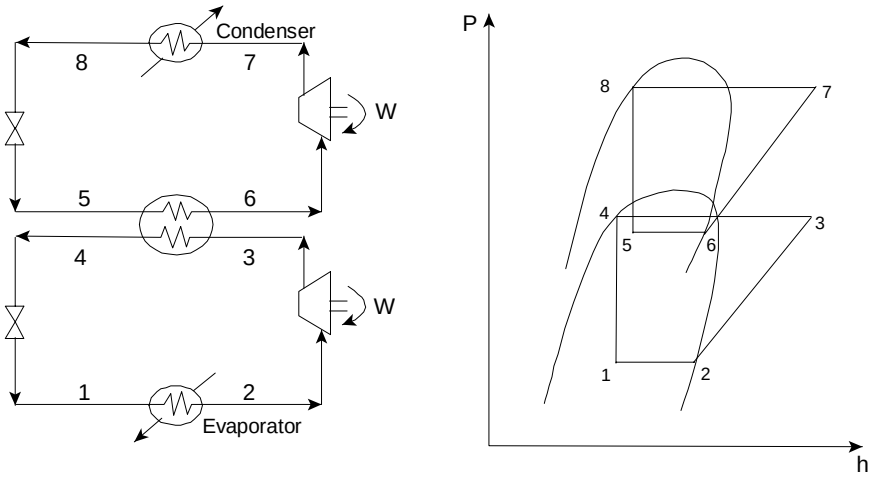

Figure 1-4. A simple cascade refrigeration system and its P-h diagram.

The reasons for using cascade refrigeration systems are two-folds. First, any single refrigerant cannot cover such a wide refrigeration temperature range. Second, in terms of energy consumption, using a single refrigerant for the whole refrigeration demand may consume more shaftwork than using multiple refrigerants. Figure 1-5 summarises the operating ranges for some commonly encountered refrigerants. We can see that ethylene as a refrigerant can be used up to 253K. Above this temperature, another refrigerant, usually propylene, is employed.

Besides suitable operating temperature ranges, there are several considerations for selecting refrigerants. Conventionally, chlorofluorocarbon (CFC) and hydrochloro-fluorocarbon (HCFC) refrigerants are widely used in domestic refrigerators and automotive air conditioners. But those refrigerants with intermediate to high ozone depletion potential (OPD) (Nimitz and Skaggs, 19920 will be totally banned in the years to come. Many efforts have already been made to find replacements with similar thermodynamic and transport properties to those banned refrigerants. Factors such as

chemical stability, health safety, flammability, and ODP, have to be taken into considerations when selecting proper refrigerants to use. Table 1-1 summarises general criteria for refrigerant acceptability.

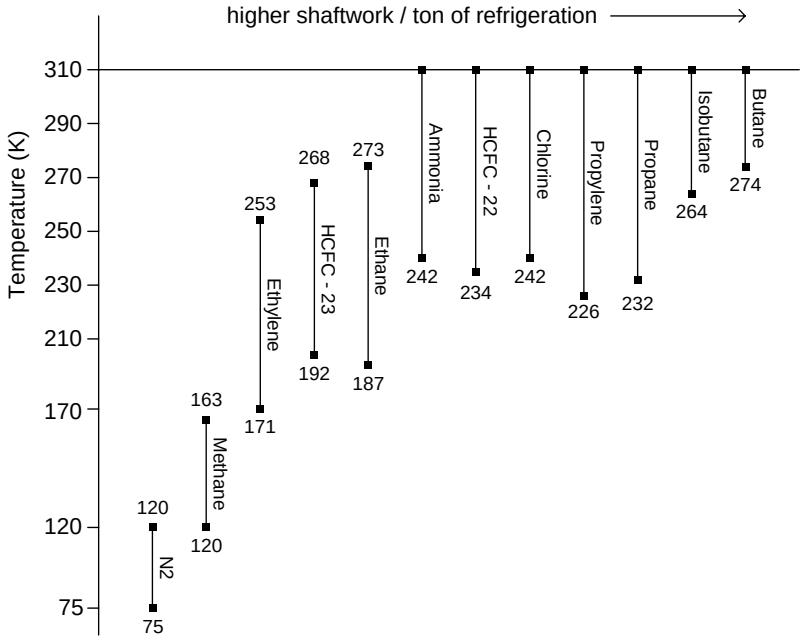

Figure 1-5. Refrigerant operating range.

Table 1-1. General criteria for refrigerant acceptability.

Chemical	Stable and inert.
Health	Non-toxic.
Safety	Non-flammable. Non-corrosive.
Environmental	Zero ozone depletion potential(ODP). Low global warming poential(GWP).
Thermodynamic	Normal boiling point and critical temperature appropriate to the application. Low liquid specific heat. Low viscosity. High thermal conductivity.
Miscellaneous	Satisfactory solubility in lubricating oil. Low freezing point. Containment in common materials. Easy leak detection. Low cost.

1.1.2 Design Options

For a refrigeration system, it is possible to improve its performance by using the following design options:

- **Economiser**: Figure 1-6(a). In an economiser, the condensed refrigerant is flashed to an intermediate pressure, where the flash vapour is returned to the suction of the compressor and the remaining liquid is further expanded to a lower temperature. As a result, the amount of vapour flowing through the lower pressure part is reduced, thus saving shaftwork.
- **Aftercooler**: Figure 1-6(a). With this option, the superheated refrigerant vapour is cooled down after compression by other available heat sink before further compression. This results in the reduction of shaftwork requirement and the aftercooling duty. Aftercoolers provide the opportunity of heat integration between refrigeration systems and processes.
- **Presaturator**: Figure 1-6(c). A presaturator has similar structure as an economiser, but the partially compressed refrigerant vapour is presaturated in the flash vessel with the expense of evaporating part of the refrigerant liquid from the corresponding economiser. This decreases the temperature of the refrigerant vapour entering the next stage of compressor, and saves shaftwork. On the other hand, presaturation may have two drawbacks: (1) it requires a higher refrigerant flow rate which may more than offset the shaftwork reduction of the single compressor, and (2) either economiser or presaturator, adding an intermediate pressure level, may cause an increase in capital cost for compressors. Several small compressors can be more expensive than a single large compressor, even though the total shaftwork requirement is reduced.
- **Desuperheater**: Figure 1-6(c). Using a desuperheater, the final stage superheated refrigerant vapour is precooled after compression by a warmer heat sink before entering the condenser. This adds the possibility of heat integration to processes.

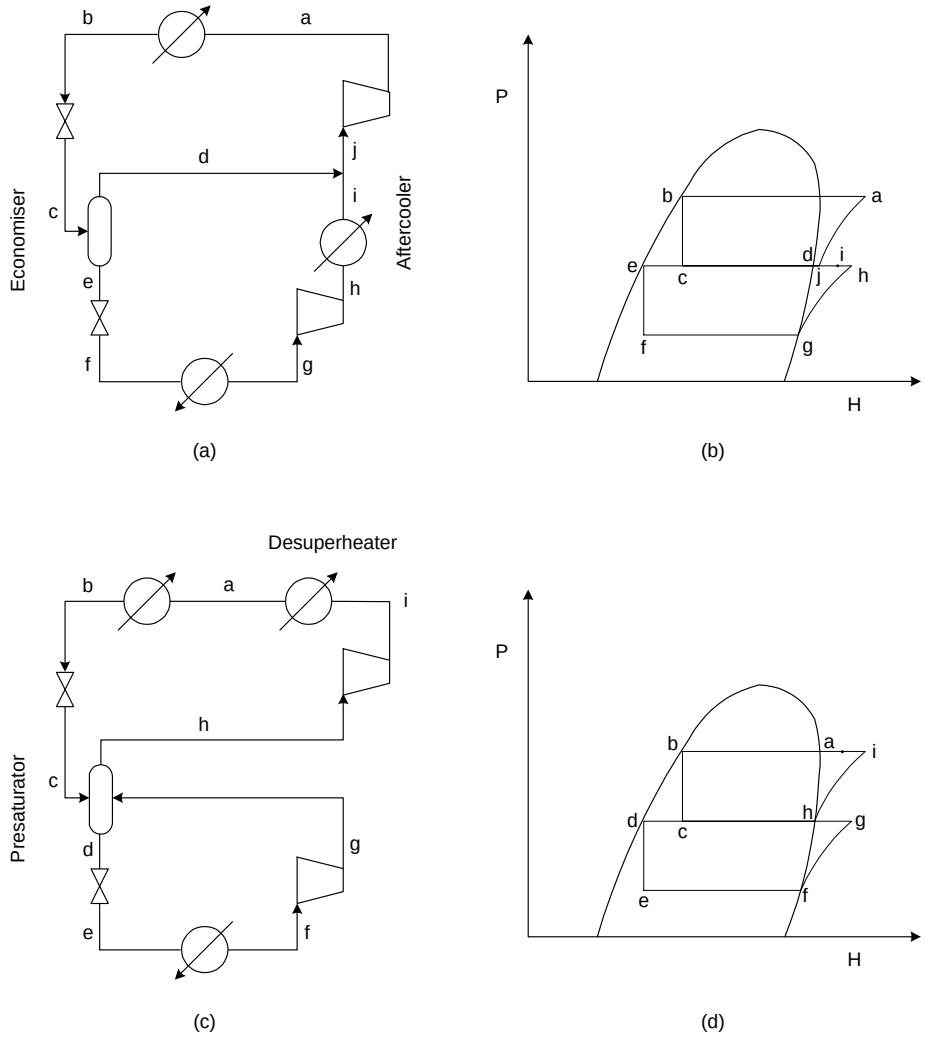

Figure 1-6. Several design options: (a) and (b) economiser and aftercooler; (c) and (d) presaturator and desuperheater.

- **Suction vapour-liquid heat exchanger**: Figure 1-7. With this option, the refrigerant vapour after evaporation undergoes heat exchange with the incoming saturated refrigerant liquid. Therefore the vapour is superheated before compression and the liquid is subcooled before expansion. In this way, the amount of remaining refrigerant liquid after expansion is increased at the expense of increasing shaftwork requirement. Another potential advantage is that cheaper material of construction for the compressor can be used, since more expensive materials of construction for compressors are required if the vapour is admitted at its saturated state or lower temperature.

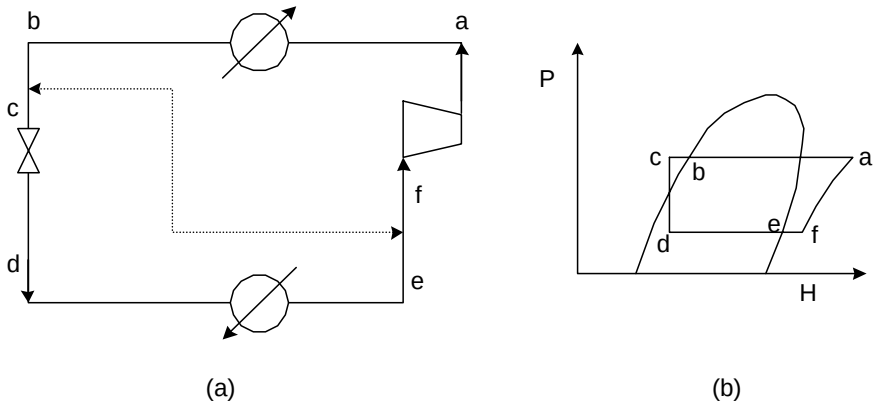

Figure 1-7. Suction vapour-liquid heat exchanger: (a) Flow diagram; (b) Pressure-enthalpy diagram.

- **Reboiling**: Figure 1-8. If there is available heat sink in the process, we can reject part of the heat into the process by adding one more condensing stage (c-d) instead of rejecting the total heat in the final condensing stage, which is usually to external cooling water. This can be described as exploring the "pocket" in the GCC. It forms a closed loop of refrigerant around the stage, and therefore reduces the total amount of required refrigerant flow.

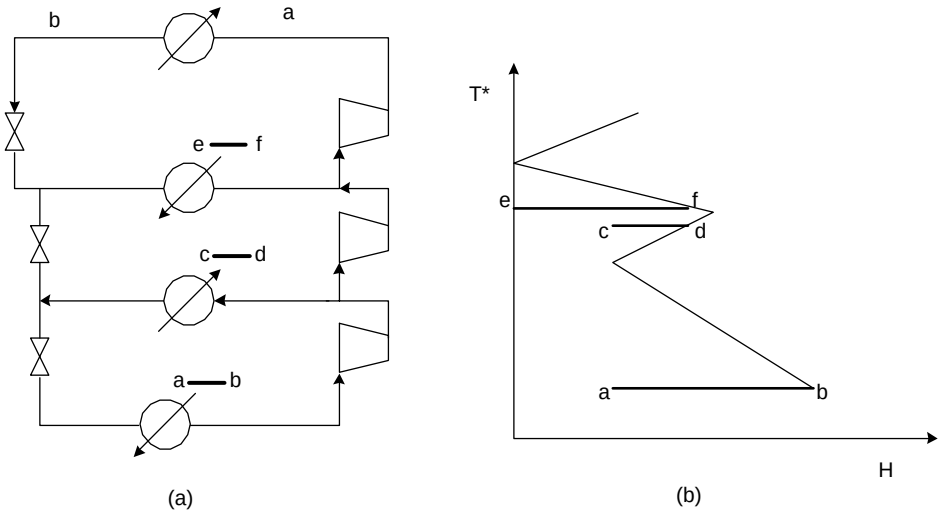

Figure 1-8. An example of using reboiling: (a) Flow diagram; (b) T-H diagram.

- **Multistage cycle**: Figure 1-9. If the refrigeration demand is distributed in a wide range of temperature, we can introduce more refrigeration levels and construct a multistage refrigeration cycle.

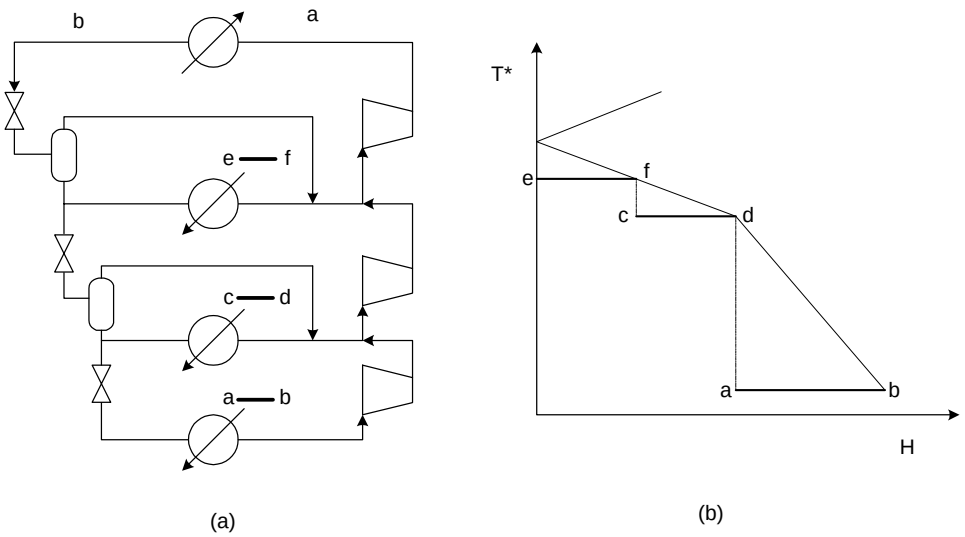

Figure 1-9. Multistage cycle: (a) flow diagram; (b) T-H diagram.

- **Cascade refrigeration system**: For very low temperature processes, it is common to use cascade refrigeration systems. As shown in Figure 1-10, a cascade refrigeration system comprises of several cycles, simple or multistage, and each cycle employs a different refrigerant.

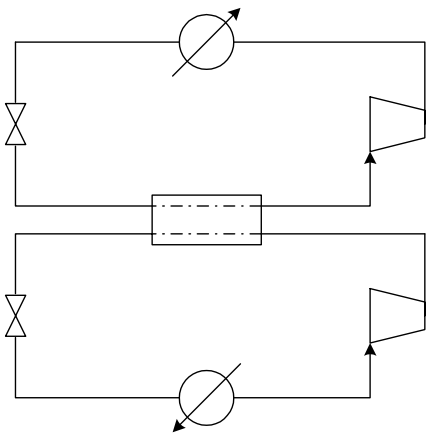

Figure 1-10. A cascade refrigeration system comprising of two cycles

1.1.3 Shaftwork Estimation

Due to the complicated interactions amongst refrigeration systems, processes and HEN, it is impractical to use rigorous simulation tools to check the impacts on refrigeration systems every time there are design changes in processes. Linnhoff and Dhole (1989) introduced an exergy-based procedure for estimating shaftwork. It estimates the shaftwork directly from the process stream data without going through the detailed refrigeration calculations. The temperature axis of the composite curves is converted to Carnot Factor to generate Exergy Composite Curves (ECC), as illustrated in Figure 1-11. The area between the ECC and utilities represent the exergy loss. We can plot the Exergy Grand Composite Curve (EGCC) by plotting the horizontal separation between the ECC. The area between the ECC is the same as the area enclosed by the EGCC. Hence the shaded area between the EGCC and utilities also represents the exergy loss.

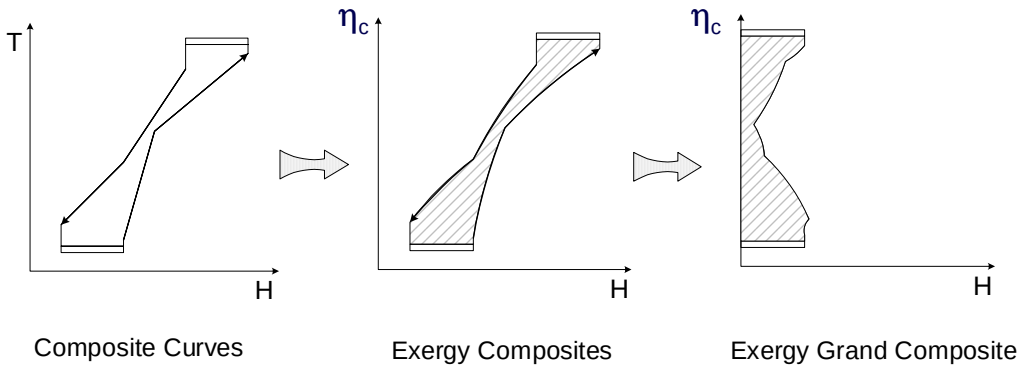

Figure 1-11. Exergy Grand Composite Curves

Using the EGCC, we can relate changes in the shaded area (Δ Area) between the EGCC and the refrigeration levels as a result of design changes to changes in refrigeration shaftwork. Figure 1-12 explains the concept. While this method enables us to evaluate the changes in the refrigeration shaftwork quickly and visually, it requires an exergetic efficiency, which is assumed to remain constant. This causes large errors in certain cases. Also, the Exergy Grand Composite Curve takes only thermal losses into consideration, and not mechanical exergy losses. Another limitation comes from the fact that shaftwork requirement of a refrigeration cycle is determined not only by the refrigeration levels, but also by the actual configuration of the system. EGCC cannot

reflects the change in shaftwork consumption when design options are introduced. Thus, this method has many limitations in practical applications.

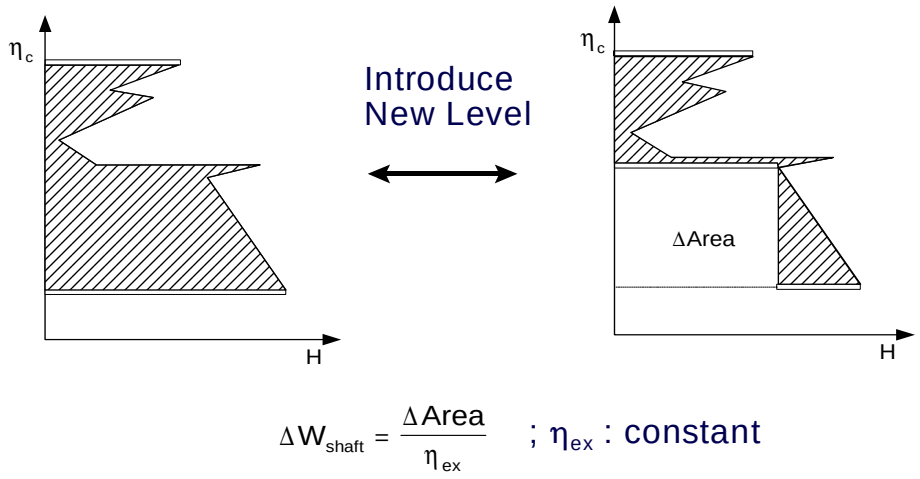

Figure 1-12. Effect of refrigeration levels on the EGCC

Lee *et al.* (2000) introduced a new shaftwork prediction method called "shaftwork targeting", by combining pinch technology and optimisation. The method starts with construction of Grand Composite Curve (GCC), and formulates the curve as a function of temperature and load. Optimisation is then applied to automatically adjust the number of levels and temperature and load of each level to reach minimum shaftwork consumption or minimum total costs. Details will be discussed later in Chapter 2.

1.2 LITERATURE REVIEW

The synthesis of refrigeration systems has caused many attentions due to its economic importance and the challenge of complex integration. Barnes and King (1974) investigated the problems of synthesising refrigeration cycles and provided a two-step approach to identify optimum cascade refrigeration systems. In the first step, a limited number of promising choices for configurations and design parameters are identified using graph decomposition principles. To minimise the cost of the configuration, the problem was represented as a network. In the network, each of the labelled node

represents a possible state of refrigerant vapour and each directed line between two such nodes implies pieces of physical equipment. Dynamic programming is then applied in the second step to this network to find the cheapest path from the starting node to the final node. Cheng and Mah (1980) developed an interaction procedure, which optimised the initial structure by considering intracycle and intercycle heat exchange and aided by heuristic guidelines. Topological relationships, as well as heuristics, are used to evaluate candidate designs of increasing complexity. An example of the heuristic rules that were employed is if either of the following criteria is met, a new level may be added:

- If the averaged compression work exceeds the initial compression work by a factor of 1.6, i.e., $\overline{\left(\frac{\partial H}{\partial p}\right)_s} > 1.6\left(\frac{\partial H}{\partial p}\right)_s\Big|_{\text{zero superheat}}$
- If the vapour fraction of the outlet stream of the corresponding valve exceeds 0.5.

The issues considered by this strategy include choice of refrigerants and temperature approaches, use of intermediate temperatures and pressures, economisers and presaturators, different materials of construction, and all permissible intercycle and intracycle heat transfers. However, the synthesis of refrigeration systems was carried out without considering the interactions between process, HEN and refrigeration systems.

Townsend and Linnhoff (1982) and Linnhoff and Dhole (1989) use a set of qualitative guidelines based on pinch technology and exergy analysis for placing heat engines and heat pumps to minimise utility consumption. The method can estimate shaftwork requirement using simple graphical tool, called Exergy Grand Composite Curve (EGCC). Since the area between the EGCC and the utility levels is proportional to the exergy loss in the heat exchanger network, the change in shaftwork requirement can be related to the change of area on the EGCC.

Shelton and Grossmann (1986) introduced a mathematical programming approach. The main idea was to finely discretise the entire temperature range providing candidate temperature levels for intermediate stages. A network superstructure was then used to represent a refrigeration system and the design problem was formulated as a mixed integer linear programming (MILP) model. In this method, many potential levels with

fixed evaporating temperature are assumed (e.g. one level per degree). Then the superstructure, which includes options of inter-evaporator, inter-condenser and presaturator, is optimised and the number of levels, level temperature and other parameters are determined simultaneously. Colmenares and Seider (1989) used a nonlinear programming model and "lumping temperature intervals" concept, which is similar to the exploration of "pockets" in GCC, to reduce the size of the model. Using this approach, a refrigeration system that operates over a temperature range can be optimised. The advantage of this approach is that it did not require fine temperature discretisation, which makes the size of problems smaller and thus easier to solve. Vaidyaraman and Maranas (1999), based on the work of Shelton and Grossmann, considered the synthesis of refrigeration systems and the selection of refrigerants simultaneously. A pre-specified list of candidate refrigerants and their individual operating ranges are provided. The superstructure representation is extended to account for more elaborate refrigerant features and allow the automatic selection of refrigerants.

In summary, recent works are mainly in two categories: (1) based on pinch technology and exergy; and (2) using mathematical programming and superstructure. Works in the first category give good understanding and insights of the integration between process and refrigeration systems. However, they cannot generate sophisticated optimal configurations and accurate information of shaftwork requirement. Methods in the second category, on the other hand, can generate design of complete refrigeration systems, but have weak insights and little understanding of the problems *per se*. Figure 1-13 summarises the features these two types of methods.

Pinch technology-based	Superstructure-based
Good insights and understabnding	"Black box" procedures
No detailed design	Complete design
Easy to apply	Difficult to initiate and apply

Figure 1-13. Comparison among recent works.

The current methods present a missing link between practicality and usability. Using pinch technology and exergy analysis, good insights can be obtained and they are easy to apply. But, they cannot generate accurate and detailed design of refrigeration systems. Therefore, this kind of methods is more suitable to the initial design stages, or at targeting phases. Superstructure-based approaches, on the other hand, address more detailed design issues but are more black-box oriented. For industrial-sized problems, applications are difficult and time-consuming to reach reasonably good and practical designs.

1.3 OVERVIEW OF THIS WORK

Optimal synthesis of industrial refrigeration systems is challenging but of great economic interests. Conventionally, heuristics, pinch technology or pure mathematical programming are applied to achieve this task. None of them satisfies the two criteria at the same time, which are easily applicable to solve large problems and capable of generating sophisticate structures. In this thesis, a new synthesis method will be proposed, which combines the power of shaftwork targeting method and mathematical programming. Shaftwork targeting optimises the major parameters of refrigeration systems and generates solutions that are near the optimal ones. The solution by shaftwork targeting also defines the upper bound of the final optimal solution for the following MINLP. The upper bound can effectively eliminate design options with shaftwork consumption higher than the upper bound. In the case study, we demonstrate that the new method not only satisfy the two criteria, but also gives the results much faster and give users greater confidence.

The first chapter gives brief introduction to the design problem of refrigeration systems and reviews previous work. The second chapter proposes a new method for the design of refrigeration systems. In the new method, disjunctive programming is used to deal with the design and enhances MINLP. In the third chapter, case studies are presented to demonstrate the procedures of the new method and also the effectiveness of the new method compared with previous work. It is shown the new method is capable of generating better design of refrigeration systems with easier initiation and faster

solutions. The new method can deal with industrial-sized synthesis problems more effectively than using either pinch technology or mathematical programming.

Reference

Barnes F. J. and King C. J., 1974, Synthesis of Cascade Refrigeration and Liquefaction Systems. *Ind. Eng. Chem. Proc. Des. Dev.* **13**, 421-433.

Cheng W. B. and Mah R. S. H., 1980, Interactive Synthesis of Cascade Refrigeration Systems. *Ind. Eng. Chem. Proc. Des. Dev*., **19**, 410-420.

Colmenares T. R. and Seider W. D., 1989, Synthesis of Cascade Refrigeration systems Integrated with Chemical Process. *Comput. Chem. Engng.*, **3**, 247-258.

Dhole V. R., Linnhoff B., 1989, Shaftwork Targeting for Subambient Plants, *AIChE Spring Meeting*, Houston, April, 1989.

Linnhoff B. Townsend D. W., Boland D., Hewitt, G. F., Thomas B. E. A., Guy A. R., Marsland R. H., 1991, *A User Guide on Porcess Integration for the Efficient Use of Energy*, The Institute of Chemical Engineers.

Nimitz J. S., Skaggs S., 1992, Estimating Tropospheric Lifetimes and Ozone Depletion Potentials of One and Two-hydrocarbons and Hydrochlorofluorocarbons, *Environ. Sci. Technol*. **26 (4)**, 739-744

Lee G. C., Zhu X. X., Smith R., 2000, "Synthesis of Refrigeration Systems by Shaftwork Targeting and Mathematical Optimisation", *ESCAPE-10*, Florence, Italy, May 2000.

Shelton M. R. and Grossmann I. E., 1986, Optimal Synthesis of Integrated Refrigeration Systems. *Comput. Chem. Engng* **10**, 445.

Townsend D. W., Linnhoff B., 1982, Designing Total Energy Systems by Systematic Methods, *The Chemical Engineer*, **March**, 91-97.

Vaidyaraman S. and Maranas C. D., Simultaneous Refrigeration Cycle Synthesis and Refrigeration Selection. *PRES'99*, Hungary, 679.

2 NEW APPROACH FOR DESIGN AND RETROFIT OF REFRIGERATION SYSTEMS

2.1 Introduction

State-of-the-art approaches for the synthesis of refrigeration systems are either pinch technology-based or superstructure-based. Pinch technology-based approaches provide good understanding and insights into the design problems. However, they cannot generate detailed optimal configurations and accurate prediction of shaftwork requirements. Superstructure-based approaches, on the other hand, generate complete structures of refrigeration systems, but offer weak insights and understanding. None of them can satisfy the needs for design of industrial problems in which a large number of process streams and practical constraints are involved. In this chapter, a new approach will be proposed for design and retrofit of refrigeration systems. This new method is based on the combination of pinch technology and mathematical programming. There are three major benefits that distinguish the proposed method to previous methods. First, the proposed method uses grand composite curve (GCC) and optimisation to continuously adjust refrigeration temperature and duty of each level, and therefore avoids unnecessary integer variables. Second, only design options are integer variables in a MINLP model in the second phase. As a consequence, the model size is much smaller than that in previous approaches. And the third benefit is the use of disjunctive programming to enhance the effectiveness and robustness of the MINLP model. The optimum design is obtained in a two-phase approach as shown in Figure 2-1.

The first phase uses the shaftwork targeting method to optimise main design variables, such as the number of levels and temperature and duty of each level. The model used in the first phase is a MINLP model, with only the number of levels as the integer variable. The results will be fed into the second phase as initial conditions. The second phase, based on a disjunctive programming-enhanced MINLP model, exploits design options

and generates the optimal refrigeration configurations. The practicality of the final design is then checked. If not satisfied, the model can readily include new constraints, such as compressor's capacity range. It should be noted that the shaftwork targeting method plays a significant role in the whole procedure. The results from the targeting method indicates the target for the next phase of design stage. More importantly, it provides good initial conditions for the next stage MINLP optimisation. The final solution from MINLP should be better or at least equal to the shaftwork targeting result. Disjunctive programming helps the MINLP model reach solutions more efficiently and behave more robust. For greater flexibility and efficiency, a hybrid form of disjunctive programming which includes conventional mix-integer constraints and disjunctions, is used.

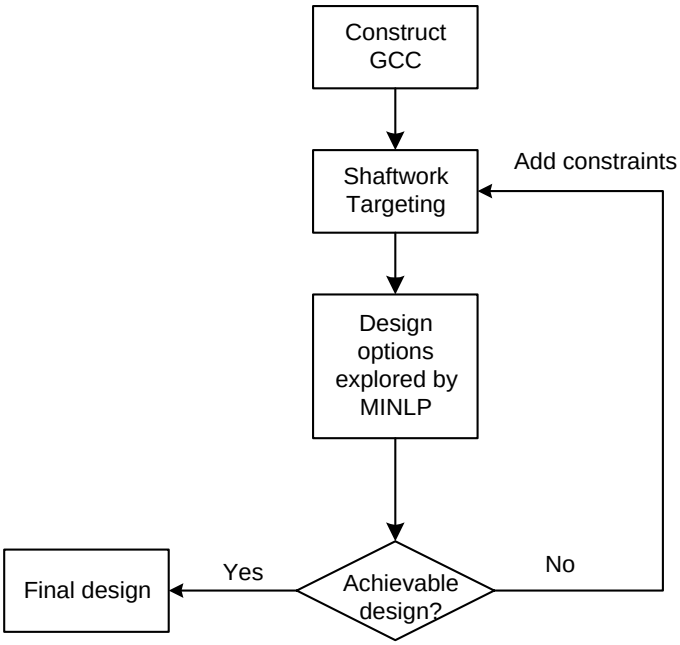

Figure 2-1. New approach for the synthesis of refrigeration systems

The proposed method is also an efficient tool to deal with retrofit of existing refrigeration systems. In retrofit cases, the shaftwork targeting method employed in the first phase is performed with the inclusion of constraints from existing equipments, such as compressors and heat exchangers. The tightness of each constraint can be adjusted according to the practical needs.

Based on the new two-phase approach, a synthesis method for cascade refrigeration system is also proposed. The method uses the partition temperature to split the whole refrigeration demands into an upper cycle and a lower cycle. The design starts from the lower cycle, and modifies the GCC for the following design of the upper cycle. In this way, each cycle is treated independently as a multistage refrigeration system. Optimisation iterates on the partition temperature to find the optimal value. Finally, the design task converges and generates the optimal configurations of a cascade refrigeration system.

2.2 Shaftwork targeting method

To achieve better energy efficiency, engineers usually consider certain design options, such as economisers, intercoolers, etc., either for new design or retrofit. To evaluate the impact of each design option, a quick and reliable method for estimating shaftwork requirement can be very useful. This kind of tool is called the shaftwork targeting method. There are some essential benefits from applying the shaftwork targeting method:

1. Set the shaftwork requirement of refrigeration system before complete design.
2. Assess the performance of the whole process prior to detailed design.
3. Allow many alternative design options to be screened quickly and estimated reliably.
4. Assess energy and capital costs.
5. Allow “user interaction” to incorporate engineers’ insight and knowledge base.

2.2.1 Calculation of Shaftwork

Simple cycle.

Consider a simple vapour-compression as shown in Figure 2-2. The problem is how to estimate the actual shaftwork requirement given the following conditions: condensing temperature T_b, evaporating temperature T_c, and compressor's polytropic efficiency, η_p.

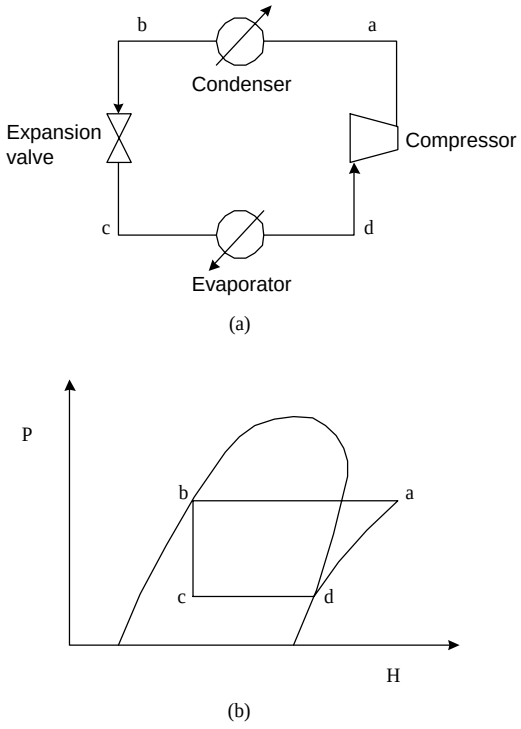

Figure 2-2. A simple vapour-compression cycle: (a) flow diagram;

(b) pressure-enthalpy diagram

The calculation procedure is performed in three steps:

1. Find the corresponding vapour pressure, P_b and P_c, by using Antoine equation:

$$\ln P^{vap} = A - \frac{B}{T + C} \tag{2-1}$$

2. Find the outlet temperature, T_a, of compressor. The polytropic function can be used to describe the compression path, where *k* is the polytropic exponent.

$$P \cdot v^k = constant \tag{2-2}$$

Given the compressor's polytropic efficiency, the outlet temperature (T_a) can be found by:

$$T_a = T_d \left(\frac{P_a}{P_d} \right)^{\gamma} \tag{2-3}$$

where

$$\gamma = \frac{k-1}{k \cdot \eta_p} \tag{2-4}$$

$$k = \frac{Cp}{(Cp - R)} \tag{2-5}$$

Cp is the average molar heat capacity at T_a and T_d.

3. Calculate the shaftwork requirement. An energy balance around the compressor gives the shaftwork requirement of compressor:

$$m = \frac{Q_{evp}}{h^d - h^c} \tag{2-6}$$

$$W_{shaft} = m \cdot \left(h^a - h^b \right) \tag{2-7}$$

The enthalpy is estimated by using the departure function of Peng-Robinson equation of state:

$$h - h^* = RT(Z-1) + \frac{T(da/dT) - a}{2\sqrt{2}\, b} \ln \left[\frac{Z + (1+\sqrt{2})B}{Z + (1-\sqrt{2})B} \right] \tag{2-8}$$

where

$$a(T) = 0.45724 \frac{R^2 T_C^2}{P_C} \cdot \alpha \tag{2-9}$$

$$b = 0.07780 \frac{RT_C}{P_C} \tag{2-10}$$

$$\sqrt{\alpha} = 1 + \kappa \cdot \left(1 - \sqrt{\frac{T}{T_C}} \right) \tag{2-11}$$

$$\kappa = 0.37464 + 1.54226 \cdot \omega - 0.26992 \cdot \omega^2 \tag{2-12}$$

$$da/dT = -0.45724 \frac{R^2 T_C^2}{P_C} \kappa \sqrt{\frac{\alpha}{T \cdot T_C}} \tag{2-13}$$

$$B = \frac{bP}{RT} \tag{2-14}$$

Thus, the enthalpy difference can be calculated between two states, $h^a - h^d$, by the following relation:

$$h^a - h^d = \left[h(T_a, P_a) - h^*(T_a, P = 0) \right] + \left[h^*(T_a, P = 0) - h^*(T_d, P = 0) \right] - \left[h(T_d, P_d) - h^*(T_d, P = 0) \right] \tag{2-15}$$

where the first and third terms of the right-hand side are computed by the departure function described above, and the second term is the enthalpy difference of ideal gas (P=0) between T_a and T_d, which is:

$$h^*(T_a, P = 0) - h^*(T_d, P = 0) = \int_{T_d}^{T_a} Cp^*(T)\, dT \tag{2-16}$$

Once the enthalpy difference has been obtained for h^a and h^d, the shaftwork requirement of the compressor for this simple vapour-compression cycle is obtained.

Multistage cycle.

A multistage cycle can be viewed as an assembly of several simple vapour-compression cycles. In multistage cycles, the compressor of each stage, except the lowest one, is subject to superheated inlet condition, which is a result of mixing of saturated stream with superheated compressor outlet from lower stage. Acceptable results can normally be obtained by correcting the temperature by mass-flow weighting. Figure 2-3 shows a detail of two intermediate stages of a multistage cycle. Refrigerant liquid L_1 evaporates at constant temperature T_1 in the evaporator and absorbs heat duty Q_1; after becoming saturated vapour, it mixes with refrigerant vapour V_1, but the mixture is still at temperature T_1. The same is for refrigerant L_2 and V_2. The outlet of first stage compressor at temperature T_{out} mixes with saturated vapour refrigerant from the second stage at temperature T_2, and the resulting mixture is at temperature T_{mix}.

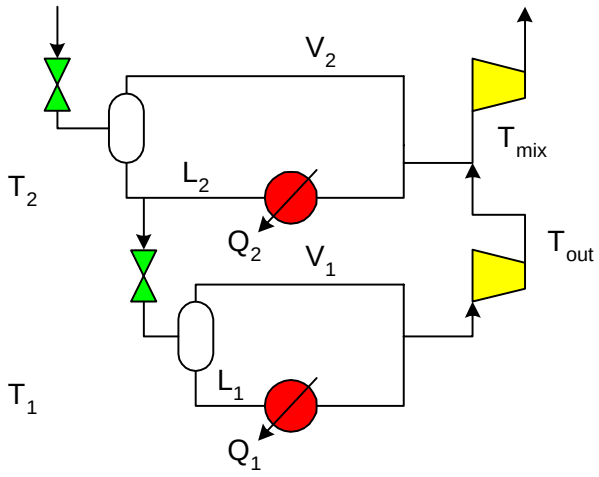

Figure 2-3. Two intermediate stages of a multistage cycle

To calculate T_{mix} by mass-flow weighting, a material and energy balance is done around the two stages and the following relations are obtained:

$$\left(L_1 + V_1\right) \cdot h_2^L = L_1 \cdot h_1^L + V_1 \cdot h_1^V$$

$$\Rightarrow L_1 \cdot \left(h_2^L - h_1^L\right) = V_1 \cdot \left(h_1^V - h_2^L\right)$$
$$= V_1 \cdot \left(h_1^V - h_1^L\right) - V_1 \cdot \left(h_2^L - h_1^L\right)$$

If both sides are divided by $V_1 \cdot \left(h_2^L - h_1^L\right)$, then we have the following relation:

$$\frac{L_1}{V_1} = \frac{H^{vap}(T_1)}{h^L(T_2) - h^L(T_1)} - 1 \tag{2-17}$$

The relation between L_1 and L_2 is more straightforward:

$$\frac{L_1}{L_2} = \frac{Q_1 \cdot \Delta H^{vap}(T_2)}{Q_2 \cdot \Delta H^{vap}(T_1)} \tag{2-18}$$

By using equations (2-17) and (2-18), the mass flow rate of each stage can be calculated. A mass-flow weighting relation then calculates T_{mix}:

$$T_{mix} = \frac{T_{out}\left(L_1 + V_1\right) + T_2\left(L_2 + V_2\right)}{L_1 + V_1 + L_2 + V_2} \tag{2-19}$$

The outlet temperature of the second stage compressor is found by using equation (2-3) in which T_{mix} replaces T_d.

Incorporation with grand composite curve

A pure mathematical programming approach discretises the whole temperature range of processes into many small temperature intervals. A large number of binary variables thus are required to represent potential active refrigeration levels, which dramatically increase the complexity of the model and make the problems difficult to solve. Contrary to conventional mathematical programming approaches, refrigeration levels and duties are treated as continuous variables in the proposed method by using grand composite curves (GCC). The GCC provides the overall source and sink temperature profiles of a

process. It allows setting the refrigerant load at any temperature level continuously, instead of discretising the temperature level and causing the problem to grow unnecessarily large. Another benefit of using GCC is that it considers the integration among the process, HEN and refrigeration system simultaneously, and the energy balance is always guaranteed.

The GCC in Figure 2-4 shows an example of placing four refrigeration levels and one heat-rejecting level. From GCC, the information of each stage's refrigeration duty and evaporating temperature can be read directly. Due to the nature of the GCC, it can be easily modelled as a series of piecewise linear functions. Optimisation can determine the optimal refrigeration levels and duties.

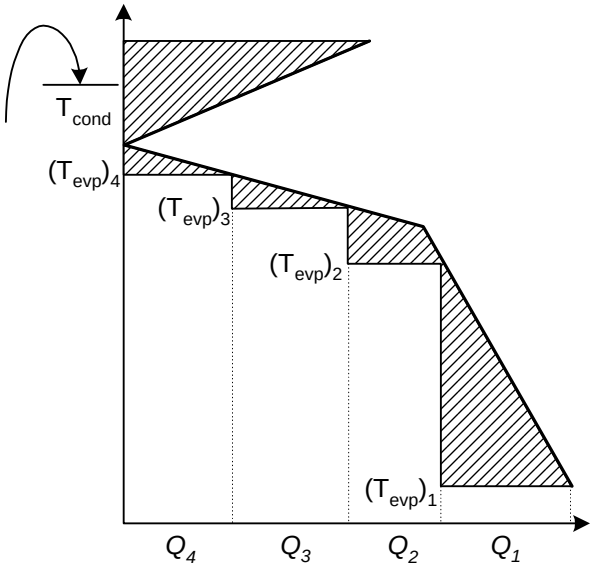

Figure 2-4. Incorporate with grand composite curve

Exploit the "pocket"

Pocket is a semi-enclosed area in the GCC, and incurs a self-contained energy balance of heat source and sink. However, there is certain amount loss of temperature driving force in heat transfer. Further saving on shaftwork requirement can be achieved by two ways. First, by adding heat rejection levels, usually a reboiling option, into the pocket, part of the heat rejected by the process into the lowest level 'a' can be disposed at below-ambient temperature level 'c', as illustrated in Figure 2-5. Second, by subcooling refrigerant before flashing by process streams, vapour fraction after flashing is therefore reduced. For the reboiling option, the reduction in total shaftwork requirement more

than compensates for installation of extra duty at level ‘d’. In other words, the saving in shaftwork requirement is very significant so it is worth of the increase in the complexity of design. The reasons for exploiting the pocket to reduce shaftwork are that the loss of temperature driving force in the pocket area is reduced and the reboiling service creates a loop of refrigerant around the lower cycle thus the total refrigerant flow rate is reduced.

For the subcooling option, saturated refrigerant liquid is subcooled close to evaporation temperature at the lower temperature level, prior to flashing through throttling valves. By doing this, the amount of vapour produced from the flash is much reduced, thus shaftwork is reduced.

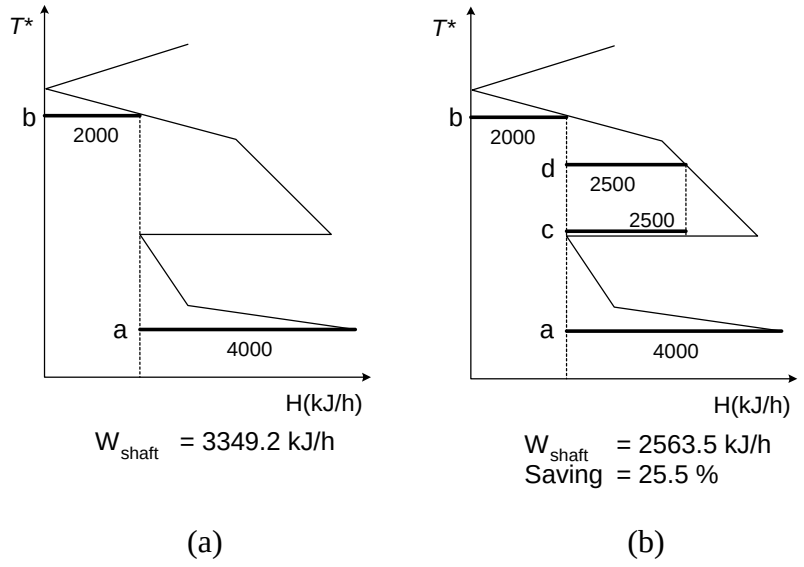

(a) (b)

Figure 2-5. Exploit the pocket by a reboiling stage: (a) the original design; (b) after including a reboiling option.

The function of a subcooler is explained in Figure 2-6. By installing a subcooler prior to the throttling valve, the saturated refrigerant liquid at point *a* is first cooled down to point *b* where the refrigerant becomes subcooled, and then flashes down to point *c*’. The vapour fraction at point *c*’ is smaller than that at point *c*, so less amount of vapour is produced after flashing.

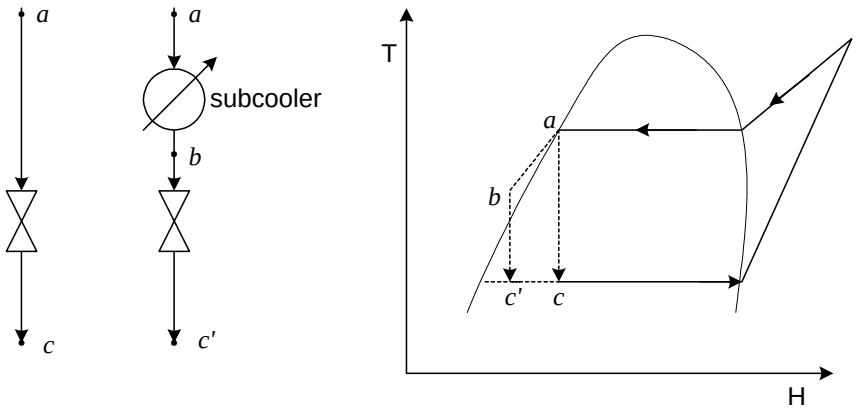

Figure 2-6. Function of a subcooler on T-H diagram.

Subcoolers can be used when suitable process streams exist in the pocket area on the GCC. Figure 2-7 explains the situation.

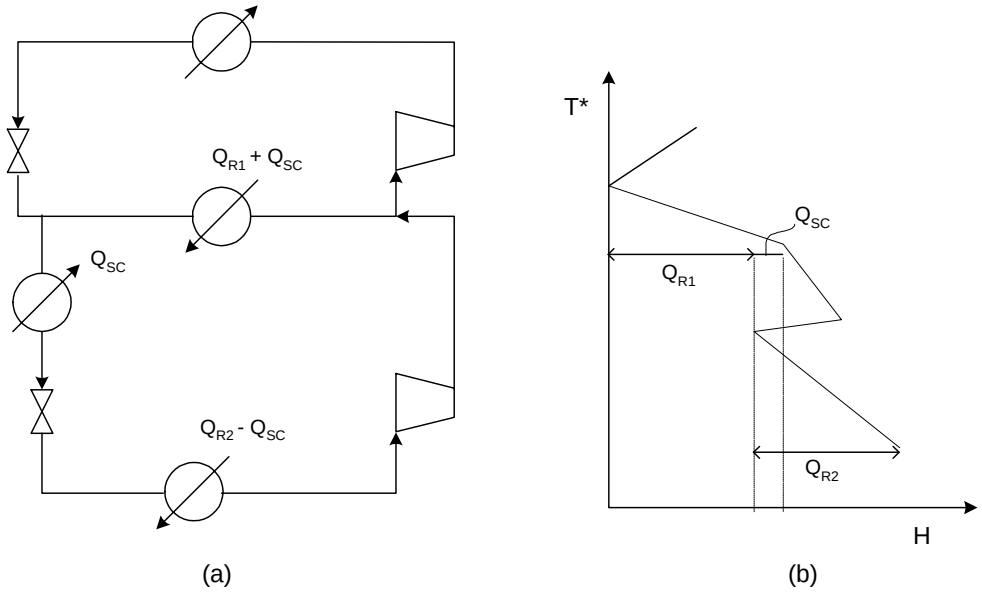

Figure 2-7. Function of the subcooler: (a) flow diagram; (b) GCC.

The revised duty for each level becomes:

Level 1 $Q_{R1} + Q_{SC}$

Level 2 $Q_{R2} - Q_{SC}$

The effect of installing subcoolers therefore can be treated as a means to shift refrigeration duty from lower levels to higher levels. The overall benefit is the reduction of shaftwork consumption.

MINLP optimisation

Optimisation based on those equations describing refrigeration systems can be carried out by a MINLP model. First, the GCC is modelled as a set of piecewise linear functions,

$$T = f(\Delta H) \tag{2-20}$$

The GCC then combines with shaftwork calculation method to determine temperature level and duty of each stage, as shown in Figure 2-8.

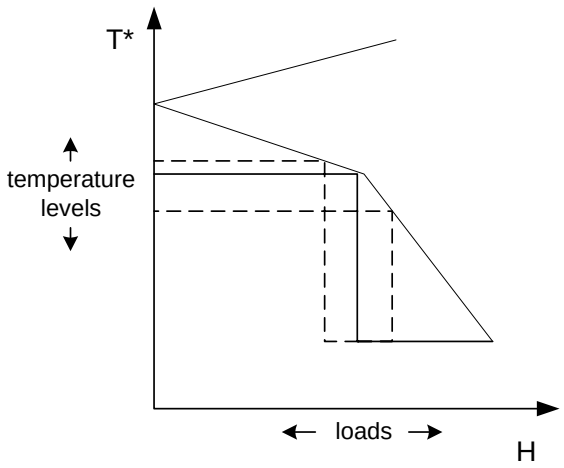

Figure 2-8. Optimisation of temperature levels and loads according to GCC

Because the GCC between each "kink" points are linear, it is straightforward to formulate the GCC by a piecewise linear approximation. So the equation of the line connecting points $\left(x^{(k)}, f^{(k)}\right)$ and $\left(x^{(k+1)}, f^{(k+1)}\right)$ is given by

$$\tilde{f}(x) = f^{(k)} + \frac{f^{(k+1)} - f^{(k)}}{x^{(k+1)} - x^{(k)}}\left(x^{(k+1)} - x^{(k)}\right) \tag{2-21}$$

For the design of a refrigeration system ignoring any design option, the degrees of freedom are n – 1, where n is the number of levels. The optimisation model is formulated as such:

$$min \quad c^{el} \cdot aot \cdot \sum_{i=1}^{n} W_{shaft,i} + cf \cdot \left(\sum_{i=1}^{n} c^{comp} + c^{HEN} \right) \tag{2-22}$$

Subject to

$$g(\xi, \varsigma) \geq 0$$

$$h(\xi, \varsigma) = 0$$

$$\xi^{l} \leq \xi \leq \xi^{u}$$

$$\xi' \subset \xi$$

ξ' : mole fraction variables

ξ : continuous variables

ς : integer variables

The first part of the objective function is the annual operating cost of compressors, and the second part is the annualised capital cost of compressors and HEN. The only integer variable in this model is the number of stages. By doing this, we can determine the optimal number of stages with optimised major parameters that achieve minimal total annual cost. The following case study demonstrates the application of the shaftwork targeting method. $g(\xi, \varsigma) \geq 0$ represents process constraints. $h(\xi, \varsigma) = 0$ is the shaftwork calculation method and other equality constraints.

2.2.2 Case study

The proposed shaftwork targeting method is demonstrated by an ammonia refrigeration system. Given the supply and target temperatures and heat capacity flowrates of four process streams (Table 2-1), the task is to design a refrigeration system using ammonia

as the refrigerant to satisfy cooling demand from the process. The cooling duty for the process streams is 190 kW. The objective here is first to find the minimum shaftwork consumption for different number of stages, and then determine the minimum total cost configuration. The main features of this case study are: (1) using GCC to place refrigeration levels; (2) increasing number of stages to reduce shaftwork consumption; (3) using MINLP to determine the optimal number of stages.

Table 2-1. Properties of the four process streams.

Stream	TS [^{o}C]	TT [^{o}C]	DH [kW]	CP [kW/ ^{o}C]	HTC [kW/^{o}C · m^{2}]
Hot 1	20.0	-45.0	-325.0	5.0	2.00
Hot 2	40.0	10.0	-30.0	1.0	2.00
Cold 1	-40.0	0.0	120.0	3.0	2.00
Cold 2	10.0	45.0	175.0	5.0	2.00

The GCC of this process is shown in Figure 2-9. Minimum temperature approach (ΔT_{min}) = 5 ^{o}C is used.

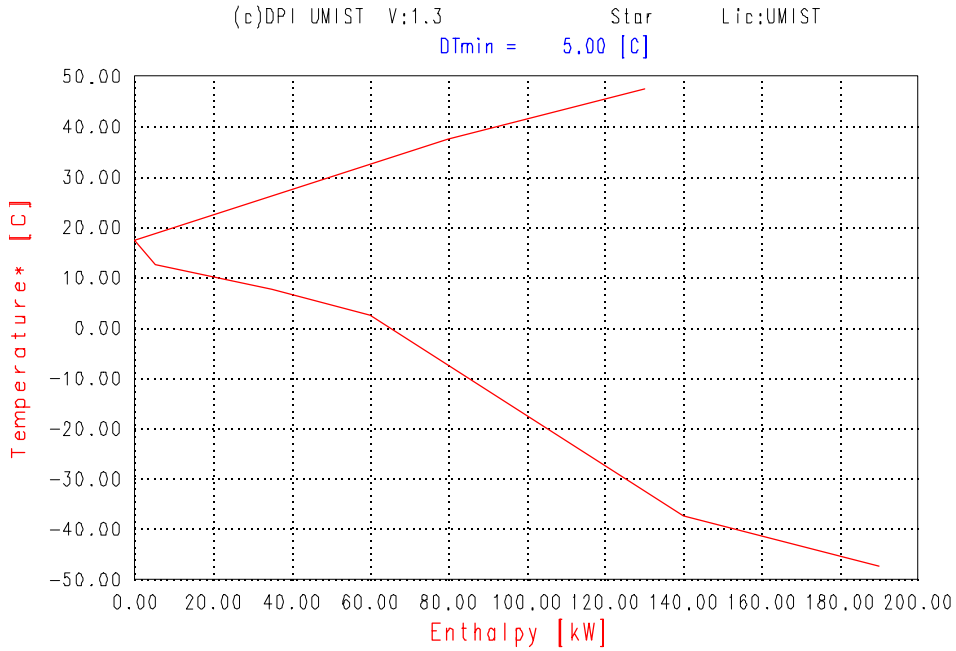

Figure 2-9. GCC of the process.

Only the part with temperature below pinch point, 17.5 ^{o}C, needs refrigeration to remove heat from the process. This part of the GCC can be formulated by a piecewise linear approximation as follows.

$$\begin{aligned} T &= 17.5 - 1.2H && 0 \le H \le 5 \\ T &= 12.5 - 0.167(H - 5) && 5 \le H \le 35 \\ T &= 7.5 - 0.2(H - 35) && 35 \le H \le 60 \\ T &= 2.5 - 0.5(H - 60) && 60 \le H \le 140 \\ T &= -50 && 140 \le H \le 190 \end{aligned} \qquad (2\text{-}23)$$

H is the accumulated refrigeration duty from the first (highest) level. T is the corresponding evaporation temperature. In the last region, the evaporation temperature is set at –50 ^{o}C, regardless of the shape of the GCC. This reflects on the fact that the lowest evaporation stage has to be at –50 ^{o}C to allow heat rejected from the process at its lowest temperature at -45 ^{o}C, with a 5 ^{o}C temperature difference. If the objective function is to minimise the shaftwork consumption, we can obtain the results in Table 2-2.

Table 2-2. Shaftwork targeting results.

No. of stages	Temperature/Load/Shaftwork of each level				Total shaftwork [kW]
1	Temperature	-50 (^{o}C)			122.96
	load	190.0 (kW)			
	shaftwork	122.96 (kW)			
2	-50 (^{o}C)	-10 (^{o}C)			79.02
	104 (kW)	86 (kW)			
	28.27 (kW)	50.75 (kW)			
3	-50 (^{o}C)	-28 (^{o}C)	3 (^{o}C)		66.40
	70 (kW)	60 (kW)	60 (kW)		
	9.67 (kW)	26.87 (kW)	29.85 (kW)		
4	-50 (^{o}C)	-33 (^{o}C)	-15 (^{o}C)	5 (^{o}C)	61.00
	56 (kW)	40 (kW)	54 (kW)	40 (kW)	
	5.84 (kW)	10.65 (kW)	17.47 (kW)	27.03 (kW)	

The shaftwork targeting method gives the optimal settings of temperature and load for each stage. We can observe the trend of reducing shaftwork requirement by increasing number of stages in Figure 2-10.

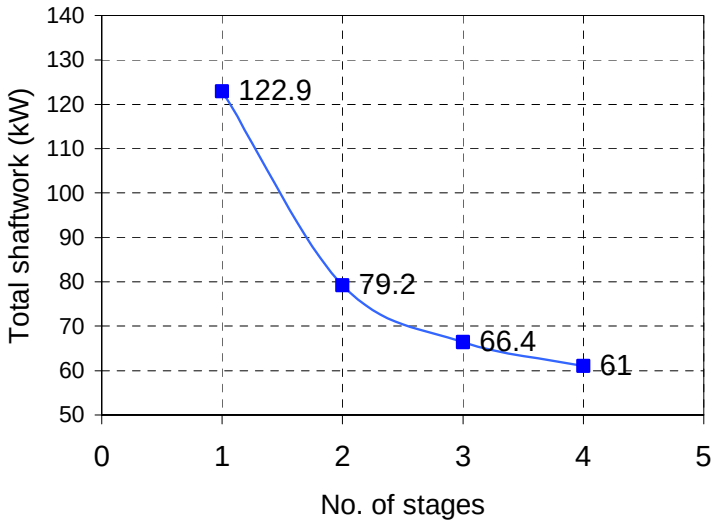

Figure 2-10. Reducing total shaftwork by increasing number of stages.

The total shaftwork shows a sharp reduction from 1-stage system to 2-stage system. The benefit diminishes when the number of stages increases. To determine the optimal configuration for minimum total cost design, we need to take capital investment into consideration. The following data are used to estimate the cost of compressors.

$$\text{Compressor cost}(£) = 57000\ (\ \text{shaft power}(kW)\ )^{0.35}$$

Electricity cost : 4.15 pence/kW-hr

Operating time per year : 8000 hours

The capital cost includes only the cost of compressors. A more thorough estimation needs to include the costs of heat exchangers, flash drums, piping, etc. The investment cost is annualised with a coefficient of 10%. Detailed results of the optimisation are shown in Table 2-3.

Table 2-3. Total cost vs. number of stages.

No. of stages	Shaftwork of each compressor (kW)	Operating cost per year (£)	Individual compressor cost (£) *	Total cost of each compressor (£)	Total cost (£)
1	122.96	40822.7	30710.87602	71533.6	71533.6
2	28.27	9385.6	18358.57164	27744.2	
	50.75	16849.0	22530.84459	39379.8	67124.1
3	9.67	3210.4	12611.71423	15822.2	
	26.87	8920.8	18035.09934	26955.9	
	29.85	9910.2	18711.3608	28621.6	71399.7
4	5.84	1938.9	10571.07982	12510.0	
	10.65	3535.8	13045.09417	16580.9	
	17.47	5800.0	15512.34205	21312.4	
	27.03	8974.0	18072.61395	27046.6	77449.8

* : annualised

After considering capital investment, 2-stage refrigeration system becomes the optimal choice for minimum total cost configuration. While the 4-stage system consumes the least shaftwork, it actually incurs the highest overall investment. In this case study, it has been demonstrated that different objective functions lead to different optimal solutions. Shaftwork targeting method can quickly estimate shaftwork requirement, so the optimisation can determine the optimal configurations of given design problems.

2.3 Disjunctive programming model

Often in the modelling of processes, we encounter the situations when logic selections need to be made, or different sets of equations apply to different design scenario. A typical example is the friction factor. It uses different equations in laminar region and in turbulent region. Although the equations are continuous, to determine the use of which equation to apply is a logic decision. The disjunctive programming, first proposed by Balas (1974, 1985), is a form to model problems in which discrete variables are restricted to values of 0 and 1 and represent certain decisions which are necessary to deal with continuous variables.

In general, a design problem is formulated as a MINLP model. However, the MINLP model has two major limitations. First, many redundant constraints in the model have to be solved at every iteration of the solution procedure, which increases the computational requirement. Second, when design options disappear from the superstructure, by setting flows to zero, equations in the MINLP model can become discontinuous due to fixed costs for the options, and deteriorate the robustness of the computations. Raman and Grossmann (1994) proposed a generalised disjunctive programming (GDP) modelling framework that overcomes these limitations by allowing a "bypass" model to take effect when a given option is eliminated from the superstructure. The GDP has the following form:

$$
\begin{aligned}
&\min \quad Z = \sum_i \sum_k c_{ik} + f(x) \\
&s.t. \quad g(x) \le 0 \\
&\qquad \bigvee_{i \in D_k} \begin{bmatrix} Y_{ik} \\ h_{ik}(x, c_{ik}) \le 0 \end{bmatrix}, \quad k \in SD \\
&\qquad \Omega(Y) = true \\
&\qquad x \in R^n \ , \ c \in R^m \ , \ Y \in \{true, false\}^m
\end{aligned}
\tag{2-22}
$$

Y_{ik} are boolean variables that establish whether a given term in a disjunction is true $[h_{ik}(x, c_{ik}) \le 0]$ or false $[h_{ik}(x, c_{ik}) > 0]$, and $\Omega(Y)$ are logical relations assumed to be in the form of propositional logic involving only the Boolean variables. x and c_{ik} are continuous variables, the latter being used to model costs associated with each disjunction. $g(x) \le 0$ represents constraints that are valid over the entire search space while the disjunction $k \in SD$ states that at lease one subset of constraints $h_{ik}(x, c_{ik}) \le 0 \, , i \in D_{ik}$ must be hold. Y_{ik} are auxiliary variables that control the part of the feasible space in which the continuous variables x lie, while the logical conditions $\Omega(Y)$, express relations between the disjunctive sets. Aldo and Grossmann (1999) proposed a hybrid model formulation for discrete-continuous non-linear problems. The model can involve disjunctions, binary variables and integer or mixed-integer constraints. The hybrid model has the following form:

$$
\begin{aligned}
&\min \quad Z = \sum_i \sum_k c_{ik} + f(x) + d^T y \qquad (2\text{-}23)\\
&s.t. \quad g(x) \le 0\\
&\qquad r(x) + Dy \le 0\\
&\qquad Ay \ge a\\
&\qquad \begin{bmatrix} Y_{ik} \\ h_{ik}(x, c_{ik}) \le 0 \\ c_{ik} = \gamma_{ki} \end{bmatrix} \vee \begin{bmatrix} \neg Y_{ik} \\ B^i x = 0 \\ c_{ik} = 0 \end{bmatrix}\\
&\qquad \Omega(Y) = true\\
&\qquad x \in R^n \ , \ c \in R^m \ , \ y \in \{0,1\} \ , \ Y \in \{true, false\}^m
\end{aligned}
$$

$r(x) + Dy \le 0$ represents the general mixed-integer algebraic formulations in which the original disjunctions are transformed into algebraic equations. $Ay \ge a$ is a set of integer inequalities and $d^T y$ are linear cost terms. This hybrid form is more convenient when the GDP form is applied to some disjunctions, or when it is not natural to express the entire model in terms of disjunctions and logic relations. Therefore, the hybrid form is more flexible than rigorous the GDP form.

Disjunctive programming can be used as a basis to formulate a mixed-integer program with 0-1 variables. The simplest representation of the disjunctions, $k \in SD$, in mixed-integer form are the "Big-M" transformation:

$$
\begin{aligned}
&h_{ik}(x, c_{ik}) \le M_{ik}(1 - Y_{ik}), \ i \in D_{ik} \ , k \in SD \qquad (2\text{-}24)\\
&\sum_{i \in D_k} Y_{ik} \ge 1 \ , \ k \in SD
\end{aligned}
$$

Therefore

When $Y_{ik} = 1$, $h_{ik}(x, c_{ik}) \le 0$

When $Y_{ik} = 0$, $h_{ik}(x, c_{ik}) \le M_{ik}$

M_{ik} is a valid upper bound. When an option is selected, its associated binary variable, Y_{ik}, is set equal to 1, so the right-hand side of the above constraint becomes 0, making

the constraint active. On the other hand, when an option is not selected, it associated binary variable is set to 0, which makes the constraint becomes virtually "unbounded" by letting the left-hand side value less or equal to a big number, M_{ik}. The fact that when an option is eliminated its associated constraints or equations are sufficiently relaxed or unbounded makes the optimisation become robust and computationally efficient. Much less time is wasted to calculate and converge those virtually non-existing equations, as conventional MINLP does. Another transformation, the convex hull proposed by Balas (1985), although often yields better-behaved formulations and tighter approximation, is more difficult to apply and only useful when the constraints in the disjunctions are linear. Therefore, in this thesis the Big-M transformation is adapted.

2.4 Design of refrigeration systems by MINLP approach

In the first phase of targeting stage, a basic refrigeration system is obtained. There are still many design options which need to be considered to reduce both capital and operating costs. These options are accounted in the second phase of design. These design options add complexity to the synthesis or retrofit task, which involves the selection of the configuration, parameters of refrigeration cycles and the matches between heat sources and sinks for each heat exchanger. A logic-based MINLP model will be used to exploit the design options in the synthesis of refrigeration systems and also in the retrofit of existing systems.

2.4.1 Review of Wu's work

The model used in this thesis was based on Wu and Zhu's work (2000). However, considerable modifications are made to improve the solution performance and results.

Wu and Zhu's method (1999) divides the whole temperature range into several temperature intervals. The refrigeration temperatures and pre-set temperatures at which the superheated vapour will enter its cooling/condensing sequence must be included in the intervals. The temperature difference within any interval must be equal or less than the allowed minimum approach temperature. Inside such cycle, refrigerant liquids, superheated vapours and suction vapours form a special heat exchanger network (HEN) with some cold utilities. The heat flow capacities are allowed to vary as well as either the inlet or outlet temperature. While suction vapours and refrigerant liquids have their supply temperature fixed, the superheated vapours have the target temperature fixed.

Liquid refrigerant streams and superheated vapours form the hot streams in the special HEN and suction vapours and cold utilities are the cold streams. The liquid refrigerant can only be subcooled by the suction vapours, while the superheated vapours can be cooled down by suction vapours and cold utilities. Figures 2-11 and 2-12 represent the heat transfer pattern between these streams.

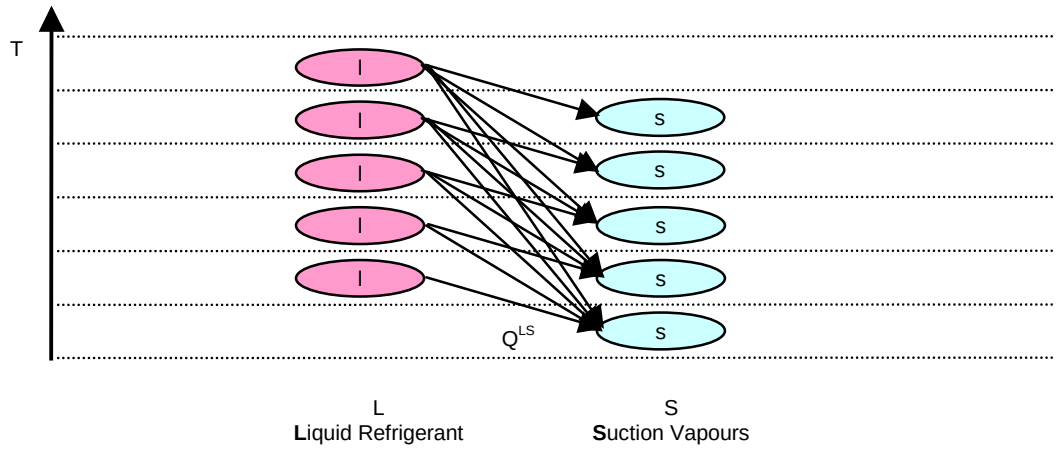

Figure 2-11. Heat transfer pattern between streams L and S.

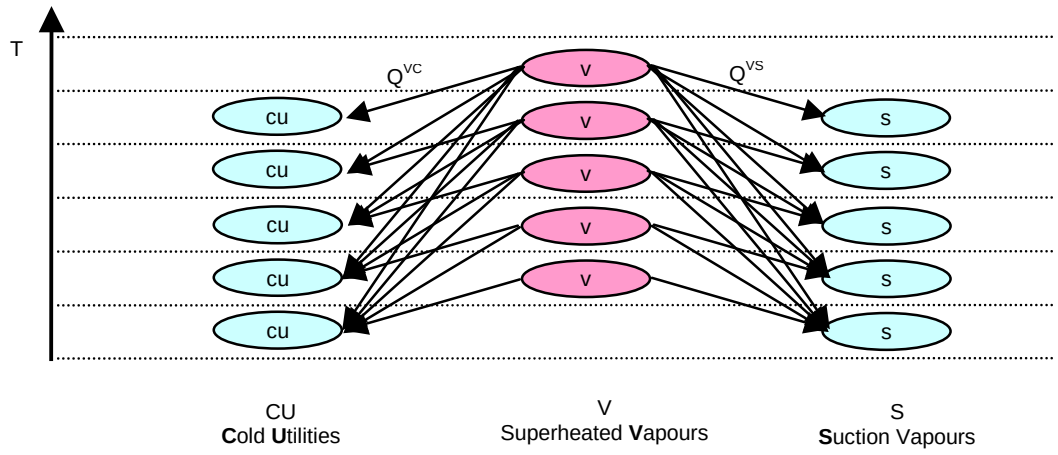

Figure 2-12. Heat transfer pattern between streams V, S and cold utilities.

The heat content for each stream in each interval is calculated as:

$$Q = FCp\Delta T \tag{2-25}$$

where ΔT represents the temperature difference in the interval. The cooling duty for the liquid refrigerant must be equal to the heat absorbed by suction vapours in all the intervals.

$$\sum Q^{L} = \sum Q^{LS} \tag{2-26}$$

The heat provided by the superheated vapours is equal to the heat transferred to suction vapour and cold utility streams.

$$\sum Q^{V} = \sum \left(Q^{VS} + Q^{VC} \right) \tag{2-27}$$

The heat absorbed by the suction vapours from the superheated vapours and liquid refrigerant should be in balance as well.

$$\sum Q^{S} = \sum \left(Q^{VS} + Q^{LS} \right) \tag{2-28}$$

Finally, the heat absorbed by the cold utilities must be equal to the heat coming from the superheated vapours.

$$\sum Q^{C} = \sum Q^{VC} \tag{2-29}$$

The rest of the equations used in the model describe basically the mass and energy balances around the different options. Some other equations are used to calculate the heat exchanger areas, inlet and outlet temperatures at certain operations. The restrictions are also included which will limit the inclusion of some equipment at the first or last level. The objective function minimises capital and operating costs. In the retrofit scenario, only the costs for extra heat exchangers and drums are included in the capital costs, meanwhile in the synthesis case, the costs of compressors are added. The operating costs include the hot and cold utility costs and electricity consumption for compressors.

2.4.2 Disjunctive programming modelling

With the base configuration obtained from the first shaftwork targeting phase, new design options are considered on top of the base structure. The combination of new design options (shown as dotted lines) and the base structure (shown as solid lines) forms a refrigeration system superstructure (Figure 2-13).

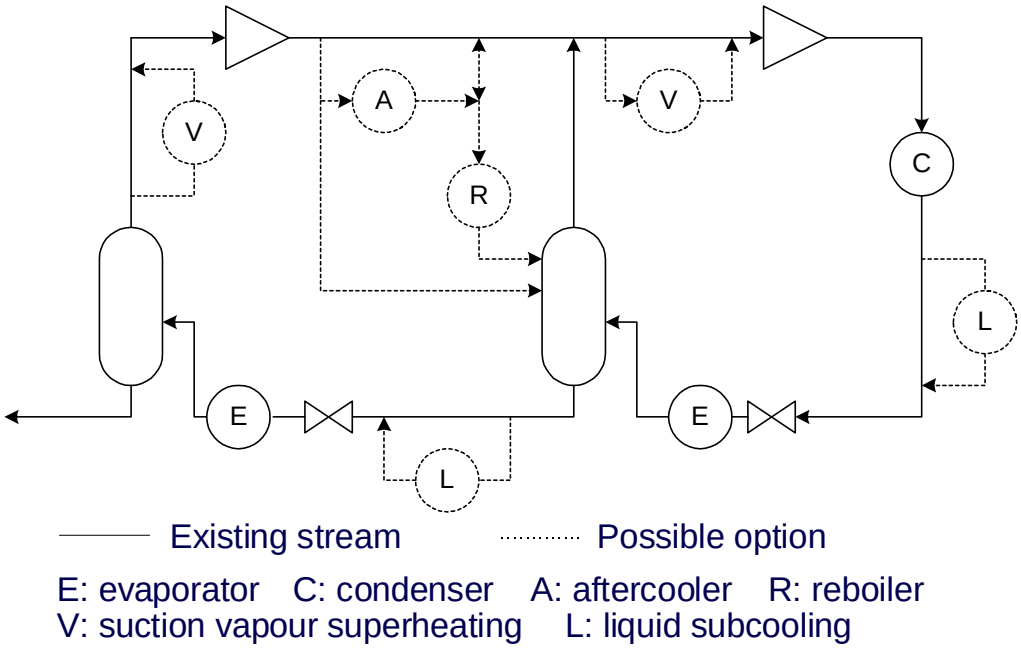

Figure 2-13. Extended refrigeration cycle superstructure.

2.4.2.1 DP modelling of V-L heat exchangers

When using a V-L heat exchanger, the refrigerant vapour after evaporation exchanges heat with the incoming saturated refrigerant liquid. Therefore the vapour is superheated before compression and the liquid is subcooled before expansion. In this way, the amount of remaining refrigerant liquid after expansion is increased at the expense of increasing shaftwork consumption per unit refrigerant flow. The overall effect, as a result, is a trade-off. Figure 2-14 shows the situation when an V-L heat exchanger is placed in the k^{th} level of a refrigeration cycle.

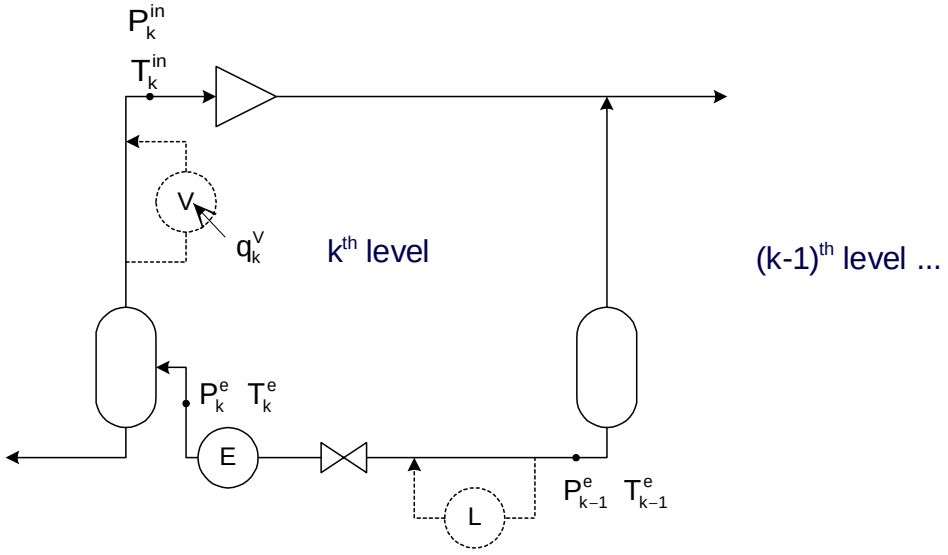

Figure 2-14. A V-L heat exchanger in the kth level.

Disjunctive programming is applied to describe the existence of an V-L heat exchanger in the kth level:

$$\begin{bmatrix} y_k^V \\ y_k^L + y_{k-1}^L + .. + y_1^L = 1 \\ P_k^{in} = P_k^e - \Delta P \\ T_k^{in} = T_k^e + \dfrac{q_k^V}{\dot{m} \cdot Cp} \\ T_k^{in} \le \sum_{i=k-1}^{1} y_i^L T_i^e - \Delta T \end{bmatrix} \vee \begin{bmatrix} \neg y_k^V \\ P_k^{in} = P_k^e \\ T_k^{in} = T_k^e \end{bmatrix} \qquad (2\text{-}30)$$

y_k^V and $\neg y_k^V$ denote the existence and non-existence of a vapour heat exchanger at the compressor's suction vapour line, respectively. When a vapour heat exchanger is placed, there must exists a liquid heat exchanger so that the energy balance is satisfied. Any liquid heat exchanger with saturated temperature higher than or equal to T_{k-1}^e is possible, but only one is needed. This condition is described by the first constraint of the left-hand side. The second and third constraints calculate the pressure drop through the vapour heat exchanger and the temperature of the compressor's suction vapour. The

forth constraint guarantees the validity of heat transfer processes. On the other hand, if the vapour heat exchanger is not placed, the conditions of compressor's inlet stream is simply set to equal to evaporator's outlet conditions. Figure 2-21 summarises the explanations of the DP formulation.

The DP modelling is then transformed into mathematical programming using "Big-M" transformation:

$$
\begin{aligned}
&\left(y_k^L + y_{k-1}^L + .. + y_1^L\right) + M\left(1 - y_k^V\right) \geq 1 \\
&\left(y_k^L + y_{k-1}^L + .. + y_1^L\right) - M\left(1 - y_k^V\right) \leq 1 \\
&P_k^{in} = P_k^e - \Delta P \cdot y_k^V \\
&T_k^{in} = T_k^e + \frac{q_k^V}{\dot{m} \cdot Cp} \cdot y_k^V \\
&T_k^{in} \leq \sum_{i=k-1}^{1} y_i^L T_i^e - \Delta T + M\left(1 - y_k^V\right)
\end{aligned}
\tag{2-31}
$$

It cab been seen that disjunctive programming is applied to model V-L heat exchangers and conventional mathematical programming for modelling pressure drop and temperature approach constraint. In this way, two different programming methods are combined nicely.

2.4.2.2 DP modelling of aftercooler

An aftercooler is considered when there is suitable external heat sink, such as air, cooling water or cold utilities. The placement of an aftercooler in the k^{th} level of a refrigeration cycle is shown in Figure 2-15.

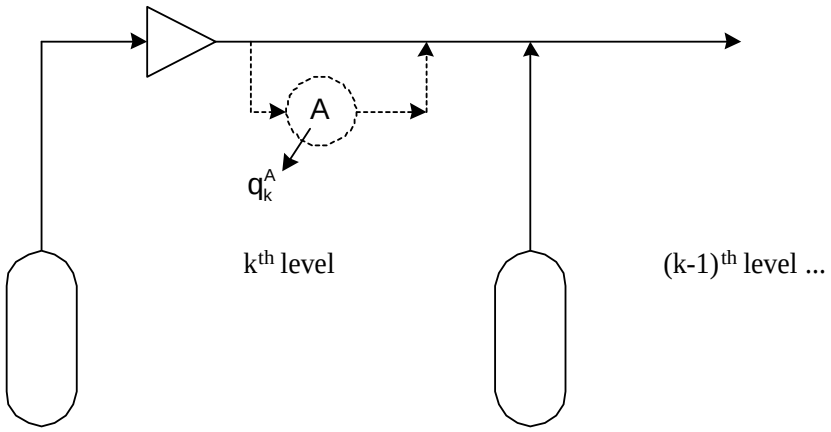

Figure 2-15. The placement of an aftercooler in the k^{th} level.

The DP formulation of the placement of an aftercooler is as follows:

$$\begin{bmatrix} y_k^A \\ P_k^{out,A} = P_k^{out} + \Delta P \\ T_k^{out,A} = T_k^{out} - \dfrac{q_k^A}{\dot{m} \cdot Cp} \\ T_k^{out,A} \geq T^{amb} + \Delta T \end{bmatrix} \vee \left[\neg y_k^A\right] \tag{2-32}$$

In the above logic expression, y_k^A and $\neg y_k^A$ denotes the existence and non-existence of an aftercooler in the k^{th} level, respectively. When an aftercooler is placed, the compressor's outlet pressure has to be increased by ΔP to compensate for the loss of pressure head. The decrease of temperature after the aftercooler is calculated by the second constraint. The third constraint guarantees the validity of the heat transfer process. On the other hand, if there is no aftercooler being placed, nothing needs to be done. The above logic expression is transformed into mathematical formulation by Big-M transformation:

$$\begin{aligned} & P_k^{out,A} = P_k^{out} + \Delta P \cdot y_k^A \\ & T_k^{out,A} = T_k^{out} - \frac{q_k^A}{\dot{m} \cdot Cp} y_k^A \\ & T_k^{out,A} + M\left(1 - y_k^A\right) \geq T^{amb} + \Delta T \end{aligned} \tag{2-33}$$

The increase in compressor outlet pressure and the decrease in temperature are described by conventional modelling, while the temperature approach constraint by the Big-M transformation.

2.4.2.3 DP modelling of reboiler

A reboiler is considered when there are suitable process streams, usually being shown as a "pocket" on the GCC. The placement of a reboiler in the k^{th} level is shown in Figure 2-16.

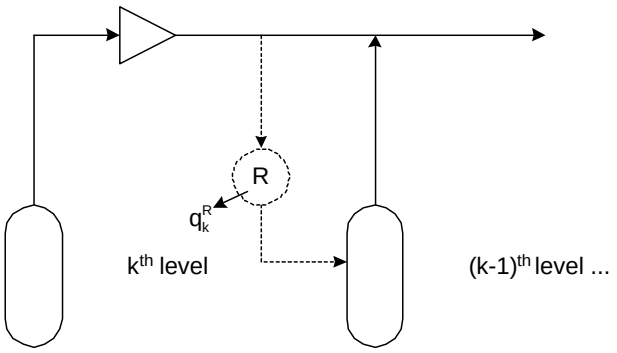

Figure 2-16. The placement of a reboiler in the k^{th} level.

The DP formulation of the placement of a reboiler is as follows:

$$\begin{bmatrix} y_k^R \\ \dot{m}_k^R = \dfrac{q_k^R}{\tilde{h}^{cond}} \\ T_k^R = T_{k-1}^e \end{bmatrix} \vee \begin{bmatrix} \neg y_k^R \\ \dot{m}_k^R = 0 \end{bmatrix} \tag{2-34}$$

Since compressor's outlet is superheated, heat rejection includes both superheat part and latent heat part. So, the definition of the effective heat of condensation ($\tilde{h}^{cond}$) is:

$$\tilde{h}^{cond} = superheat\ change + latent\ heat\ change \tag{2-35}$$

Figure 2-17 illustrates the definition schematically.

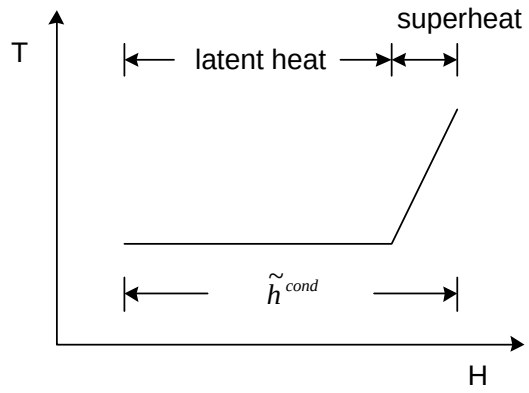

Figure 2-17. The definition of the effective heat of condensation.

When a reboiler is placed, the first constraint in equation (2-54) calculates the amount of refrigerant flow that can be accepted by the reboiler according to the available duty of heat sinks. The second constraint sets the temperature of the reboiler's outlet stream equal to the saturated temperature. If there is no reboiler placed, simply let the refrigerant flow through the reboiler be zero.

When the above logic expression being transformed into mathematical formulation, it becomes:

$$\begin{aligned} \dot{m}_k^R &= \frac{q_k^R}{\tilde{h}^{cond}} \cdot y_k^R \\ T_k^R &\le T_{k-1}^e + M(1 - y_k^R) \\ T_k^R &\ge T_{k-1}^e - M(1 - y_k^R) \end{aligned} \tag{2-36}$$

2.4.2.4 DP modelling of presaturator and economiser

When an economiser is installed, the condensed refrigerant is flashed to an intermediate pressure, where the flash vapour is returned to the suction of the compressor.

Theoretically, an economiser can be simulated as a refrigeration level with zero evaporator duty. When a presaturator is placed, the compressed refrigerant vapour is presaturated in the flash vessel with the expense of evaporating part of the refrigerant liquid from the previous level. The dotted line in Figure 2-18 represents a presaturator option.

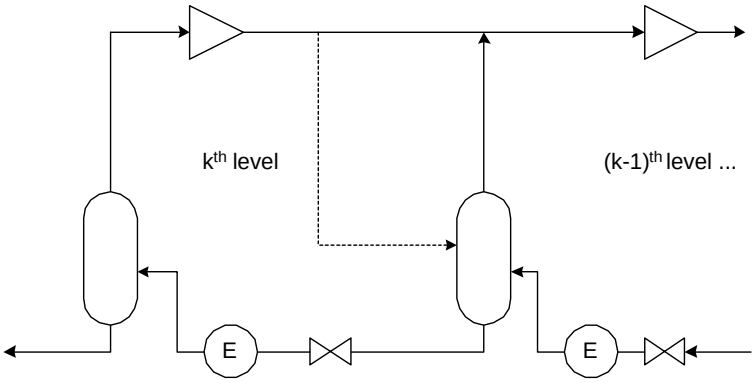

Figure 2-18. A presaturator option represented as the dotted line.

The major difference between a presaturator and an economizer is that, an economizer always reduces the overall shaftwork consumption with extra capital costs, but a presaturator, also with extra capital costs, does not always help reduce shaftwork consumption. The reason to discuss the two options together is that they can not co-exist simultaneously in the same stage.

For installing a presaturator, the DP model is:

$$\begin{bmatrix} y_k^P \\ \dot{m}_{k-1}^{cin,P} = \dot{m}_{k-1}^{cin} + \dfrac{\dot{m}_k^{cout} \cdot Cp \cdot \left(T_k^{cout} - T_{k-1}^{e}\right)}{h_{k-1}^{vap}} \end{bmatrix} \vee \left[\neg y_k^P\right] \tag{2-37}$$

For installing an economizer, the DP model is:

$$\begin{bmatrix} y_k^C \\ q_k^E = 0 \end{bmatrix} \vee \left[\neg y_k^C\right] \tag{2-38}$$

Since a presaturator and an economiser are not possible to co-exist in the same level, the following constraint is therefore required:

$$y_k^P + y_k^C \le 1 \tag{2-39}$$

The complete mathematical formulations that describe the selection of the two options can be expressed as:

$$\begin{aligned} &\dot{m}_{k-1}^{cin,P} = \dot{m}_{k-1}^{cin} + \frac{\dot{m}_k^{cout} \cdot Cp \cdot \left(T_k^{cout} - T_{k-1}^{e}\right)}{h_{k-1}^{vap}} \cdot y_k^P \\ &q_k^E \le M\left(1 - y_k^C\right) \\ &q_k^E \ge -M\left(1 - y_k^C\right) \\ &y_k^P + y_k^C \le 1 \end{aligned} \tag{2-40}$$

2.5 Synthesis of cascade refrigeration systems

Usually when processes demand refrigeration over a very wide temperature range, cascade refrigeration systems are employed. These systems are economically significant in key processes such as ethylene cold-end process, natural gas liquefaction, and in numerous other chemical processes. The study of cascade refrigeration systems is therefore of high economic interests and importance. In this section, a new method for the design of cascade refrigeration systems and the optimal tuning of partition temperatures will be proposed.

A cascade system comprises several cycles, and each cycle employs a different refrigerant. Condensing heat from a lower cycle is mechanically upgraded and rejected to an upper cycle. Since a vapour stream from a compressor is superheated, the rejection involves transferring of both superheat and latent heat. In real cascade refrigeration systems, the superheated compressor outlet vapour is cooled and condensed in several steps:

- If the outlet temperature is higher than ambient, the superheated vapour is usually first partially desuperheated by external heat sinks such as air or cooling water.
- The vapour might be further desuperheated by suitable process streams (e.g. a column reboiler or a side-reboiler).
- The vapour is totally condensed by using an upper cycle as a heat sink. If the upper cycle has several evaporation levels, the refrigeration is usually distributed among each level.

Partition temperature (Figure 2-19) is the temperature that separates each cycle, and is equal to the lowest evaporating temperature level of the upper cycle. Adjacent temperature levels are the two neighbouring evaporating temperature levels of the upper cycle and lower cycle. Partition temperature is an important factor affecting the shaftwork requirement of the whole cascade system. Wu *et al.* (2000) uses the incremental COP ratio to determine the position of partition temperature. The incremental COP ratio is the ratio of the incremental COP of the refrigerant in the upper cycle to the incremental COP of the refrigerant in the lower cycle. However, we found the incremental COP ratio approach cannot reflect the actual situations in real designs. The partition temperature is affected not only by the energy consuming nature of refrigerants used, but also by the refrigeration duties of the upper and lower cycles. An example is: in a propylene-ethylene cascade refrigeration system for ethylene recovery plants, usually the total refrigeration duty of propylene cycle is much larger than that of ethylene cycle. Although propylene is a more efficient (i.e. has higher incremental COP) than ethylene, the optimal partition temperature is sometimes found to be close to the first evaporation level of propylene cycle instead of the last evaporation level of ethylene cycle. Using Wu's approach, the prediction would be the later.

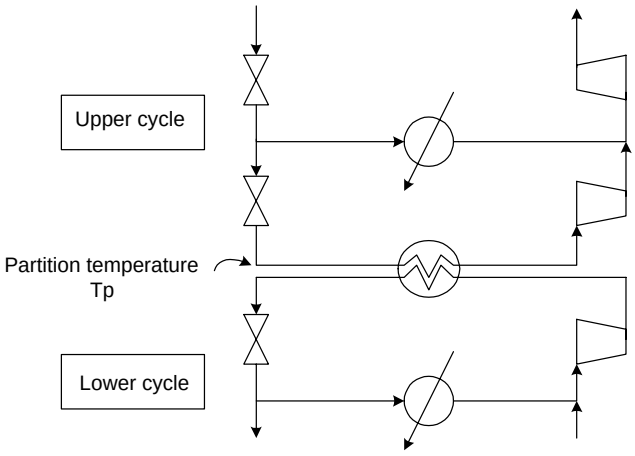

Figure 2-19. Partition temperature, Tp.

We can draw the shaftwork vs. partition temperature change curves for the upper cycle and lower cycle respectively, and use these two curves to determine the optimal position of partition temperature. As seen in Figure 2-10, the shaftwork consumptions of the upper cycle and the lower cycle change according to different partition temperatures. A lower partition temperature would reduce the shaftwork of the lower cycle but increase that of the upper cycle. Consequently, the overall shaftwork consumption curve exhibits as a convex function from which an optimal partition temperature can be identified.

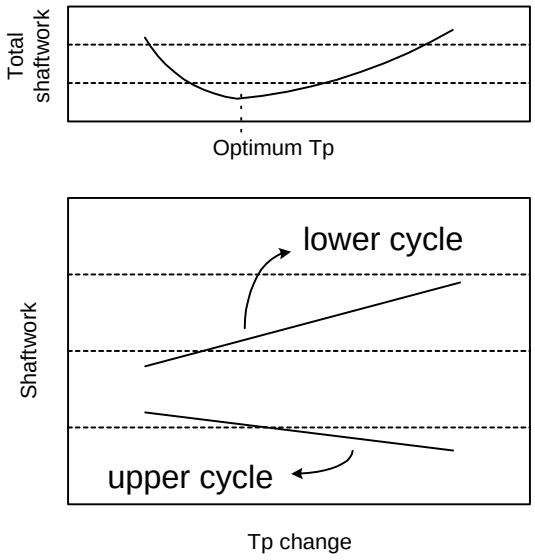

Figure 2-20. The effect of partition temperature on the total shaftwork requirement.

The proposed method for synthesis of cascade refrigeration systems is illustrated in Figure 2-21. The overall procedures have to start from the lower cycle to the upper cycle. The reason is that the design of a lower cycle can be done without the consideration of a coupled upper cycle. However, the design of an upper cycle has to include the heat rejection from a lower cycle.

The design procedure of cascade refrigeration systems starts with an initial partition temperature that splits the process cooling demands into upper part and lower part. It first does the design of the lowest part of the refrigeration load. The two-phase method introduced in previous sections is employed to determine the optimal configurations for the lower refrigeration cycle.

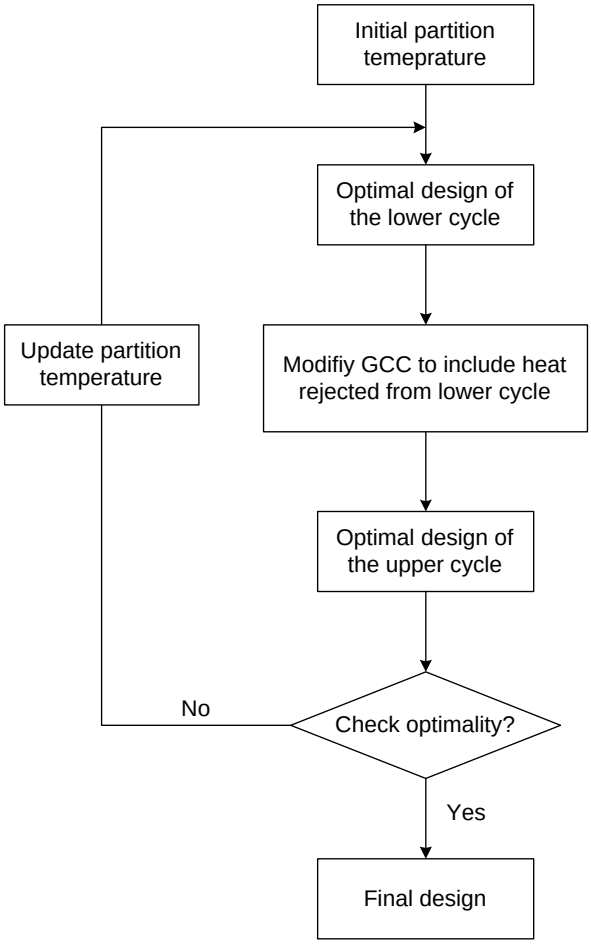

Figure 2-21. The synthesis of cascade refrigeration systems.

Then the GCC is modified to include the heat rejection streams from the lower cycle. The procedure is shown in Figure 2-22.

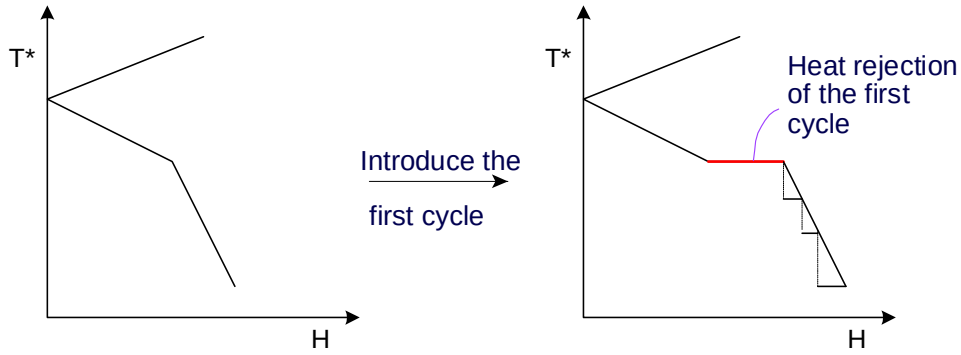

Figure 2-22. Design of the lower refrigeration cycle and the modification of the GCC.

The modified GCC combines with the shaftwork targeting method to determine the design of the upper cycle, as Figure 2-23 illustrates. In this way, the design of each cycle for the cascade refrigeration system is always the same as the design of a multistage refrigeration system.

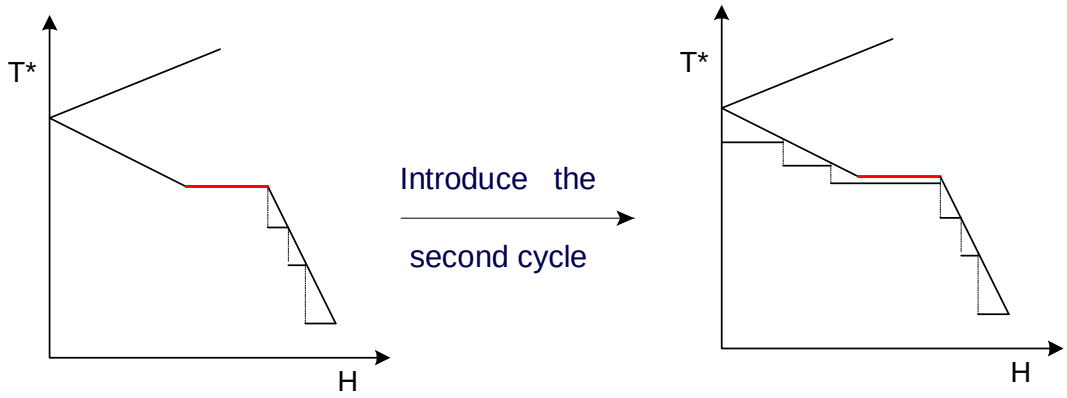

Figure 2-23. Design of the upper cycle by using the modified GCC.

Since a cascade refrigeration system uses several different refrigerants in different cycles, the suitable operating temperature ranges for each refrigerant have to be included into the optimisation model:

$$T_i^U \le Evap\_T_{ij} \le T_i^L$$

$$T_i^U \le Cond\_T_{ij} \le T_i^L \qquad i \in \{1..N\},\ j \in \{1..J\} \tag{2-41}$$

The subscript *i* means the number of refrigerant types, and *j* indicates the cycle in which the refrigerant is used. T_i^U and T_i^L denotes the upper bound and the lower bound of refrigerant *I*, respectively. By including these two constraints, the partition temperature is guaranteed to be within the operating temperature range of the refrigerant which the upper cycle employs.

2.6 Discussions

Although pure mathematical programming approaches acquires a lot of interests recently and many successful applications have been reported, they require extensive computation time, especially when applies to large-sized problems, and often difficult to manipulate and maintain. They are usually very sensitive to the initial conditions, thus consumes considerable trial-and-error time in initialisation. Often only well-trained "experts" can operate and maintain their usages well. On the other hand, pinch technology approach is more favoured by industries. However, it can tell only "guidelines" instead of detailed designs. Its applications therefore are usually confined in the conceptual design stage.

The significance of the proposed approach is that it combines the power of mathematical programming and the GCC in a systematic way. The overall procedures are initiated by shaftwork targeting method in the first phase. Shaftwork targeting method optimises only major design parameters and the integration with processes. As a result, the optimal solutions are converged fast. The optimal results are then treated as the initial conditions for the MINLP model in the second phase. Unlike in conventional superstructure approaches, the second phase of the proposed method starts with near

optimal conditions obtained from the first phase. The reduced superstructure used in the second phase contains only design options but no discretised temperature intervals. The solution time therefore is greatly minimised. The results from the first phase also play another important role in the overall procedures: any design option found beneficial in the second phase should help reduce shaftwork consumption concluded from the first phase. That is to say, the optimal results from shaftwork targeting method set the upper bound of the final optimal designs.

Another important distinction of the proposed method is the practicality for industrial applications. Conventional MINLP model require extensive solution time and experts to operate and maintain. Even a feasible solution is reached, it is hard to guarantee the optimality. On the contrary, the proposed method is easy to apply and is almost independent of the problem size. No matter how complex a problem is, the method summaries it by using the GCC. Only shaftwork targeting method in the first phase deals with the GCC, the second phase is virtually “blind” to the complexity of the processes and concerns only design options for improvement. Table 2-4 summaries the comparison.

Table 2-4. Comparison between conventional MINLP and the proposed method.

	Previous pure mathematical programming	New Method
Initial conditions	Trial-and-error ??hours	Shaftwork targeting <10 sec
Design options	MINLP	MINLP (smaller problem size)
Final solution	Optimality ?	Simpler design Lower shaftwork Greater confidence
Total solution time	Depends on luck. Uncontrollable.	Usually < 10 min
Applicability to industry-sized problems	Difficult. Needs experts and specific softwares.	Easy. Almost independent of the problem size.

2.7 Conclusions

A new approach for the synthesis and retrofit of refrigeration systems has been proposed in this chapter. It combines the advantages of two different methods to produce optimal designs. The shaftwork targeting method is used as the first phase. The method is simple to understand and doesn't require a lot of manipulation for the process data. The result is obtained swiftly and it is used as the basic configuration for the second phase. It provides the number of levels, the temperatures, shaftwork consumption and evaporators and condenser duties.

The second phase can be used as a fine-tuning phase for the basic configuration obtained in the shaftwork estimation, or it can be used as a retrofit tool. The approach is given by the disjunctive-programming-enhanced MINLP model, which includes

different design options to improve the performance and cost of the cycle. The logic based modelling approach is found to be robust and flexible. The pressure drop effect can also be considered in this phase. It greatly helps make design or retrofit tasks more realistic.

Consequently, an optimal design is achieved in much shorter time than using any of the previous methods. This reduction mainly comes from two aspects. First, the shaftwork targeting method in the first phase generates basic configurations in seconds with arbitrary initial conditions. Unlike conventional MINLP approach, no time is wasted in the trial-and-error search of proper initial conditions. The base configurations obtained in the first phase are usually near-optimal. Second, the MINLP model in the second phase deals with a smaller superstructure, as only design options need to be considered.

Nomenclature

Parameters and variables

cf : Annulisation factor.

c^{el} : Electricity cost.

c^{comp} : Compressor cost.

c^{HEN} : Capital cost of a HEN.

Cp : Heat capacity of ideal gas.

h : Specific enthalpy.

h^{L} : Liquid enthalpy.

h^{V} : Vapour enthalpy.

h^{*} : Specific enthalpy of ideal gas.

$\tilde{h}^{cond}$: The effective heat of condensation.

H^{vap} : Latent heat of vaporisation.

k : The polytropic exponent.

L : Liquid flow rate.

$\dot{m}_k^{cin}$: The compressor inlet flow rate in the kth level.

$\dot{m}_k^{cin,P}$: The compressor inlet flow rate with the existence of a presaturator in the kth level.

$\dot{m}_k^{cout}$: The compressor outlet flow rate in the kth level.

$\dot{m}_k^{R}$: The refrigerant flow rate in a reboiler of the kth level.

M : An arbitrary large number used in Big-M transformation.

P : Pressure.

P_C : Critical pressure of a substance.

P_k^e : Evaporation pressure of the kth level.

P_k^{in} : Inlet pressure of the kth compressor.

$P_k^{out,A}$: The outlet pressure of an aftercooler in the kth level.

P^{vap} : Saturated vapour pressure.

q_k^A : The amount of heat transferred into an aftercooler in the kth level.

q_k^R : The amount of heat transferred into a reboiler in the kth level.

q_k^V : The amount of heat transferred into a V heat exchanger in the kth level.

Q : The amount of heat transfer.

Q_{evp} : Duty of an evaporator.

R : Universal gas constant.

T : Temperature.

T_a : Compressor outlet temperature in a simple cycle.

T_b : Condensing temperature in a simple cycle.

T_c : Evaporating temperature in a simple cycle.

T_C : Critical temperature of a substance.

T_{cond} : Condensation temperature.

T_a : Compressor outlet temperature.

T_b : Condensing temperature in a simple cycle.

T_d : Compressor inlet temperature, saturated vapour.

T_{out} : Compressor outlet temperature in a multistage cycle.

T_{mix} : Weight-averaged mixing temperature to a compressor's inlet.

T^{amb} : The ambient temperature.

T_k^e : Evaporation temperature of the kth level.

T_k^{in} : Inlet temperature of the kth compressor.

T^L : A vector containing the lower bounds of temperature variables.

$T_k^{out,A}$: The outlet temperature of an aftercooler in the kth level.

T_k^R : Reboiling temperature.

T^U : A vector containing the upper bounds of temperature variables.

T_P : The partition temperature.

V : Vapour flow rate.

v : Specific volume.

W : Work.

y_k^A : A binary variable denotes the existence of an aftercooler in the kth level.

y_k^C : A binary variable denotes the existence of an economiser in the kth level.

y_k^P : A binary variable denotes the existence of a presaturator in the kth level.

y_k^R : A binary variable denotes the existence of a reboiler in the kth level.

y_k^V : A binary variable denotes the existence of a V heat exchanger in the kth level.

Z : Compressibility.

Greek letters

ξ : Continuous variables.

ς : Integer variables.

η_p : Polytropic efficiency.

ω : Acentric factor.

Ω : Logic relations in a disjunctive programming model.

Reference

Balas, E., 1974, Disjunctive Programming: Properties of the Convex Hull of Feasible Points, MSRR #348. Carnegie Mellon University, Pittsburgh, PA.

Balas, E., 1985, Disjunctive Programming and a Hierarchy of Relaxations for Discrete Optimization Problems, *SIAM J. Alg. Disc. Meth*., **6**, 466-486.

Lee G. C., Zhu X. X., Smith R., 2000, "Synthesis of Refrigeration Systems by Shaftwork Targeting and Mathematical Optimisation", *ESCAPE-10*, Florence, Italy, May 2000.

Linnhoff, B., Dhole, V. R., 1989, Shaftwork Targeting for Subambient Plants, *AIChE Spring Meeting*, Houston, April, 1989.

Raman, R., Grossmann, I. E., 1994, Modelling and Computational Techniques for Logic Based Integer Programming, *Computers chem.. Engng*., **18 (7)**, 563-578.

Sinnott, R. K., 1996, *Coulson & Richardson's Chemical Engineering*, Volume 6, Butterworth-Heinemann.

Vecchietti, A., Grossmann, I. E., 1999, LOGMIP: a Disjunctive 0-1 Non-linear Optimizer for Process System Models, *Computers chem. Engng*., **23**, 55-565.

Wu, G. D., Zhu, X. X., 2000, Design and retrofit of Integrated refrigeration Systems, *PhD Thesis*, UMIST, Manchester, UK.

3 CASE STUDIES

3.1 Introduction

A new method for the synthesis of complex refrigeration systems is proposed in previous chapter. This chapter will show the applications of the new method on two case studies. The first case study demonstrates the combination of this synthesis method for refrigeration systems with heat exchanger network (HEN) design method. By using shaftwork targeting method to achieve minimal cost design, optimal number of levels and temperature and duty of each level can be determined. The second case study shows the practicality of the proposed method on industrial applications. An ethylene-propylene cascade refrigeration system is designed for an ethylene cold-end process. Results will be compared with Wu's (2000).

3.2 Case study I – Optimal design of refrigeration system and HEN

The proposed design method for synthesis of refrigeration systems can actually combine with conventional HEN design methods. The integrate solution treats evaporation levels in refrigeration systems as cold streams and heat rejection streams as hot streams. By including them into problem table, a complete HEN for the integration of refrigeration systems and processes can be obtained. The benefit is that since the HEN design methods have been well developed, the design of refrigeration systems can be treated as a front-end stage and easily combined with HEN design.

Table 3-1 shows four process streams. ΔT_{min} is $5^{o}C$. The task is to design a refrigeration system using ammonia as refrigerant to satisfy cooling demand from the process.

Table 3-1. Process stream data for case study I.

	Ts (C)	Tt (C)	DH (kW)	CP (kW/C)
H1	20.0	-50.0	350.0	5.0
H2	25.0	5.0	20.0	1.0
C1	-25.0	0.0	75.0	3.0
C2	10.0	30.0	200.0	10.0

In the first phase, the shaftwork targeting method uses the GCC constructed from the four process stream data to optimise major parameters. The same cost estimation equations as in 2.2.2 Case Study are used. Figure 3-1 shows the targeting results for different number of levels. For operating cost, the benefits of adding more number of levels diminish very quickly. On the other hand, the compressor cost increases as more number of levels and machines are installed, and it offsets the operating cost saving when the number of levels exceeds three. As a result, a two-stage refrigeration system is found to be optimal in terms of overall costs.

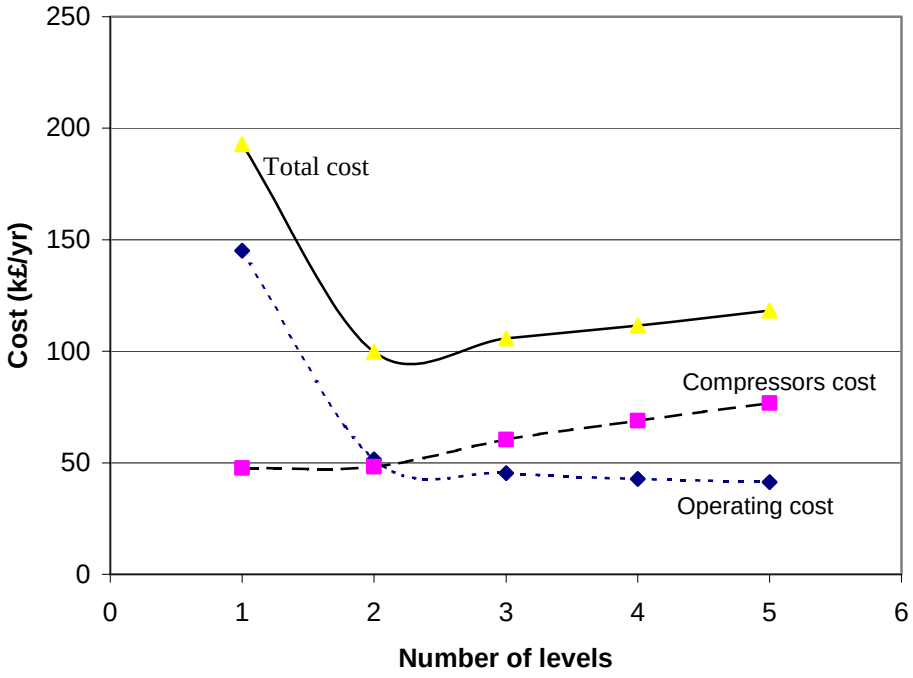

Figure 3-1. Number of levels vs. costs.

A summary of the design results is shown in Table 3-2. It consumes totally 153.24 kW in compressors' shaftwork, and the overall COP as 1.7.

Table 3-2. Design results of the three-stage ammonia refrigeration system.

No. of level	Temperature (^{o}C)	Duty (kW)	Shaftwork (kW)	Comp. Outlet (^{o}C)	Comp. Cost (k£)	Ref. flowrate (kg/hr)
1	-52.50	130.19	21.93	58.89	167.97	355.57
2	-26.46	129.81	131.31	257.71	314.25	889.50

Figure 3-2 shows the balanced grand composite curve of the results. Three evaporation levels are plot against the GCC. Heat rejection comprises two parts: superheat and latent heat. The superheat of the compressor's outlet vapour is rejected to the process itself. Part of latent heat of condensation is rejected to the process, and part to ambient air at 25 ^{o}C. It is easy to see the advantages of the proposed method are that the design procedures are systematic and results are presented clearly and concisely.

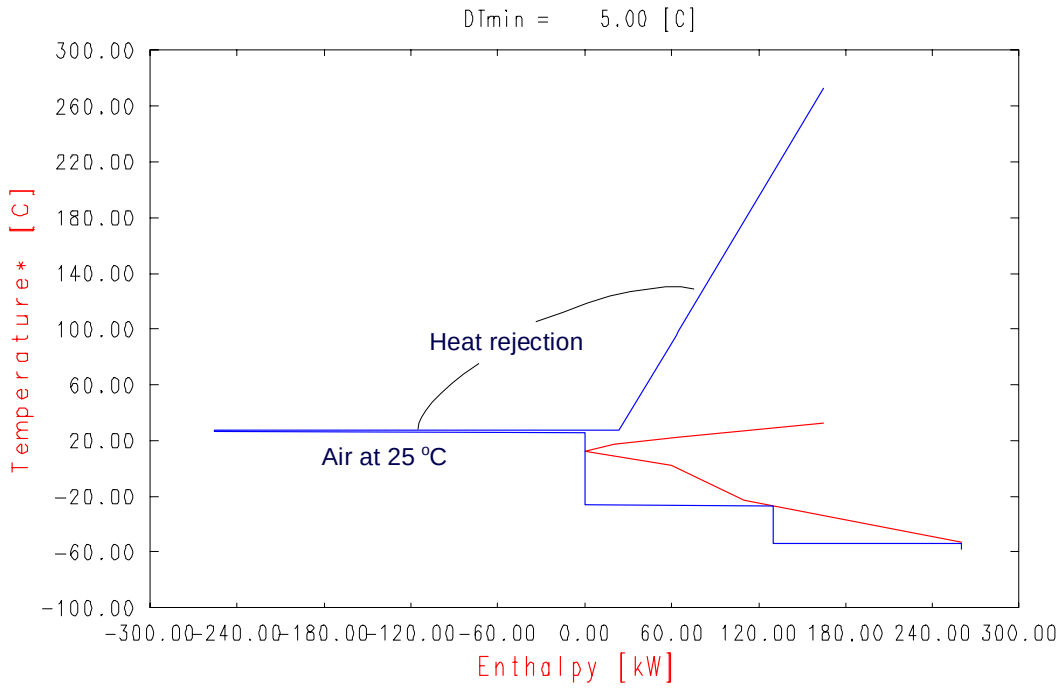

Figure 3-2. Balanced GCC of the final design.

In the second phase, the design results from the first phase are used as initial conditions for MINLP optimisation. A superstructure is constructed to include all possible design options, such as aftercooler, economiser or V-L heat exchanger. The results from the second phase, as shown in Figure 3-3, suggest that an aftercooler which removes superheat from the first level compressor outlet vapour can reduce overall shaftwork to 146.1 kW while incurs minimal extra capital investments.

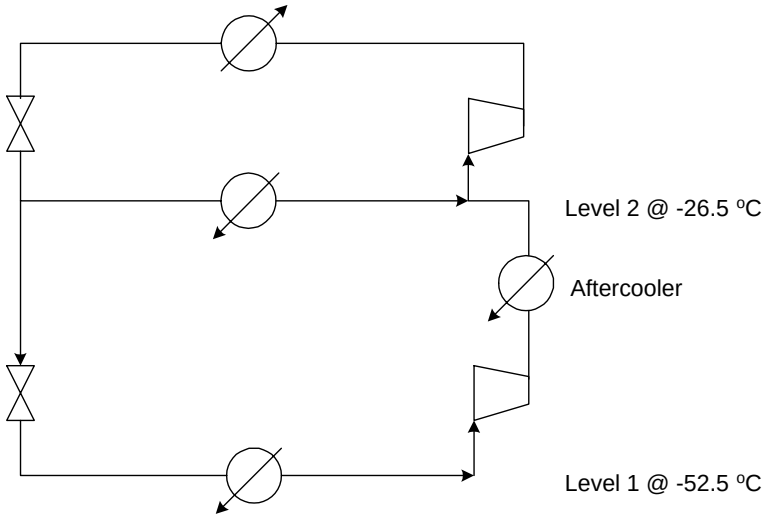

Figure 3-3. Configuration of the refrigeration system.

Completing the design of the refrigeration system, the procedures migrate to the design of HEN. A problem table is constructed to include evaporation levels as cold streams and heat rejection as hot streams. Table 3-3 shows the modified problem table.

Table 3-3. The modified problem table.

	Ts (C)	Tt (C)	DH (kW)	CP (kW/C)
H1	20.0	-50.0	350.0	5.0
H2	25.0	5.0	20.0	1.0
C1	-25.0	0.0	75.0	3.0
C2	10.0	30.0	200.0	10.0
Ref level 1	-52.5	-52.0	130.2	260.4
Ref level 2	-26.5	-26.0	129.8	259.6
Superheat	275.5	31.0	151.2	0.6
Condensing	30.5	30.0	262.0	524.1

The design of the HEN is done by SPRINT (DPI, UMIST, 2000). Figure 3-4 shows the complete configuration of the HEN. The refrigeration absorbs heat from H1 and H2, and H1 and H2 also exchange heat with C1 and C2. The superheat of compressor outlet is rejected to C2. Part of condensing latent heat is rejected to C2, and part is absorbed by ambient air. It can be seen that the final design of HEN thoroughly agrees with what the balanced GCC (Figure 3-2).

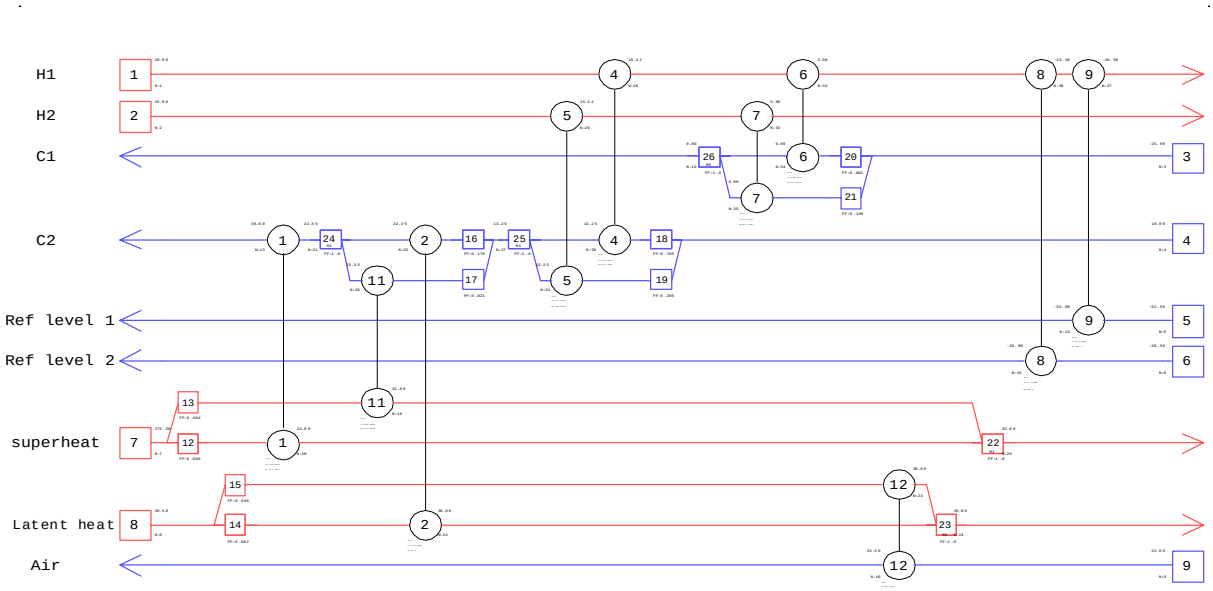

Figure 3-4. The final design of HEN comprising of process streams and the refrigeration system.

This case study demonstrates the combined use of the proposed method for refrigeration systems and conventional HEN design method. The overall procedures are systematic and clearly presented by GCC. By modifying the problem table to include streams from the designed refrigeration systems, conventional HEN design methods are able to generate complete solutions giving the necessary information such as number of heat exchangers, position and duty of each heat exchanger and the overall costs of the HEN.

3.3 Case Study II – An ethylene cold-end process

In this case study, the interest focuses on the ethylene cold-end process. An ethylene recovery plant comprises of several parts: the hot-end utilities, the raw gas compression train, the gas separation system, and the cold-end utilities. In the cold-end utilities, a refrigeration system interacts with the process through the HEN and cold box. Figure 3-5 illustrates the ethylene recovery plant diagrammatically.

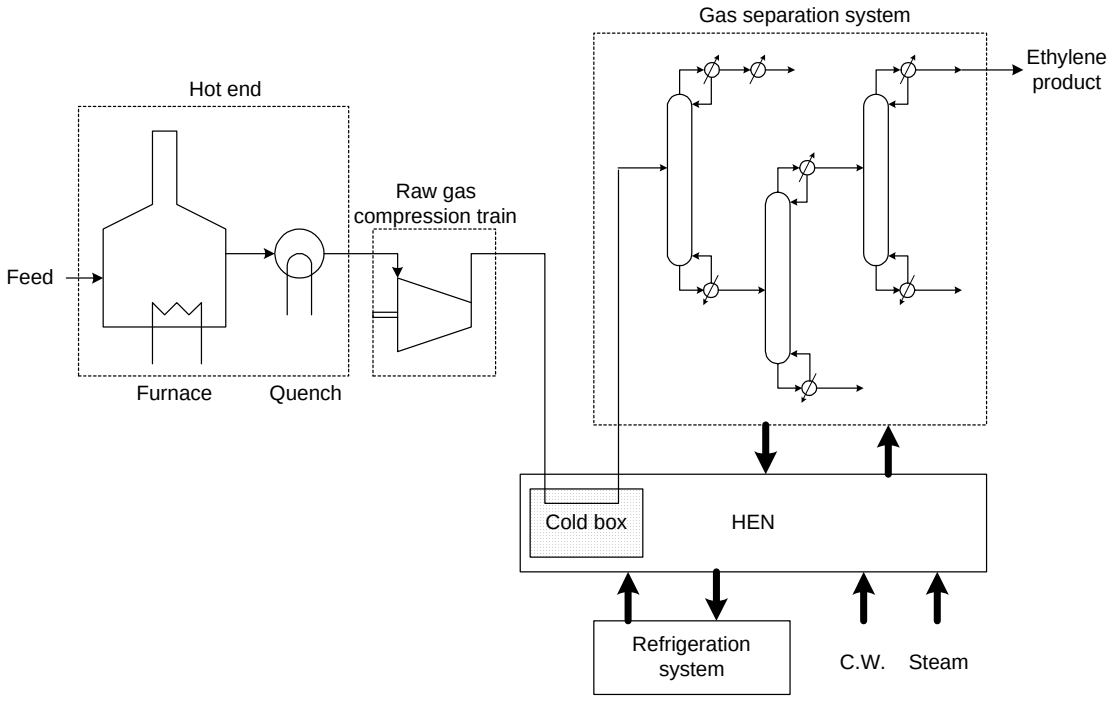

Figure 3-5. An ethylene recovery plant.

Results from the case study will be compared with that in Wu's work (2000), in which a synthesis of an ethylene-propylene cascade system based on a pure MINLP model was proposed.

3.3.1 Basis for the case study

The first step of the proposed method is the construction of the GCC from process stream data. The relevant streams to be included in the process, along with their supply and target temperatures, enthalpy changes and overall heat transfer coefficients are shown in Table 3-4.

Table 3-4. Temperatures, enthalpy changes and overall heat transfer coefficients for base case streams.

ID	Stream	TS (°C)	TT (°C)	ΔH (MW)	U (kW/m^2°C)
HS1	Deethaniser condenser	-14	-15	-3.780	0.300
HS2	Ethylene condenser	-22	-23	-15.911	0.300
HS3	Process gas	27	-98	-18.985	0.300
HS4	Demethaniser condenser	-96	-98	-1.568	0.300
CS1	Naphtha feed	23	78	7.296	0.300
CS2	Demethaniser reboiler	7	8	3.634	0.300
CS3	Ethylene reboiler	-1	0	14.651	0.300
CS4	Ethylene product	-27	23	6.373	0.300
CS5	Tail gas and hydrogen	-100	-18	2.870	0.100
CS6	Ethane recycle	-27	23	0.185	0.300

The Grand Composite Curve (GCC) for the previous data is shown in Figure 3-6.

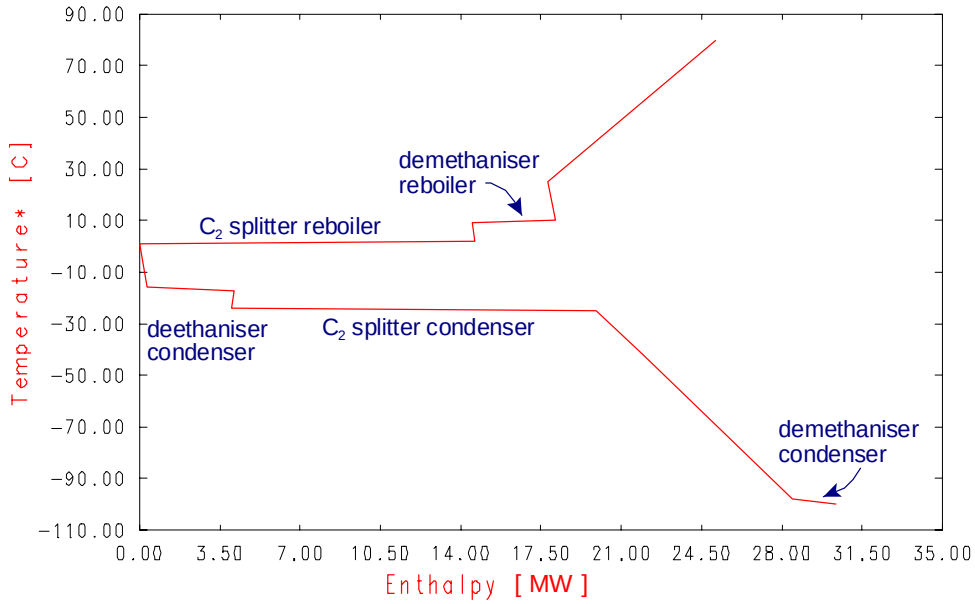

Figure 3-6. Grand Composite Curve (ΔT_{min}=5°C)

The data for the utilities, capital costs and equipment performances is shown in Table 3-5. For comparison purpose, the same cost estimation equations as in Wu's work (2000) are employed here.

Table 3-5. Utilities, capital costs and equipment performances.

Utilities	**TS**	**TT**	**Cost (MM$/MW/yr)**
Cooling water (CW)	23°C	33°C	0.015
Quench water (QW)	82°C	72°C	0.027
Refrigeration at t	t °C	t °C	6.175× (33-t)
Shaftwork			0.300
Equipment	**Capital Costs (MM$/yr)**		
Single stage compressor	= 0.2197+0.3515×W		W: MW
Compressor driver	= 0.1152+0.0614×W		W: MW
Heat exchanger (I)	= 0.0740×A		A:1000m^2
Heat exchanger (II)	= 0.002064+0.0720×A		A:1000m^2
Flash drum	= 0.04		50m^3
Equipment Performance			
Mechanical efficiency	98%		For all drivers
Polytropic efficiency	80%		For all compressors

3.3.2 Pressure drop model

The configuration obtained in Wu's work for the ethylene cycle in which the pressure drop is not considered is shown in Figure 3-7 and Table 3-7.

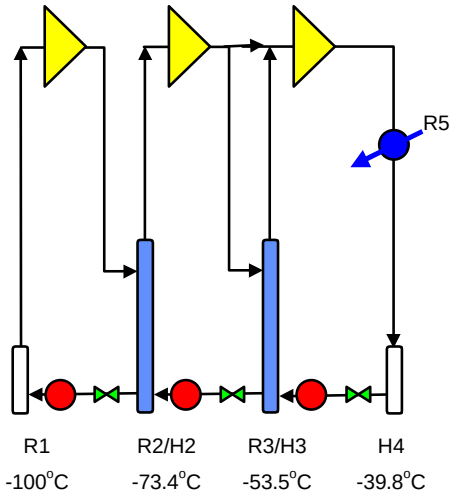

Figure 3-7. Wu's optimal ethylene cycle

Table 3-7. Wu's optimal results of the ethylene cycle

Utility costs	**Requirement**	**Costs**
Cold utility	9.169MW	4.360 MM$/yr
Shaftwork	3.113MW	0.934 MM$/yr
Capital costs	**Number / Size**	**Costs**
Compressor	One compressor with three stages	1.369MM$/yr
Driver	One steam turbine	0.306MM$/yr
Flash drum	2 flash drums	0.080MM$/yr
Heat exchanger	12.56×10^3 m^2, 5 matches related with the cycle	0.915MM$/yr

The operation costs are 5.294 MM$/yr, the capital costs are 2.670 MM$/yr and the total cost is 7.964 MM$/yr.

The new model can consider the pressure drop across some of the heat. The pressure drop values used for evaporator and condenser are in Table 3-8.

Table 3-8. Pressure drop values for heat exchangers

Heat Exchanger	Pressure Drop, kPa
Evaporator	15
Aftercooler	10

The results obtained with these values are shown in the configuration in Figure 3-9 and Table 3-9.

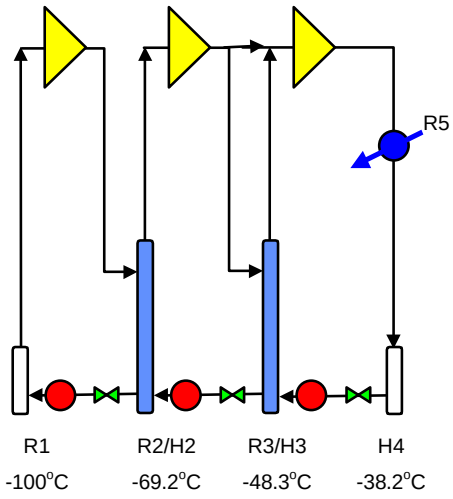

Figure 1-9. Optimal ethylene cycle with pressure drop included

Table 3-9. Optimal results of the ethylene cycle with pressure drop included

Utility costs	Requirement	Costs
Cold utility	9.408MW	4.473 MM$/yr
Shaftwork	3.462MW	1.039 MM$/yr
Capital costs	**Number / Size**	**Costs**
Compressor	One compressor with three stages	1.491MM$/yr

Driver	One steam turbine	0.328MM$/yr
Flash drum	2 flash drums	0.080MM$/yr
Heat exchanger	9.581×10^{3} m^2, 5 matches related with the cycle	0.733MM$/yr

The operation costs for this new design are 5.512 MM$/yr, the capital costs are 2.632 MM$/yr to get a total cost of 8.144 MM$/yr.

The compression ratio is one of the parameters which is more affected when the pressure drop calculation is included. It allows a better and more realistic compressor design. Table 3-10 shows the difference in compression ratio values between the original and the modified models.

Table 3-10. Compression ratio for the original and modified models

	Compression ratio	
Stage	**Original model**	**Modified model**
1	3.324	4.688
2	2.220	2.361
3	1.654	1.259

The value of compression ratio is increasing, as the pressure drop calculations are included. The increase is more noticeable in the lower levels where the compression ratio will be more sensitive to small changes.

In the case study, the pressure drops across heat exchangers are considered as constant parameters. However, more accurate estimations of pressure drops, such as in Hewitt *et al*. (1994), for heat exchangers can be used.

3.3.3 SYNTHESIS OF REFRIGERATION CYCLES

The refrigeration cycle to be synthesised in this chapter is the same as that in Wu's work. The data for the cycles has already been given before in this chapter.

The new synthesis method starts with building up the GCC from collected process stream data. The GCC is then fed into the shaftwork targeting method to generate the refrigeration system with an optimised number of stages, optimised temperature levels and loads of each stage. Table 3-11 summarises the shaftwork targeting results.

The results show a three-stage ethylene refrigeration cycle and a two-stage propylene cycle with one stage reboiling at 4 ^{o}C. The partition temperature is still –44 ^{o}C. Comparing to the base case, by shaftwork targeting we already achieve a lower shaftwork consumption. The result from shaftwork targeting is then used as an initial condition for the following MINLP optimisation to generate a complete structure.

Table 3-11. Shaftwork targeting results.

Ethylene refrigeration system			
No. of levels	Temperature (^{o}C)	Duty (MW)	Shaftwork (MW)
1	-100	3.52	0.52
2	-82.5	2.39	1.06
3	-60	2.80	1.73
Total			3.31

Propylene refrigeration system			
No. of levels	Temperature (^{o}C)	Duty (MW)	Shaftwork (MW)
1	-44	12.35	0.72
2	-28.3	19.61	4.24
3	4	-18.50	3.67
Total			8.63

Heat rejection level (to cooling water) : 36^{o}C

Once the basic configuration is obtained for each cycle, the information is used in the second phase to produce final configurations. The design for the ethylene cycle from Wu's work is shown in Figure 3-10 and from the proposed method is in Figure 3-11.

In Wu's approach, the ethylene refrigeration cycle is a three-stage refrigeration system. It has a presaturator installed at both the second and the third stages. All condensing heat is rejected to the propylene cycle at condensing temperature -40 °C. The total shaftwork consumption is 3.52 MW and total costs 7.96 M$/yr.

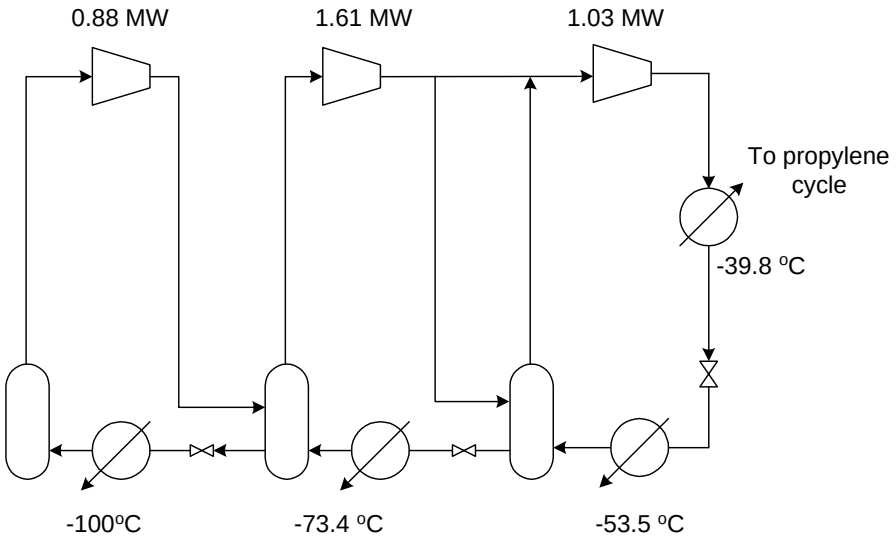

Figure 3-10. The design of ethylene cycle in Wu's work.

The design of ethylene cycle from the proposed method is a three-stage refrigeration system, with only one flash drum and one presaturator at the third stage. It consumes total shaftwork 3.11 MW and costs overall 7.17 M$/yr. Comparing to the base case, the new ethylene cycle has not only 12% lower shaftwork consumption, but also a simpler configuration. The total cost is 10% lower than the base case.

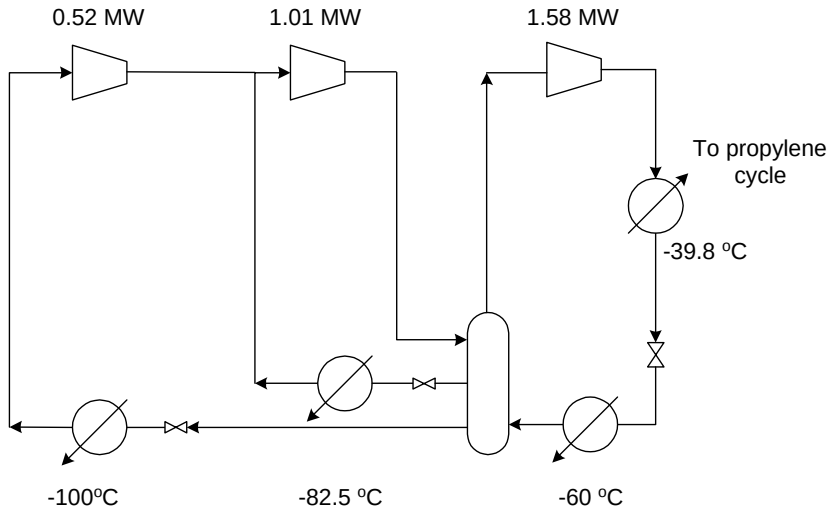

Figure 3-11. Solution by the new method for the ethylene cycle.

The design for the propylene cycle in Wu's work is shown in Figure 3-12 and Figure 3-13 shows the results from the new method.

The propylene cycle has two evaporation stages and two reboiling stages. It has a presaturator installed at the second stage and one economiser at -7.6 ^{o}C. The overall shaftwork consumption is 9.70 MW and the total cost is 10.83 M$/yr.

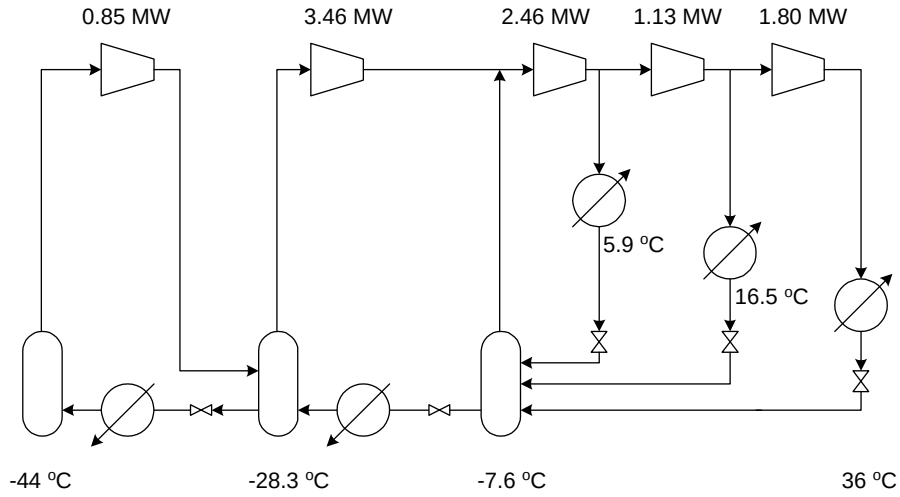

Figure 3-12. Wu's optimal propylene cycle

Interestingly, the design of propylene cycle by the proposed method is exactly the same as the shaftwork targeting result. We have two evaporation stages and one reboiling stage at 4 °C. It consumes 8.63 MW shaftwork and costs overall 9.85 M$/yr. The shaftwork consumption is 11% lower than that of the Wu's. The configuration is also simpler, for the new design has only one reboiling stage instead of two reboiling stages as the base case has. The total cost is therefore 9% lower.

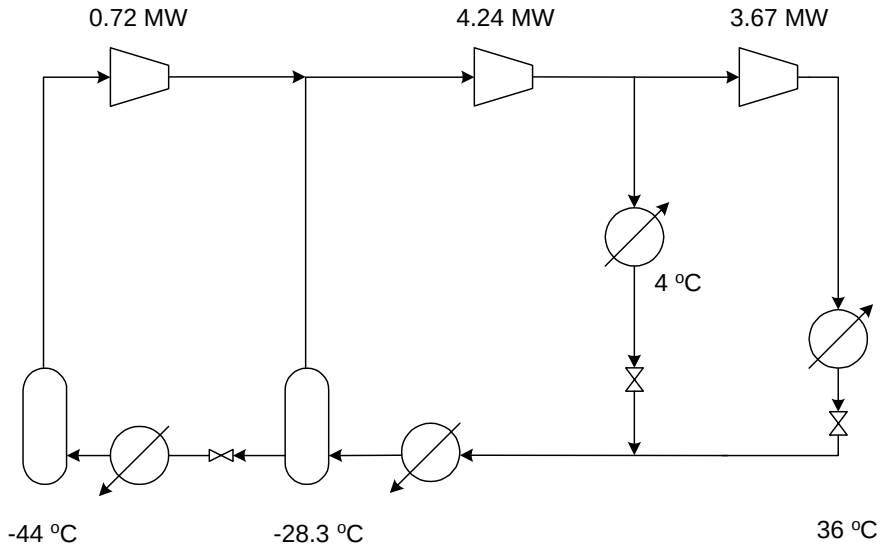

Figure 3-13. Solution by the new method for the propylene cycle.

As it can be seen, the design results for the ethylene and propylene cycles are cheaper and simpler than that obtained from the previous method. In both cycles, the shaftwork targeting method produces near optimal results, where in the second phase only minor modifications where found, mainly related to the shaftwork consumption. The Table 3-12 summarises the comparison of the results from different methods.

Table 3-12. Comparison between base case, shaftwork targeting and the new approach

	Base Case	Shaftwork Targeting	New Method
No. of flash drums	6	6	3
No. of compressors	8	6	6
Total shaftwork	13.22	11.94	11.74
Total cost	18.79	17.65	17.02

When we plot the temperature level and load of each stage of the new design against the base case on the GCC, as shown in Figure 3-14, we can easily see why the improvement is achieved. In the ethylene cycle, the new design has better settings of temperature and load of each stage. In the propylene cycle, the new design has only one reboiling stage to cover a wider heat rejection range than the base case, which uses two reboiling stages. The base case ignores the fact that each heat rejection stage has both superheat rejection and condensing heat rejection parts.

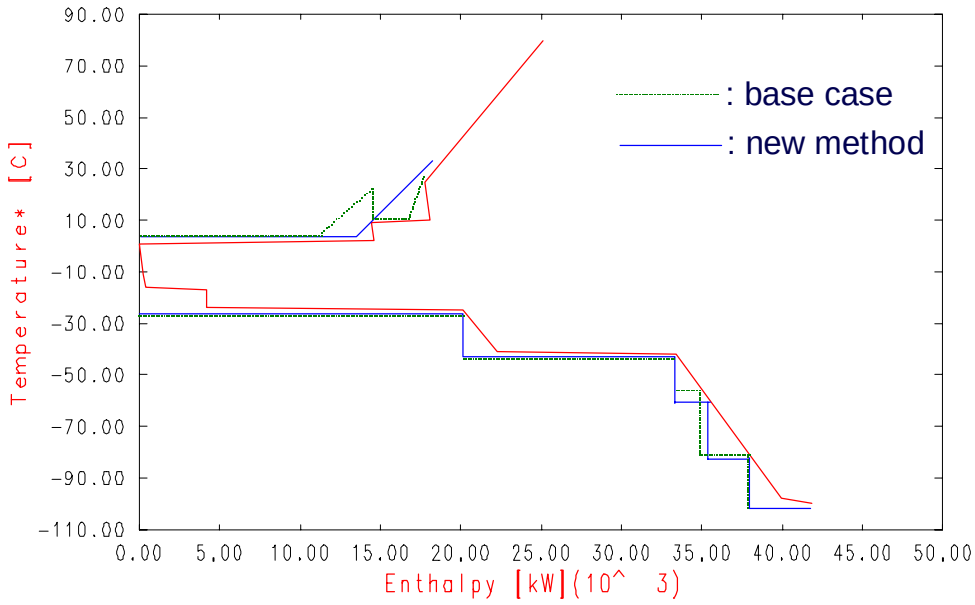

Figure 3-14. Comparison on the GCC.

3.4 Conclusions

In the first case study, it has been demonstrated that the proposed method can be combined with conventional HEN design method to generate complete design of refrigeration systems and associated HEN. Shaftwork targeting method can determine the optimal number of levels, and temperature and duty of each level by minimising total costs. Then design options are explored in the second phase by disjunctive programming-enhanced MINLP model.

The proposed method has been demonstrated in the second case study on synthesis of an ethylene-propylene cascade refrigeration system. The shaftwork targeting method in the first phase generates base configurations. The second phase uses this base configuration as initial conditions for the MINLP model. The results obtained from this new method show an improvement compared with the previous pure MINLP approaches. The overall design of the ethylene-propylene cascade refrigeration system is obtained in much shorter time than that by previous methods. The final configurations are cheaper and simpler. The shaftwork targeting method plays an important role in the overall procedures, as it not only generates good initial conditions to alleviate the efforts of the optimisation in the second phase, but the base configurations are near optimal. One of the important advantages of this new method is that results can be displayed clearly and concisely by GCC.

Reference

Hewitt, G. F., Shires, G. L. and Bott, T. R., 1994, *Process Heat Transfer*, CRC Press, Boca Raton, U.S.A.

Part 2.

Optimal Design of Mixed-Refrigerant Systems

4. SYNTHESIS OF SINGLE - STAGE MIXED - REFRIGERANT SYSTEMS

4.1 Introduction

Many LNG facilities have been built or are under construction. Early plants used cascade cycles. There are difficulties concerned with maintaining the many machines needed for cascade cycles. The continuing development of new methods to reduce net power and capital costs is important in the LNG industry.

Gas liquefaction processes are always capital intensive, because of major use of installed equipment and large energy requirement in operations. A large part of investment is in the liquefier, which usually makes up around 25~50 % of the total cost. Thus, optimal design and operation of a liquefaction process offers huge potential energy and cost benefits.

A mixed refrigerant (MR) system uses a mixture as refrigerant instead of using several pure refrigerants in conventional multistage or cascading refrigeration systems. Unlike pure refrigerants and azeotropic mixtures, the temperature and vapour and liquid composition of non-azeotropic mixtures do not remain constant at constant pressure as the refrigerants evaporate or condense. The composition of the mixture is selected such that the liquid refrigerant evaporates over a temperature range similar to that of the process cooling demand. A mixture of hydrocarbons (usually in the C1 to C5 range) and nitrogen is normally used to provide the desired refrigerant characteristics (e.g. close matching of the hot and cold composite curves, with small temperature driving forces over the whole temperature range) for the specific refrigeration demand. Small temperature driving force leads to near-reversible operation, thus better thermodynamic efficiency and lower power requirement. Also, an MR system features a simpler machinery configuration and fewer maintenance problems.

The concept of using a mixture as refrigerant has been around for a long time. The earliest application can be traced back to 1936, when W. J. Podbielniam (1936) devised a mixed component refrigerant system having three stages of throttling, and a single compressor in a close cycle. Thereafter, several variations and applications have been introduced (Haselden et al (1957); Perrett (1968); Gaumer and Newton (1971)). MacKenzie and Donnelly (1985) demonstrated that MR systems are more efficient than turbo-expander systems in a natural-gas-liquid (NGL) recovery process. More recently, due to the growing concern of the impact of ozone depletion by certain chlorofluorocarbon (CFC)-based refrigerants, there is an urgent need to replace high ozone-depletion-potential (ODP) refrigerants by environmentally benign ones (Steed, 1989). Using mixed refrigerants is one of the most promising solutions (Radermacher, 1989). Lamb et al (1996) and Bensafi and Haselden (1994) demonstrated that MR systems can achieve high energy efficiency and thus power saving. They reported up to 30% energy saving compared with systems using pure R22. However, the way they determined the best composition of refrigerant mixture is experimental.

Duvedi and Achenie (1997) used an MINLP approach to the design of refrigerant mixtures that have the desired attributes, such as low ODP. However, the approach was limited to small number of refrigerant components and assumptions made in the MINLP model were far from the reality. First, they assumed the refrigerant mixtures leaving the condenser or the evaporator were at their saturated states. However, this assumption is untrue, since in reality the refrigerant mixtures leaving the condenser should be subcooled and the mixtures leaving the evaporator should be superheated. Second, they assumed the evaporating and condensing temperatures were the average of the inlet and outlet saturated temperatures. In practical operations the evaporating and condensing temperatures of refrigerant mixtures usually cover a wide range from ambient down to -160 ^{o}C. For such a wide temperature range, the second assumption is poor. In design of MR systems, we need to be concerned not only with the minimisation of energy and capital costs, but also the temperature profiles of the evaporation and the condensation. Usually, the temperature approach within the heat exchangers of MR systems is as low as 1~3 ^{o}C.

Patel and Teja (1982) proposed an improved equation of state for predicting the thermodynamic properties of refrigerant mixtures. Lee et al. (1992) improved the

Patel-Teja equation of state to be a purely predictive model for mixture property calculations.

One major application of the MR systems is in the LNG industry (Kinard and Gaumer, 1973). The refrigeration facilities can be categoried according to the general type of refrigeration cycle used: conventional cascade refrigeration systems, and MR systems. In fact, the birth of the concept of using a mixture as refrigerant is due to the awareness of the difficulty in maintaining classical cascade refrigeration machines. For such a wide temperature range in LNG process, usually from ambient temperature down to around -160 °C, cascade refrigeration systems require typically three different multistage refrigeration cycles. Each cycle typically comprises three stages, as shown in Figure 4-1. On the other hand, MR systems have only one compression train and simpler machinery configuration, as shown in Figure 4-2.

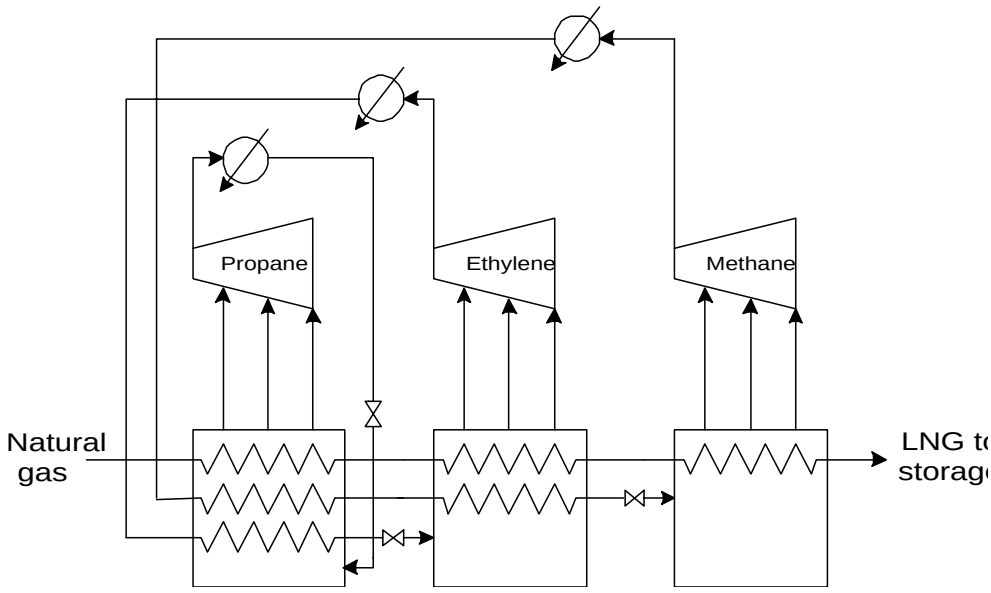

Figure 4-1. A cascade refrigeration system for LNG.

An efficient process can be designed by judicious manipulation of operating pressure and the composition of the circulating mixed refrigerant, and by proper arrangement of heat exchangers. Because of the ability to alter the refrigerant evaporation temperature profile by changing refrigerant composition, MR systems have lower heat transfer irreversibilities within heat exchangers, thus saving power. Furthermore, by

changing refrigerant composition, more efficient utilisation of all available heat transfer surface and actual compressor characteristics can be achieved.

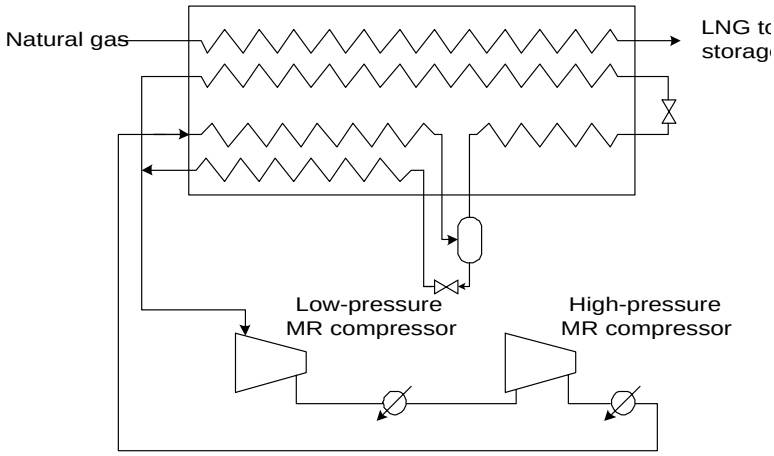

Figure 4-2. A two-stage MR system for LNG.

The PRICO process (Price and Mortko, 1996), as shown in Figure 4-3, is the simplest form of MR system.

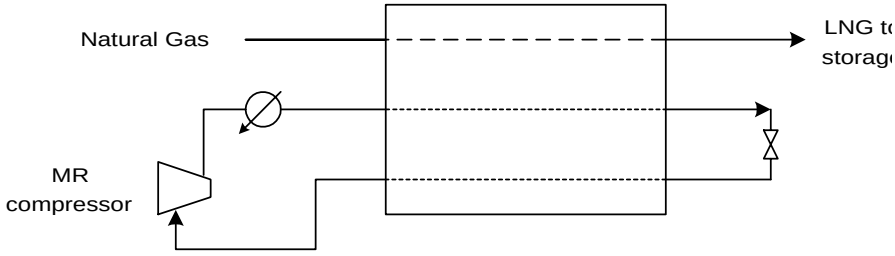

Figure 4-3. The PRICO process – a single-stage MR systrem.

Its major function is to convert natural gas (NG) to liquid state for transportation and/or storage at atmospheric pressure by using a single-stage MR system. It is also applicable to natural gas liquid (NGL) extraction (high ethane recovery) from NG. Mixed refrigerant is compressed and passes through the main hear exchanger where it is condensed. It is then expanded across a Joule-Thomson valve and returns counter-currently through the heat exchanger back to the compressor. Natural gas enters the heat exchanger at ambient temperature and exits as liquefied natural gas. The main heat exchanger is a plate-and-fin with a brazed aluminium core. Figure 4-4 shows the three streams in the heat exchanger: the NG-LNG stream, the warm refrigerant stream

(before Joule-Thomson valve) and the cold refrigerant stream (after Joule-Thomson valve).

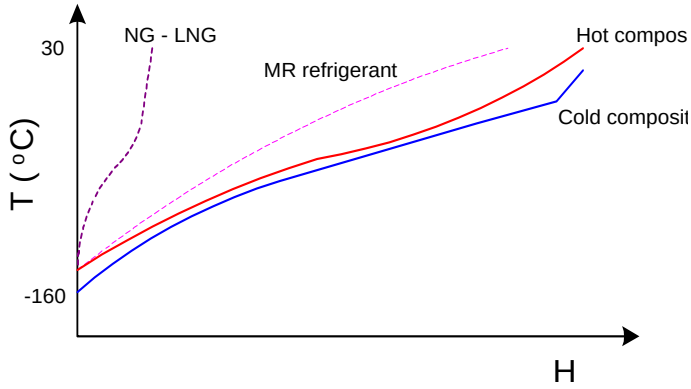

Figure 4-4. The composite curves of the PRICO process.

The NG-LNG stream and the warm refrigerant stream can be combined as a hot composite curve, while the cold refrigerant stream alone forms the cold composite curve. We denote two ends in the composite curves as the high-pressure (HP) end and the low-pressure (LP) end. To achieve higher efficiency, the design of the MR systems can be evolved to more complex schemes, such as multistage MR systems, propane-precooled MR systems or cascade MR systems.

However, in practice, MR systems are generally considered to have lower efficiency than conventional cascade cycles (Finn et al., 1999), because even though the temperature driving force is smaller, the circulation flow of the refrigerant is much higher. The main reason is usually poor matching between the hot and cold composite curves of the existing plants, and hence a higher flow rate of refrigerant is required to avoid temperature crosses occurring within the heat exchanger. The solution of improving the performance of MR system therefore lies in better selection of refrigerant composition. However, due to the high complexity of the problem, the selection of refrigerant composition has been done by trial-and-error and guided only by heuristics. No systematic synthesis of MR system has been proposed so far.

In summary, the difficulties in the design of MR systems mainly come from two sources. First, the complex nature of the thermodynamic and physical properties of mixtures makes computation of MR systems expensive and highly non-linear. Second,

the small temperature approach between the profiles of evaporation and condensation and the wide temperature range, make MR systems extremely sensitive to the change of operating conditions, especially change of composition of refrigerant mixtures.

In this thesis, we shall propose a novel methodology for the systematic synthesis of MR systems by a combined mathematical programming/thermodynamic approach, which can generate optimal design solutions and good understanding of design problems, and deliver greater confidence to the users. The basic idea is to try to find a set of refrigerant compositions that can give the best match between hot and cold composite curves under given pressure levels (condensing and evaporating pressures) and refrigerant flow rate. If the search is successful, then pressure levels and/or the refrigerant flow rate are reduced progressively and the procedure of finding the best-matching refrigerant composition repeated iteratively. The procedure terminates when no set of valid refrigerant compositions can be found. In other words, there are always temperature crosses inside the heat exchanger and no further improvement is possible. We can propose three different forms of objective function: minimise crossover, minimise sum of crossover, and minimise shaftwork requirement. It has been found that each objective function has its strengths in different situations, and better optimisation results can be obtained by switching to different objective functions during one optimisation task. The strength of this approach is that it integrates the power from the mathematical programming and thermodynamics. While mathematical programming can produce accurate information and optimal solution for the process operating conditions, thermodynamics expresses the evolution of the solution procedures in a visual way so that the users have understanding and confidence in the solution.

To test the viability of this methodology, three case studies on a PRICO process have been carried out. The first case demonstrates a 21.3% shaftwork saving by the new method, when compared with commercial PRICO processes. The second case study, by switching to different objective functions during optimisation, achieves a 25% saving in shaftwork consumption. The third case study investigates the effect of using different degrees of temperature shifting on the change of shaftwork requirement. Based on this preliminary success on single-stage MR systems, this methodology can

further be extended to the design and retrofit of more complex MR systems, i.e. multistage MR systems and propane-precooled MR systems (APCI process).

4.2 Pure Refrigerant vs. Mixed Refrigerant

Conventional refrigeration systems, domestic or industrial, employ single-component refrigerants. In most situations, the temperatures of the heat source or sink vary during the heat transfer process, while the evaporating and condensing temperatures of pure refrigerants are constant. As a result, there are inevitably pinch points in the evaporators or condensers, as seen in Figure 4-5.

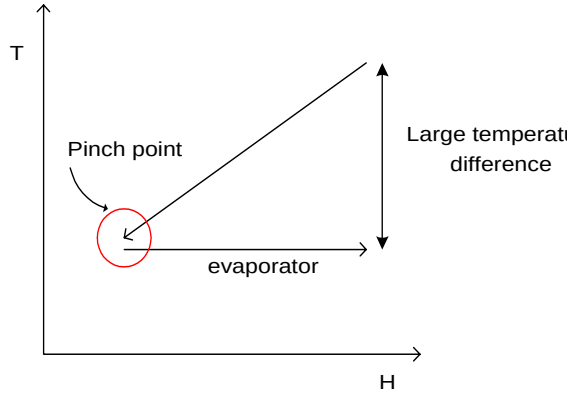

Figure 4-5. Temperature profiles within an evaporator when using a pure refrigerant.

The large temperature difference at one end of the heat exchanger leads to irreversibility that in turn reduces the efficiency of the refrigeration system. Also, a certain pure refrigerant may be suitable for the existing operating conditions. But, once the operating conditions change, another pure refrigerant might be more desirable. A possible solution would be to replace the existing refrigerant by a new one, but this is not practical. Finally, if the difference between the condensing and evaporating temperature gets larger, the pressure ratio across the compressor increases and consumes more shaftwork.

The problem of using pure refrigerants is mainly from the fact that the thermodynamic properties of a pure refrigerant, the operating conditions imposed by a

refrigeration system and a particular application might not match well with each other. When a mixed refrigerant is used, we can overcome this problem by selecting the composition of a refrigerant mixture, or variations of the design of refrigeration systems.

According to Gibbs Phase Rule, the number of degrees of freedom of a system, having C components, M independent reactions and Q phases, is calculated as:

$$F = C - M - Q + 2 \tag{4-1}$$

Thus, the specification of $C - M - Q + 2$ intensive variables of the individual phases completely fixes the thermodynamic state of each phase. For pure refrigerant systems, the degrees of freedom are:

$$F = C - M - Q + 2 = 1 - 0 - 2 + 2 = 1 \tag{4-2}$$

We have only either temperature or pressure to choose as our degree of freedom. For the MR systems of C components, the number of degrees of freedom becomes:

$$F = C - M - Q + 2 = C - 0 - 2 + 2 = C \tag{4-3}$$

This suggests that at a given pressure the boiling (or dew) temperature of the mixed refrigerant will be a function of composition and hence we have more degrees of freedom than pure refrigerant systems. If the gap between the condensing and evaporating temperatures gets larger, the pure refrigerant system needs to increase the difference between condensing and evaporating pressures as well, while for the MR systems, it can only alter the refrigerant composition and keep the same pressure levels. This greatly enhances a refrigeration system's flexibility and saves a significant amount of shaftwork when operating conditions change.

The major difference between pure refrigerants and mixed refrigerants is the shape of the temperature profile during phase transition, as illustrated in Figure 4-6. Therefore, by using a suitable refrigerant mixture, the average temperature difference is closer to

the minimum temperature difference, thus reducing the heat transfer losses compared with a pure refrigerant. Changing the refrigerant composition, flow rate, evaporating/condensing pressures or configuration of the heat exchanger can alter the shape of the refrigerant evaporating line for a mixed refrigerant. If the operating conditions change in the process, we can adjust the refrigeration system to maintain desirable performance by changing the refrigerant composition.

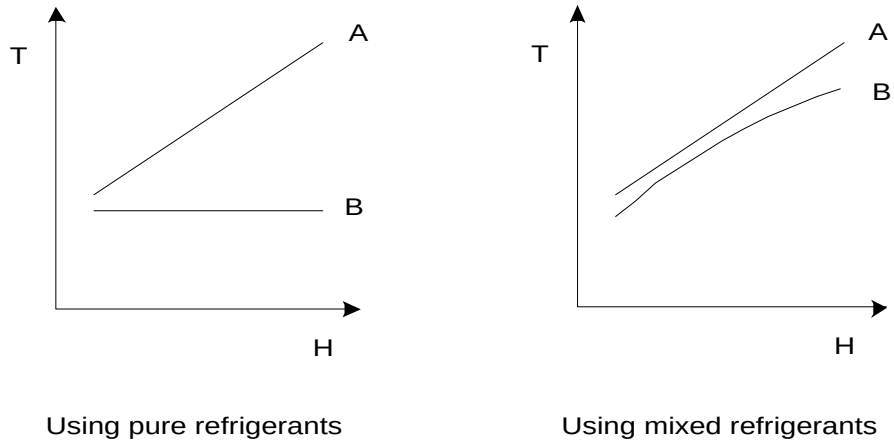

Figure 4-6. Comparison between using pure refrigerants and mixed refrigerants.

The challenges in selecting the composition of mixed refrigerant lie firstly in that, since we deal with very small temperature differences between the hot and cold composite curves and we need complex phase equilibrium calculations, it is necessary to use rigorous thermodynamic property calculations to obtain the accurate information necessary. This not only increases the difficulty of modelling for the problem, but also adds to the non-linearity when carrying out optimisation. The design of MR systems usually exploits multistream heat exchangers, which is already a challenging problem in itself. Figure 4-7 shows a temperature cross between hot and cold composite curves.

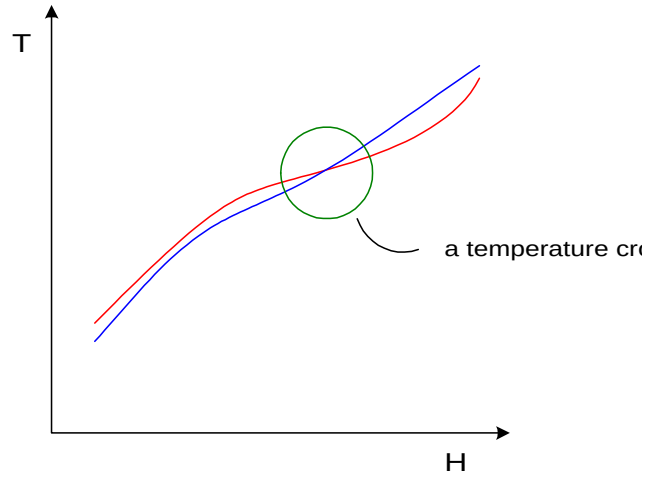

Figure 4-7. A temperature cross between hot and cold composite curves.

To guarantee valid heat transfer, we must avoid temperature crosses in the heat exchanger. The final consideration is the wetness in the inlet stream of the compressor. The mixed refrigerant flow, after being evaporated in the heat exchanger, becomes the inlet stream to the compressor. It would be damaging to certain types of compressors if the inlet stream contains some amount of wetness. The situation is illustrated in Figure 4-8.

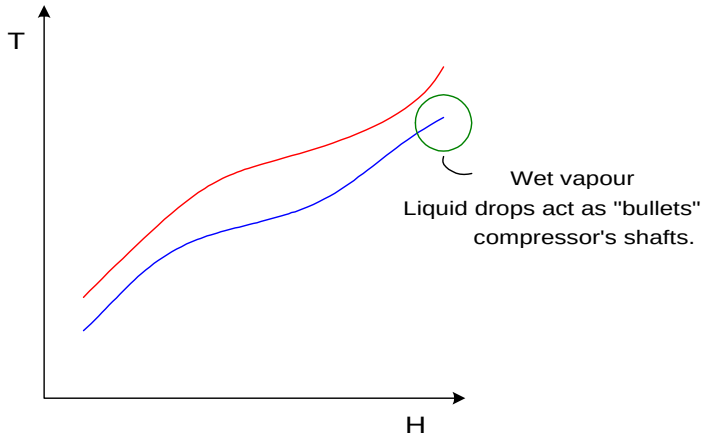

Figure 4-8. Composite curves when compressors' inlet stream having wetness.

In conclusion, from the considerations discussed so far, the desired hot and cold composite curves, as shown in Figure 4-9, should have the following features. (1) Hot and cold composite curves should be close and parallel to each other, thus heat transfer can be carried out with a near-constant temperature driving force distribution.

(2) No temperature crosses should occur. (3) Vapour should be superheated at the end of cold composite curve, which is the refrigerant evaporating line.

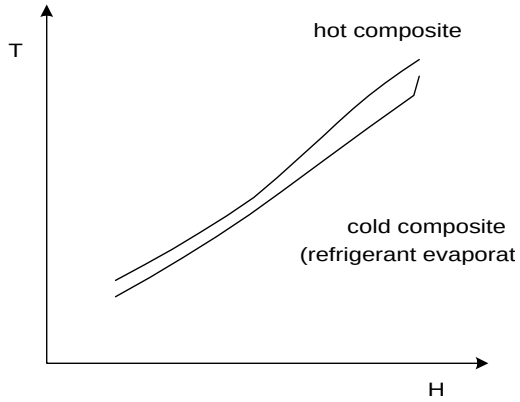

Figure 4-9. The composite curves for the ideal conditions.

4.3 Thermodynamic Properties Estimation for Refrigerant Mixtures

Although the concept of using mixed refrigerant for refrigeration systems of gas liquefaction has been known for a long time, to extend the concept beyond laboratory stage to plant operation requires two necessary tools. First, we need the ability to accurately predict the physical and thermodynamic properties of the mixtures. Second, we need the availability of models to calculate the material and energy balances, while utilising the thermodynamic and physical properties. The accurate prediction of phase equilibrium for vapour-liquid ratios and values of enthalpy is essential for the hydrocarbon mixtures in natural gas and in mixed refrigerants. With the temperature approaches within the heat exchangers being as small as 3~5 ^{o}C, a slight difference between the true performance and the predicted design performance can lead to large deviations on the surface area or shaftwork requirements.

In the study of phase equilibrium of a two-phase mixture, we need to know the partial mole properties of each component in the mixture. The starting point of all vapour-liquid equilibrium (VLE) calculations is the equilibrium criterion:

$$\bar{f}_i^{\,L}(T,P,x) = \bar{f}_i^{\,V}(T,P,y) \tag{4-4}$$

Calculation of the fugacity of each component in a mixture can be achieved by one of two different approaches: the ϕ – approach and the γ – approach.

ϕ – approach: by using ideal gas mixture as the reference,

$$\phi_i = \frac{\bar{f}_i}{x_i P} = \exp\left[\frac{1}{RT}\int_0^P \left(\overline{V}_i - \overline{V}_i^{\,IGM}\right)dP\right] \tag{4-5}$$

where the supercscript IGM refers to an ideal gas mixture property. ϕ is the fugacity coefficient. The fugacity coefficient can be calculated by applying an equation of state (EOS). For example, if Peng-Robinson EOS is used, the fugacity coefficient can be calculated by:

$$\begin{aligned} ln\,\phi_i(T,P,x) = {} & \frac{B_i}{B}\left(Z^V - 1\right) - ln\left(Z^V - B\right) \\ & - \frac{A}{2\sqrt{2}B}\left[\frac{2\sum_j x_j A_{ij}}{A} - \frac{B_i}{B}\right] ln\left[\frac{Z^V + \left(1+\sqrt{2}\right)B}{Z^V - \left(1+\sqrt{2}\right)B}\right] \end{aligned} \tag{4-6}$$

where

$$A = \frac{aP}{(RT)^2} \tag{4-7}$$

$$B = \frac{bP}{RT} \tag{4-8}$$

$$a(T) = 0.45724\frac{R^2T_c^2}{P_c}\alpha(T) \tag{4-9}$$

$$b = 0.0778\frac{RT_c}{P_c} \tag{4-10}$$

$$\sqrt{\alpha} = 1 + \kappa\left(1 - \sqrt{\frac{T}{T_c}}\right) \tag{4-11}$$

and

$$\kappa = 0.37464 + 154266\omega - 0.26992\omega^2 \tag{4-12}$$

where ω is the acentric factor.

γ – approach: by using ideal solution as the reference,

$$\bar{f}_i(T,P,x) = x_i \gamma_i(T,P,x) f(T,P) \tag{4-13}$$

where γ is the activity coefficient. The activity coeficient can be calculated by usig correlative models. For example, for a binary mixture, if we have experimental data for γ_1 and γ_2, we can use the one-parameter Margules equation to fit the model to the data. The one-parameter Margules equation is:

$$G^{EX} = Ax_1x_2 \tag{4-14}$$

but from the Gibbs-Duhem equation,

$$G^{EX} = \left(x_1 ln\,\gamma_1 + x_2 ln\,\gamma_2\right)RT \tag{4-15}$$

So we can write

$$ln\,\gamma_1 = \frac{\Lambda}{RT} x_2^2 \tag{4-16}$$

and

$$ln\,\gamma_2 = \frac{\Lambda}{RT} x_1^2 \tag{4-17}$$

where Λ is an adjustable parameter.

With the two approaches, the calculation of vapour-liquid phase equilibrium can be achieved by two different ways. The ϕ - ϕ approach uses an equation of state to describe both phases, and the γ - ϕ approach applies an activity coefficient model for

the liquid phase and an equation of state for the vapour phase. For the ϕ - ϕ approach, the VLE becomes:

$$\bar{f}_i^L(T,P,x) = x_i P \phi_i^L(T,P,x) = \bar{f}_i^V(T,P,y) = y_i P \phi_i^V(T,P,y) \qquad (4\text{-}18)$$

where

$$\phi_i^L(T,P,x) = \frac{\bar{f}_i^L(T,P,x)}{x_i P} \quad \text{and} \quad \phi_i^V(T,P,y) = \frac{\bar{f}_i^V(T,P,y)}{y_i P} \qquad (4\text{-}19)$$

If the γ - ϕ approach is applied, the VLE becomes

$$\bar{f}_i^L(T,P,x) = x_i \gamma_i^L(T,P,x) P_i^{SAT}(T) \phi_i^L(T,P,x) = \bar{f}_i^V(T,P,y) = y_i P \phi_i^V(T,P,y) \qquad (4\text{-}20)$$

Due to advancing computer power, the ϕ - ϕ approach tends to be favoured, since good phase equilibrium calculations can be made over a wide range of temperatures and pressures, including near the critical region. Furthermore, not only the vapour-liquid ratios and the compositions of the phases can be accurately predicted, but also other relevant properties, such as densities and enthalpies. In this thesis, the ϕ - ϕ approach will therefore be used throughout.

Patel and Teja (1982) proposed a better equation of state for predicting the thermodynamic properties of refrigerant mixtures. Lee et al. (1992) improved the Patel-Teja equation of state to be a purely predictive model for mixture property calculations. In this thesis, the Peng-Robinson EOS will be used, mainly because it is well developed and widely recognised. Moreover, since most commercial simulators have Peng-Robinson EOS as an option for thermodynamic property calculations, the results from this study can be compared with simulation results if the same EOS is employed.

4.4 Characteristics of Key Design Variables

In the design of MR systems, three key variables play a dominant role in affecting the overall performance. These are the pressure levels of condensation and evaporation, the refrigerant flow rate and the refrigerant composition. Here we discuss the individual characteristics of those variables, respectively:

1) Pressure levels

In the MR refrigeration cycle, the mixed refrigerant evaporates and condenses at two constant pressure levels, while both the evaporating and condensing temperatures vary over a wide range. Let us use an example to demonstrate the effect of pressure levels. In the PRICO process as the base case, which is shown in Figure 4-10a, the condensing and evaporating pressure levels are at 42 bar and 3.4 bar respectively. When the hot and cold composite curves are checked, there is a temperature cross at the HP end of the heat exchanger. To avoid the temperature cross, the difference between the two pressure levels can be increased such that the condensing and evaporating pressures are 48 bar and 3.4 bar respectively. As shown in Figure 4-10b, the problem of temperature cross is avoided by widening the gap for the HP end but at the same time increasing the shaftwork requirement.

Another significant point is that changing the LP end pressure has a large effect on the LP end temperature, while changing the HP end pressure has a large effect on the HP end temperature difference. However, it will inevitably increase the shaftwork requirement if we increase the difference between the two pressure levels.

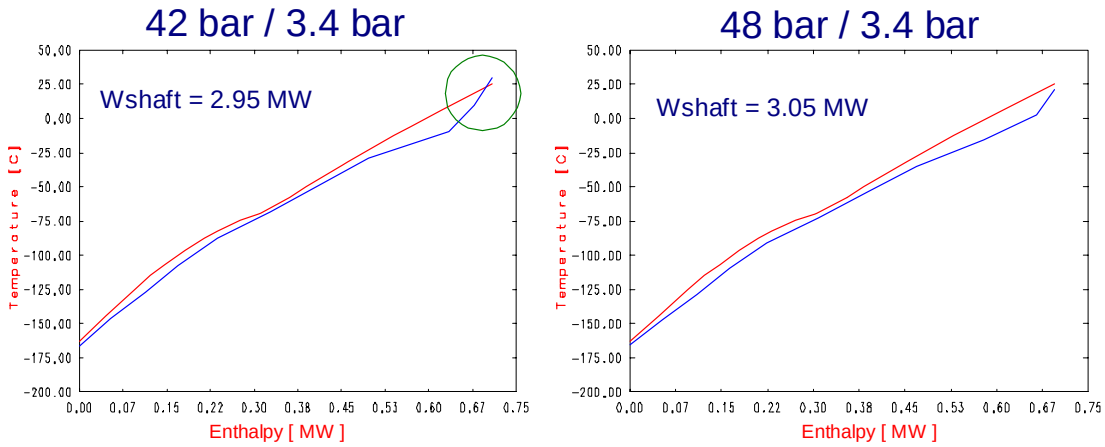

(a) (b)

Figure 4-10. The effect of changing pressure levels.

2) Refrigerant flow rate

Increasing the refrigerant flow rate can widen the gap between the hot and cold composite curves. We use the same base case to demonstrate the effect of the refrigerant flow rate. As shown by Figure 4-11a, where the refrigerant flow rate of the base case is 3.2 kmol/s, the hot and cold composite curves are crossed at the HP end. Increasing the refrigerant flow rate to 3.5 kmol/s, it can be seen that the temperature cross has been successfully avoided.

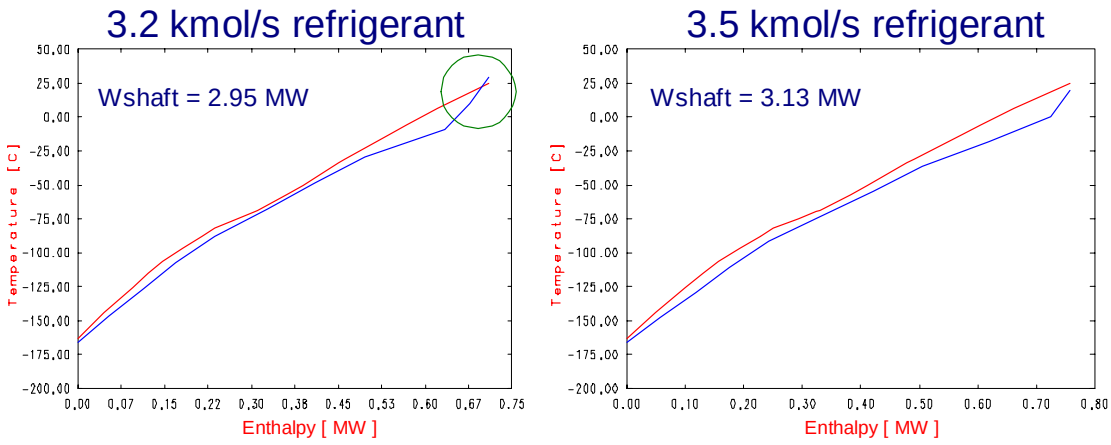

(a) (b)

Figure 4-11. The effect of changing refrigerant flow rate.

However, the shaftwork requirement has also increased. It should be noted that if the refrigerant flow rate is too low, it is difficult, if not impossible, to avoid temperature

crosses in the heat exchanger. Equally, if the refrigerant flow rate is too high, there will always be a certain amount of wetness in the inlet stream to the compressor, which should be avoided. Therefore, the refrigerant flow rate can be changed only within a range. Increasing the refrigerant flow rate also inevitably increases the shaftwork requirement.

3) Refrigerant composition

In typical MR systems, more than four different components are usually employed for the refrigerant mixture. According to the Gibbs phase rule, we have *C* degrees of freedom in MR systems. Considering the introduction of new components or replacing an existing component by a new one, there is more freedom to adjust to achieve better performance of our MR systems. Consider the same base case to demonstrate the effect of changing refrigerant composition. In Figure 4-12a, we face the same temperature cross problem.

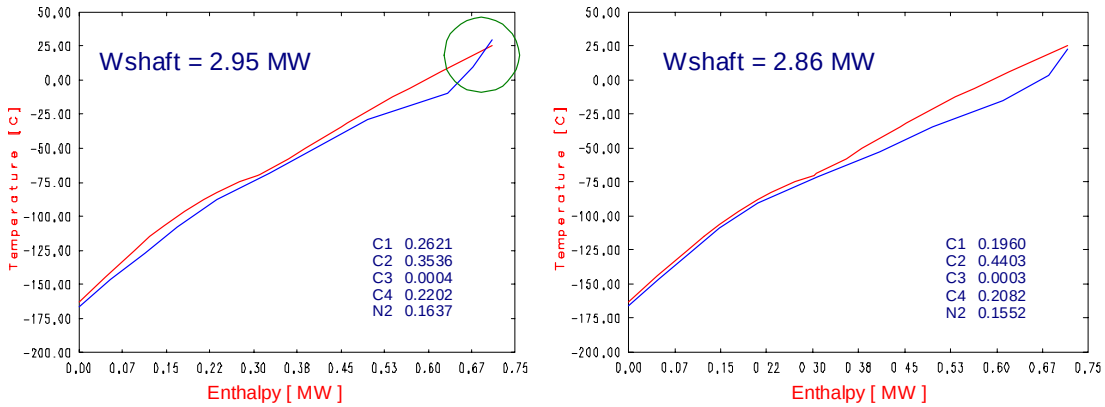

(a) (b)

Figure 4-12. The effect of optimising refrigerant compositions.

By applying the optimal selection method of refrigerant composition, which will be introduced later, we get another set of refrigerant compositions that successfully avoid the temperature cross problem and decrease the shaftwork requirement at the same time. Unlike the previous two variables, by optimising composition, it is not inevitable that removing a temperature cross results in higher shaftwork consumption. Since either pressure levels or refrigerant flow rate can be changed only within certain range, the refrigerant composition is the most flexible and significant variable when designing MR systems.

4.5 New Method for Selection of Mixed Refrigerant Composition

The major difficulty in formulating the problem for selection of refrigerant composition comes from the highly interactive relationship between the variables, and the tight composite curves. Any change in the refrigerant composition, condensing/evaporating pressures or the refrigerant flowrate will alter the shape and position of the hot and cold composite curves. Thus changing the refrigerant flowrate will also change the horizontal length of the two composite curves. Consequently, any small change in the variables might be more than enough to violate the desired features and even invalidate the heat transfer. A pure mathematical programming approach is opaque to the users, who need to have a thorough understanding and confidence of the procedures and solutions. Due to the highly non-linear nature of the problem, optimisation can be easily halted at infeasible points or trapped at local optimum. Without sufficient insight and understanding, it is difficult to make further improvement.

In this work, we propose a strategy of selecting mixed refrigerant composition by a combined NLP/thermodynamic approach. By using thermodynamics, the complex design problem can be displayed visually and the interaction between variables can be lumped together as the hot and cold composite curves. The NLP optimises the design variables to achieve the optimal solution for a given objective function. "Perfect" matching between the hot and cold composite curve would indicate that the two lines are exactly parallel to each other. The strategy is to find the refrigerant composition within the given refrigerant set (say, C1 to C4 and nitrogen) so that the hot and cold composite curves can be most parallel to each other. The overall procedure of the strategy is shown in Figure 4-13.

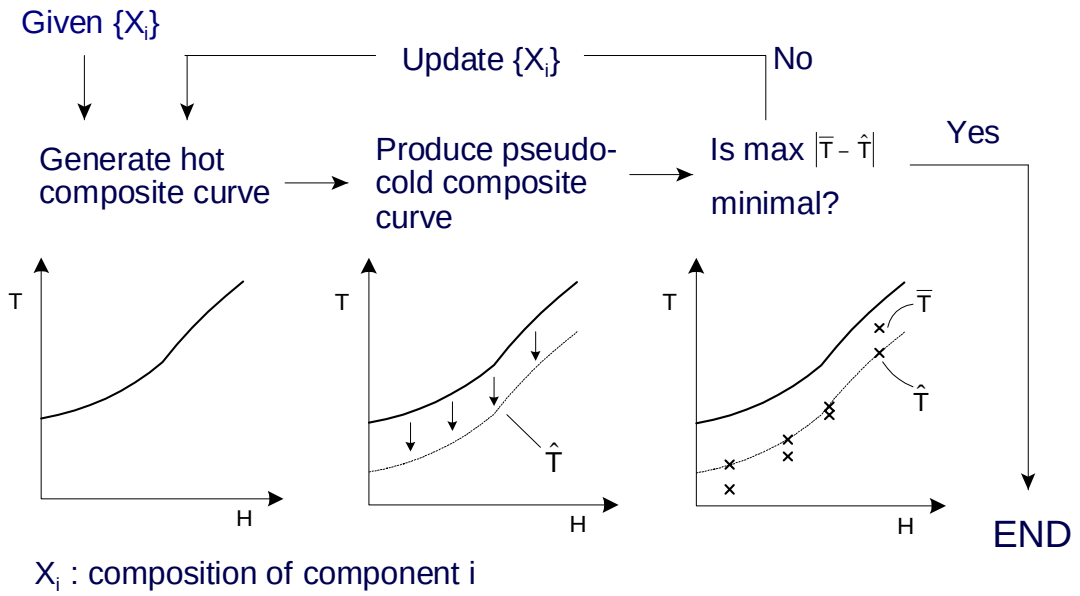

Figure 4-13. The strategy for optimal selection of refrigerant compositions.

The method starts with an initial setting of refrigerant composition, flow rate and pressures for evaporation and condensation of refrigerant. First, the hot composite curve for the given operating conditions is generated. Then, we shift the hot composite curve down by a certain temperature difference, say 5°C, to generate the "pseudo-cold" composite curve. The pseudo-cold composite curve serves as a "target" for the optimisation to achieve by changing composition. An NLP model is used to perform an optimisation to find the best composition that can achieve the minimum value of the objective function. The whole spectrum of the composite curves is sliced into N intervals. Within each interval *i*, the material and energy balances calculate the temperature of the pseudo-cold composite, $\overline{T}_i$, and of the real cold composite, $\hat{T}_i$. The optimisation algorithm continuously updates the composition of refrigerants. When it agrees with the optimality criteria of optimisation, the method concludes the best refrigerant composition.

An NLP model is used to optimise the composition of refrigerant mixtures to target desired properties. A general form for such problem is:

Problem NLP

$$\text{Minimise } f(\xi) \qquad (4\text{-}21)$$

Subject to

$$g(\xi) \geq 0$$

$$h(\xi) = 0$$

$$\xi^l \leq \xi \leq \xi^u$$

$$\xi' \subset \xi$$

ξ' : mole fraction variables

ξ : continuous variables

In the above, ξ is a vector of all continuous variables, and ξ' is a subset of ξ that represents the mole fraction of each component in a refrigerant mixture. ξ^u and ξ^l are specified upper and lower bounds. For ξ', the upper bound is 1 and the lower bound, 0. In addition to ξ', ξ includes all thermodynamic and physical properties of interest, such as the bubble and dew point temperature of a refrigerant mixture, the latent heat of vaporisation and condensation of a refrigerant mixture, and the specific heat of a vapour phase mixture.

Objective function

There are three different possible forms of objective function:

1) Minimise crossover: minimise the single biggest ΔTmin violation, as shown in Figure 4-14. Since we only consider the single biggest ΔTmin violation, we may ignore the change of other ΔTmin violations. The objective function can be expressed as:

$$\text{Minimise} \quad max\left(\left|\overline{T_i} - \hat{T}_i\right|\right) \qquad i \in N$$

$$\text{Subject to} \quad \hat{T}_i < \overline{T_i} + \delta \qquad i \in N \tag{4-22}$$

meaning of minimisation of the single biggest temperature violation. The temperature constraint guarantees that everywhere the cold composite curve is below the hot composite, so the heat transfer is always valid.

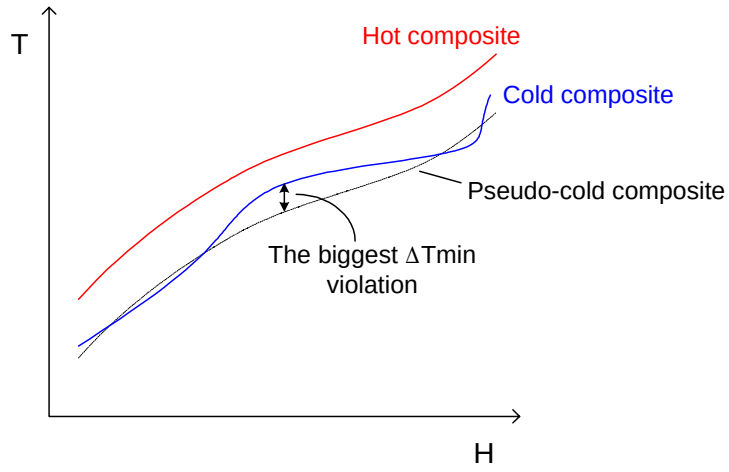

Figure 4-14. Illustration of "Minimise crossover" as the objective function.

2) Minimise sum of crossover: minimise the sum of the overall ΔTmin violation, as shown in Figure 4-15. The objective function can be written as:

$$\begin{aligned} &\text{Minimise} && \sum_{i=1}^{N} max\left\{0,\ \left(\overline{T_i} - \hat{T}_i\right)\right\} \\ &\text{Subject to} && \hat{T}_i < \overline{T_i} + \delta \qquad i \in N \end{aligned} \tag{4-23}$$

If $(\overline{T_i} - \hat{T}_i) \le 0$, the amount of temperature violation has no effect on the objective function. Compared with minimising the single biggest temperature violation, this objective function takes more thorough consideration of the whole shape of the hot and cold composite curves.

For the same temperature shift for the pseudo-cold composite curve, it often leads to higher shaftwork requirement than using "Minimise crossover". The reason is that, although the results from "Minimise sum of crossover" agree more closely with the pseudo-cold composite curve, the results from "Minimise crossover" have overall smaller temperature driving force between the hot and the real cold composite curves. Nevertheless, it can be improved by decreasing the degree of temperature shifting for the pseudo-cold composite curve.

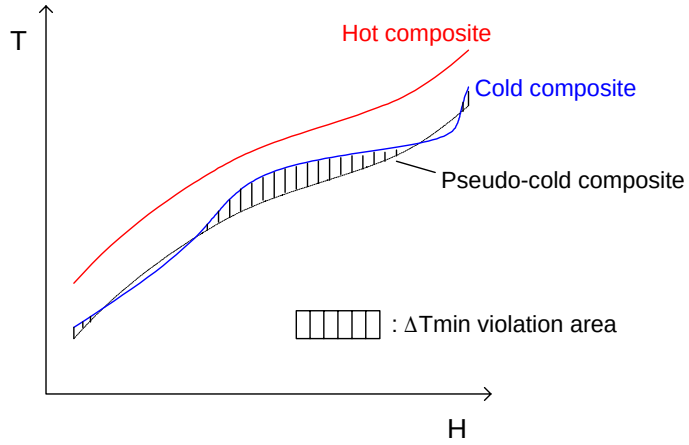

Figure 4-15. Illustration of using "Minimise sum of crossover" as the objective function.

3) Minimise shaftwork requirement: using this as the objective function can often result in the least shaftwork requirement among the three types of objective functions and seems the most "straightforward" way of defining our objective function:

$$\text{Minimise} \quad \sum_{j=1}^{M} WS_j$$

$$\text{Subject to} \quad \hat{T}_i < \overline{T_i} + \delta \qquad i \in N \tag{4-24}$$

Since it ignores the shape of the composite curves, it sometimes gets a refrigerant composition that would cause wetness in the inlet stream of the compressor. This objective function works best when the refrigerant flow rate and condensing/evaporating pressure ratio have been significantly reduced, that is, approaching the end of optimisation task. Under such conditions, the optimisation is free from the problem of wetness, and can usually give the lowest shaftwork requirement.

Equality constraints

The equality constraints in this problem formulation are mainly the balance equations and the calculation of physical properties. The balance equations are made around a

differentiated segment of the heat exchanger, as shown in Figure 4-16. The equality constraints are listed as follows:

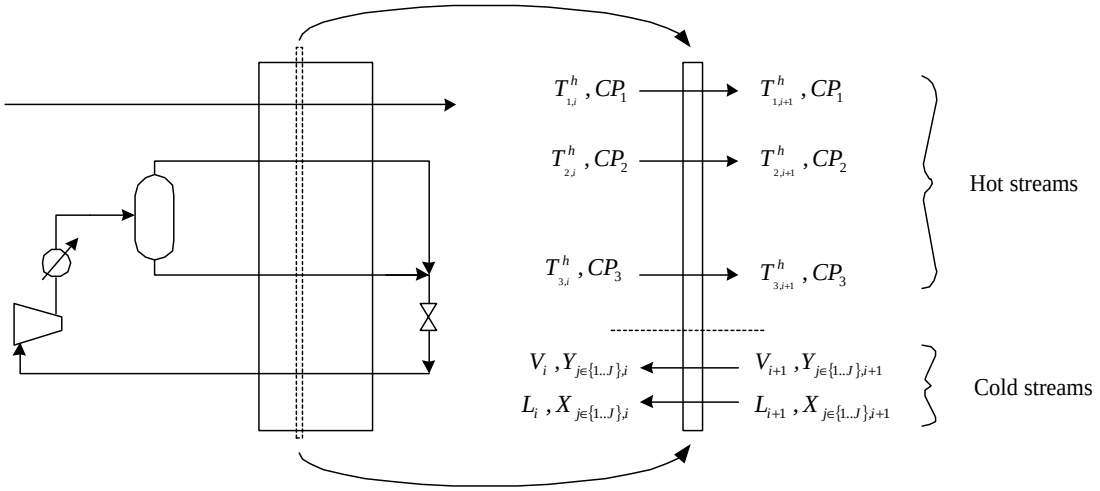

Figure 4-16. System boundary for balance equations.

mass and composition balance

$$L_i + V_i = L_{i+1} + V_{i+1} \tag{4-25}$$

$$X_{j,i} \cdot L_i + Y_{j,i} \cdot V_i = X_{j,i+1} \cdot L_{i+1} + Y_{j,i+1} \cdot V_{i+1} \qquad \forall i \in \{1 \ldots N\}\ ; \forall j \in \{1 \ldots J\} \tag{4-26}$$

energy balance

$$L_i \cdot h_i^L + V_i \cdot h_i^V = L_{i+1} \cdot h_{i+1}^L + V_{i+1} \cdot h_{i+1}^V + \sum_k CP_k \cdot \left(T^h_{k,i} - T^h_{k,i+1}\right) \qquad \forall i \in \{1 \ldots N\}\ ; \forall k \in \{1 \ldots K\} \tag{4-27}$$

The last term on the right hand side of Eq. (4-27) is the energy influx at segment *i*. The refrigerant mixture at segment *i* absorbs the energy influx of this amount and evaporates part of liquid, $L_i - L_{i+1}$, to satisfy the energy balance.

phase equilibrium

$$Y_{j,i} \cdot \phi_j^V\left(p,\hat{T},\overline{Y}\right) = X_{j,i} \cdot \phi_j^L\left(p,\hat{T},\overline{X}\right) \qquad \forall i \in \{1\ldots N\}\ ;\forall j \in \{1\ldots J\} \tag{4-28}$$

As discussed previously, the phase equilibrium is formulated by the ϕ - ϕ approach. The Peng-Robinson EOS is applied to calculate the fugacity coefficients for both vapour and liquid phases. An iterative computation is needed for this constraint. However, this constraint can be implicitly included into the calculation of evaporation temperature of a refrigerant mixture, since an equilibrium state has to be reached to find the evaporation temperature and the corresponding vapour phase composition. Details will be given later.

sum of mole fractions

$$\sum_j Y_{j,i} = 1 \qquad \forall i \in \{1\ldots N\}\ ;\forall j \in \{1\ldots J\} \tag{4-29}$$

$$\sum_j X_{j,i} = 1 \qquad \forall i \in \{1\ldots N\}\ ;\forall j \in \{1\ldots J\} \tag{4-30}$$

This constraint ensures that the mole fractions of all components that make up the mixture add up to 1 in either vapour or liquid phases.

evaporation temperature of a mixture, $\hat{T}$

$$\hat{T} = T\left(P,\overline{X}\right) \tag{4-31}$$

The calculation of the bubble-point temperature and vapour composition for a liquid of know composition at a pressure P. An initial guess is needed for the bubble-point temperature and the vapour mole fractions, and then Eq. (4-29) and the equality of component fugacities, Eq. (4-28), are checked for each component with the fugacities calculated by an equation of state. Details of the calculation can be found from Sandler (1999).

generating of $\overline{T}$

$$\overline{T}_i = \tilde{\tilde{T}}_i - \delta \qquad \forall i \in \{1 \ldots N\} \qquad (4\text{-}32)$$

It is worth emphasising that $\tilde{\tilde{T}}_i$, the local temperature of the hot composite curve, is calculated each time the NLP model is initiated or the composition is updated by the optimiser. So the hot composite curve and the pseudo-cold composite curve are not fixed in this method. The way to generate the hot composite curve can be found in Linnhoff *et al*. (1991).

physical property constraints

$$h_i^L = h^L\left(P, \hat{T}, \overline{X}\right) \qquad (4\text{-}33)$$

$$h_i^V = h^V\left(P, \hat{T}, \overline{Y}\right) \qquad \forall i \in \{1 \ldots N\} \qquad (4\text{-}34)$$

By using the Peng-Robinson EOS, the enthalpy of the vapour and liquid phases of a refrigerant mixture can be calculated in a departure function form with reference to ideal gas mixture:

$$h^V\left(P, \hat{T}, \overline{Y}\right) - h^{IGM}\left(P, \hat{T}, \overline{Y}\right) = RT(Z_m - 1) + \frac{T\left(\frac{da_m}{dT}\right) - a_m}{2\sqrt{2}b_m} ln\left[\frac{Z_m + \left(1+\sqrt{2}\right)B_m}{Z_m + \left(1-\sqrt{2}\right)B_m}\right] \qquad (4\text{-}35)$$

where the subscript m indicates a mixture property, and the superscript IGM means a property of an ideal gas mixture. Changing the superscript from V to L, Eq. (4-35) also applies to liquid phase mixtures.

After-throttling and after-mixing refrigerant temperature

$$\begin{aligned} & T_{to} = f\left(T_{ti}, P_{ti}, P_{to}, \overline{X}_{ti}\right) \\ & s.t. \quad h_{to} = h_{ti} \end{aligned} \tag{4-36}$$

The above equation states that the after-throttling refrigerant temperature is a function of temperature, pressure and compositions of throttle inlet liquid and throttle outlet pressure, subject to isenthalpic changes.

pressure profile constraint

$$P_i = P_{i+1} \qquad \forall i \in \{1 \ldots N\} \tag{4-37}$$

Although no frictional pressure drop is assumed within a heat exchanger in this study, the constraint can be changed to accommodate the condition once the pressure profile is know inside the heat exchanger by using the form:

$$P_i = P_{i+1} + \sigma \qquad \forall i \in \{1 \ldots N\} \tag{4-38}$$

where σ is the pressure drop between each interval.

Inequality constraints

The inequality constraints are of two types: the mole fraction constraint for each component in a refrigerant mixture, and the temperature approach constraint within a heat exchanger. They are as follows:

mole fraction constraint

$$0 \le Y_{j,i} \le 1 \quad ; \quad 0 \le X_{j,i} \le 1 \qquad \forall i \in \{1 \dots N\} \; ; \forall j \in \{1 \dots J\} \qquad (4\text{-}39)$$

temperature approach constraint

$$\hat{T}_i < \overline{T_i} + \delta \qquad \forall i \in \{1 \dots N\} \qquad (4\text{-}40)$$

This constraint states that everywhere the temperature of the cold composite curve should be colder than that of the hot composite curve. In this way, heat transfer validity within a heat exchanger is enforced.

No matter which type of objective function is used for composition optimisation, we should always check the hot and cold composite curves to see if the results are viable.

4.6 Systematic Synthesis of MR Systems

Based on the success of the proposed method for the optimal selection of refrigerant composition, we can develop a systematic method for the synthesis of MR systems. Figure 4-17 explains the methodology. The procedure commences from an initial setting of refrigerant flow rate, composition, and pressure levels for condensation and evaporation. The initial guess of refrigerant composition can be arbitrary, although the "initial condition" does affect the optimisation results. As for the initial refrigerant flow rate and pressure levels, we initially choose generous values for them, so as to leave room for the optimisation to reduce their values.

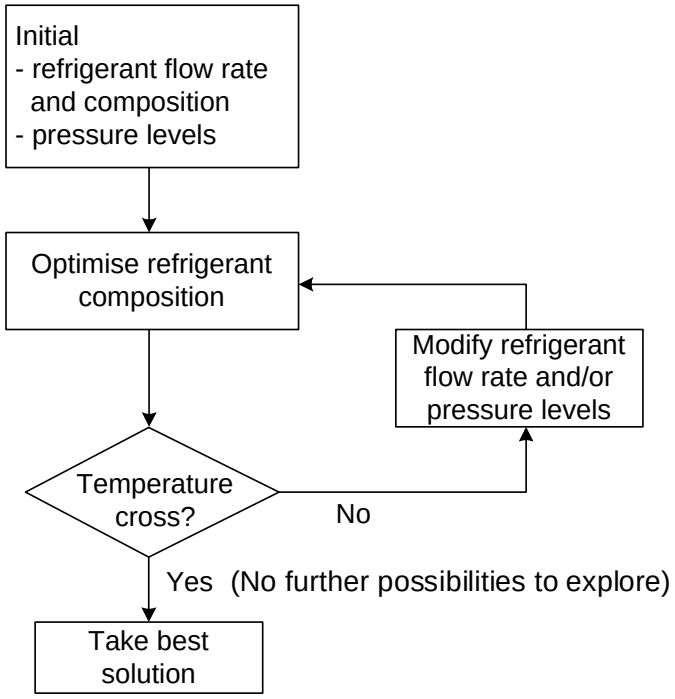

Figure 4-17. Proposes synthesis strategy of MR systems.

For the design task of the PRICO process for LNG, a reasonable range for refrigerant flow rate is 3 ~ 4 times NG flow rate, condensing pressure within 40 ~ 50 bar and evaporation pressure within 4 ~ 5 bar. If the optimal selection of refrigerant composition is successful under given refrigerant flow rate and pressure levels (evaporating and condensing), the refrigerant flow rate and/or pressure levels are adjusted or reduced and the procedure returns to the composition selection stage. After several iterations, the procedure terminates when either the refrigerant flow rate is too small or the pressure levels of condensing and evaporating are too close, so temperature crosses always occur in the heat exchanger. Therefore, no further improvement is possible by changing refrigerant compositions, and the optimisations reach the final design of the MR system by picking the best solution. Modifying the refrigerant flow rate or pressure levels can be done based on heuristics, judgement or optimisation. The choice of different objective functions, as will be illustrated in the "Case study" later, can affect the final results. Nevertheless, it is arguable which is the best solution to pick. Very possibly, the solution that gives the lowest shaftwork requirement may incur extra large heat transfer area and thus capital costs. Pua et al. (2000) has discussed this issue and combined the work presented in this thesis with a

design method for the synthesis of plate-fin heat exchanger networks. The results show a trade-off between shaftwork saving and heat exchanger network cost investment, and give better guidelines for picking the most economic solution to minimise total cost. Table 4-1 summarises seven cases with different compositions, minimum temperature approach and shaftwork requirements. It can be seen that with decreasing ΔTmin, the heat transfer area requirement is increased, and hence the pressure drop. When both shaftwork cost and heat exchanger network capital cost are taken into consideration, a trade-off between the two can be found by plotting them on Figure 4-18. A minimum total cost is found in case 4, in which neither the shaftwork requirement nor the HEN area are minimum, but the overall cost has the most favourable value. The study shows that an optimal MR system should be a trade-off between shaftwork consumption and heat exchanger network cost. An optimisation that only minimised shaftwork might lead to sub-optimal overall design.

Table 4-1.

Case	Composition	ΔT_{min}	W_{shaft} (kW)	HEN_V (m^3)	$HEN_{\Delta P}$ (kPa)
1	C1: 0.192 N2: 0.158 C2: 0.342 C4: 0.131 C3: 0.178	3.050	2937	3.004	25.4
2	C1: 0.190 N2: 0.159 C2: 0.342 C4: 0.131 C3: 0.178	2.207	2794	4.521	27.1
3	C1: 0.211 N2: 0.136 C2: 0.343 C4: 0.131 C3: 0.179	2.108	2712	4.667	27.5
4	C1: 0.220 N2: 0.125 C2: 0.344 C4: 0.130 C3: 0.180	1.668	2649	5.527	28.8
5	C1: 0.222 N2: 0.126 C2: 0.332 C4: 0.131 C3: 0.191	1.350	2545	7.543	29.1
6	C1: 0.223 N2: 0.131 C2: 0.312 C4: 0.136 C3: 0.197	1.156	2423	8.956	30.3
7	C1: 0.226 N2: 0.119 C2: 0.317 C4: 0.138 C3: 0.200	0.487	2342	13.015	32.1

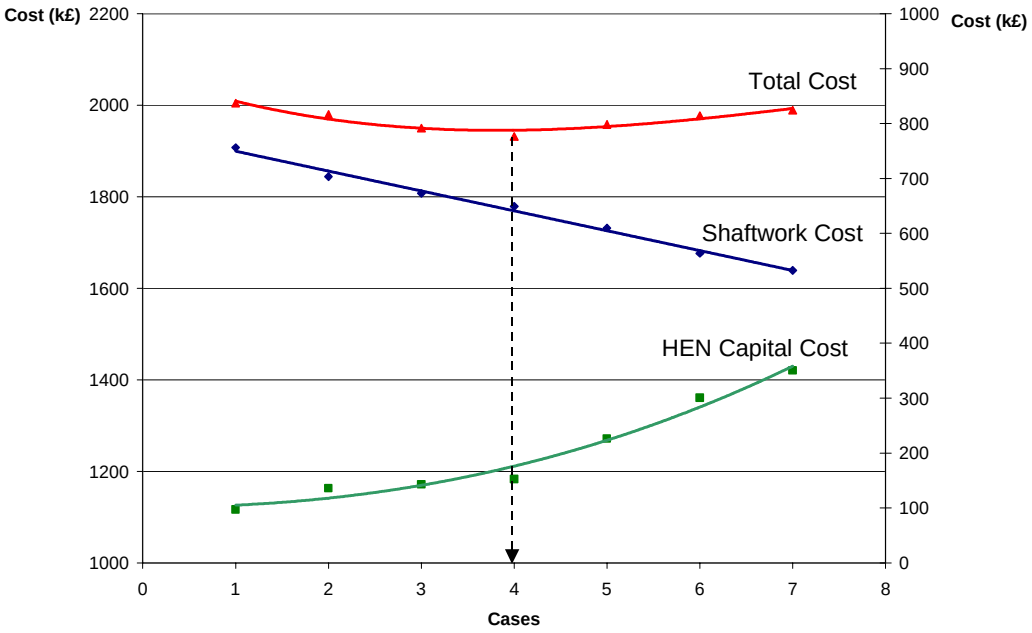

Figure 4-18. Trade-off between shaftwork cost and HEN capital cost.

A novel design methodology of subambient refrigeration systems using mixed refrigerants is then proposed. It comprises two main parts: optimal selection of refrigerant compositions and a method of design of compact multistream heat exchangers. The procedures start with the optimal selection of refrigerant compositions, as proposed in this thesis. In this stage, the operating costs of a series of near-optimal designs are found. The information is then fed to the second phase, in which the optimal synthesis of multistream heat changers (cold boxes) is performed (Pua *et al.*, 1999). From the second phase, the capital costs of each case are determined. In the third phase, the objective function is defined as the sum of operating costs and capital costs. The optimal design, which has the lowest overall costs, is fed back to the first phase as the initial conditions. The whole procedure converges to a final design when the optimal solution is close to the initial condition, which is the optimal result of the previous run, within the pre-defined convergence allowance. The overall procedures are shown in Figure 4-19.

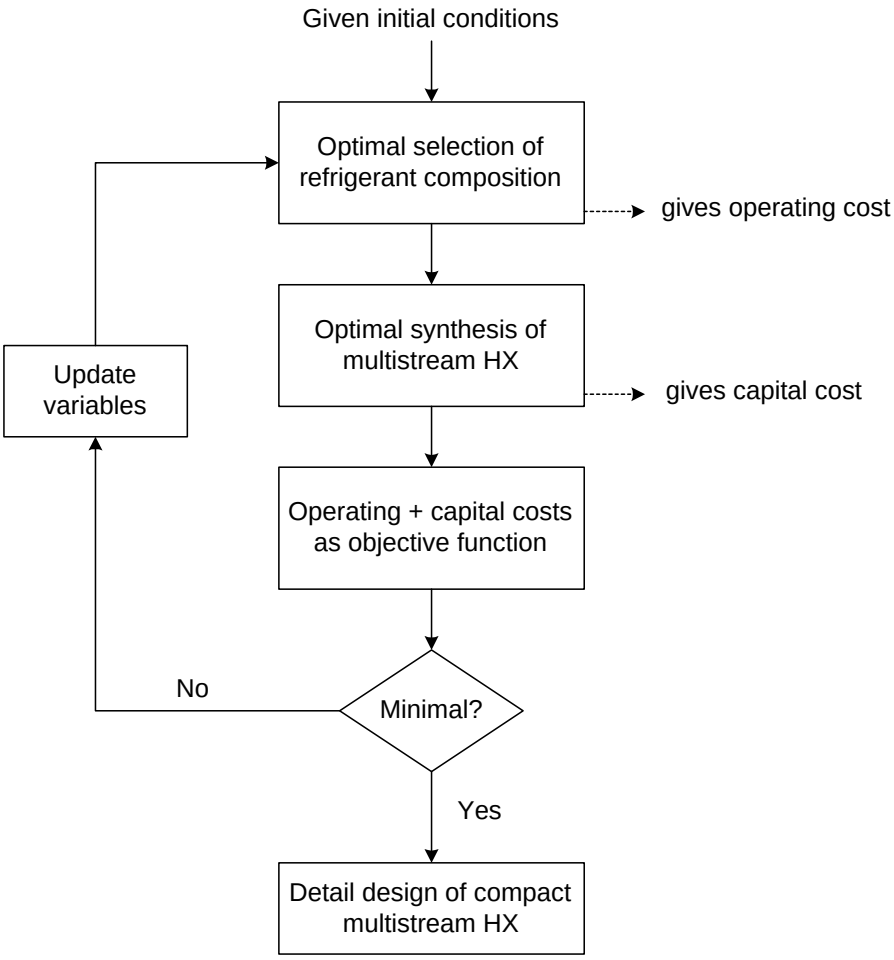

Figure 4-19. Complete design method of MR systems considering HEN costs.

It is interesting to note that a feasible solution is not required as the initial starting point to carry out the optimisation. The use of the pseudo-cold composite curve helps to correct the infeasible intermediate solutions towards feasible ones. After the first run of the optimisation, a feasible set of refrigerant composition will be found under a specified refrigerant flow rate and pressure ratio.

The method is readily extended to more complex MR systems. Figure 4-20 shows a 4-stage MR system, which splits the expansion of liquid refrigerant into four stages and still has only one compression train.

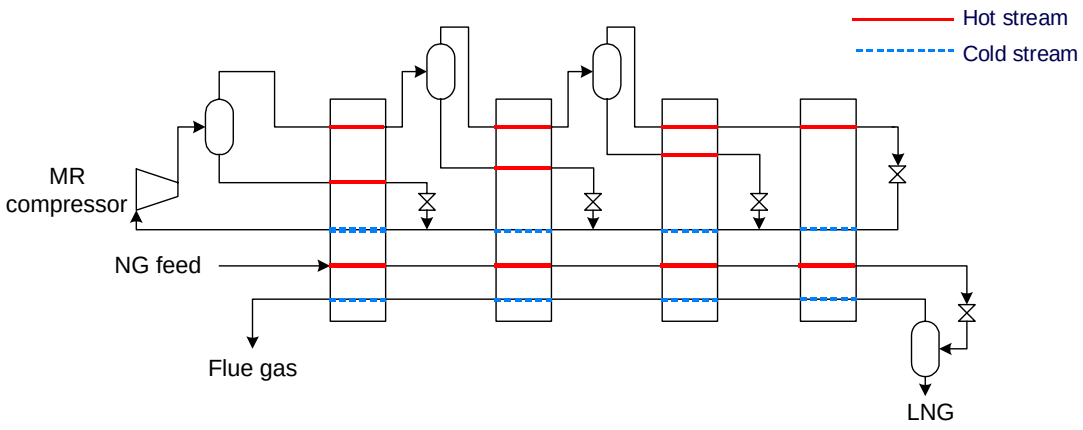

Figure 4-20. A four-stage MR system.

No matter how complex the system is, there will be only one hot composite curve and one cold composite curve. Therefore, by considering the match between hot and cold composite curves, this method readily applies to the synthesis of more complex MR systems by changing the modelling of the NLP, but more degrees of freedom (flow rates and pressures of each splitting) must be optimised.

4.7 Case study

Three case studies will be used to demonstrate the new synthesis method of MR systems by using the PRICO process as our base case, as illustrated in Figure 4-21.

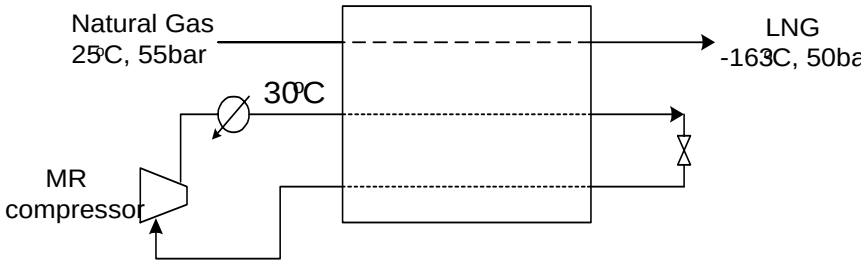

Figure 4-21. The design task – a PRICO process.

Here the natural gas enters the heat exchanger at ambient temperature and high pressure, and is to be liquefied by the mixed refrigerant flowing countercurrently though the heat exchanger. The refrigerant then passes the compressor to recover its

pressure back to the condensing condition. After the partial condenser, normally cooled by cooling water, the refrigerant is only partially condensed. Since there is no other heat sink in the process that can totally condense the refrigerant, it must be condensed by the cold refrigerant itself.

Case study 1 is to design the PRICO process to achieve the lowest shaftwork consumption by the new method. "Minimise sum of crossover" is employed as the default objective function. In case study 2, different objective functions are used, expecting to achieve further energy saving. Shifting of the hot composite curve by a chosen temperature difference forms the pseudo-cold composite curve. Certainly, the degree of shifting should have a significant effect on the final optimal solutions. In case study 3, different temperature shifts are tested to see how the optimisation results are influenced.

Table 4-2 lists the segmented natural gas feed stream. We can see that in the temperature range of -70.10 ^{o}C to -82.26 ^{o}C, the CP of the feed stream is exceptionally high, which implies a major liquefaction process has happened.

Table 4-2. The segmented natural gas feed stream

Stream	Ts	Tt	DH	CP
	[^{o}C]	[^{o}C]	[kW]	[kW/^{o}C]
1.1	25.00	-6.03	-1861.5	60.0
1.2	-6.03	-34.09	-1964.3	70.0
1.3	-34.09	-57.65	-1885.0	80.0
1.4	-57.65	-70.10	-2490.0	200.0
1.5	-70.10	-74.55	-1780.0	400.0
1.6	-74.55	-82.26	-3084.0	400.0
1.7	-82.26	-96.50	-1424.0	100.0
1.8	-96.50	-115.00	-1850.0	100.0
1.9	-115.00	-163.00	-3840.0	80.0

Case Study 1

To demonstrate this methodology, we start from using "Minimise sum of crossover" as the objective function. The optimisation steps are in Table 4-3.

Table 4-3. The optimisation steps.

	Pressure levels (bar)	Composition (wt %)	Refrigerant flow rate (kmol/s)	Shaftwork (kW)
Initial	4.0 / 46.0	C1: 28.9 C2: 37.5 C3: 16.5 C4: 4.8 N2: 12.3	4.0	X (Temperature cross)
1	4.0 / 46.0	C1: 15.7 C2: 46.4 C3: 3.5 C4: 4.65 N2: 19.8	4.0	34852.3
2	4.0 / 45.0	C1: 18.7 C2: 45.1 C3: 0.0 C4: 18.1 N2: 18.2	3.8	32610.6
3	3.8 / 43.0	C1: 20.1 C2: 42.44 C3: 4.5 C4: 17.1 N2: 15.9	3.6	30912.6
4	3.8 / 42.0	C1: 24.1 C2: 39.8 C3: 0.36 C4: 21.5 N2: 14.3	3.4	28763.9
5	3.7 / 40.0	C1: 18.5 C2: 47.0 C3: 0.01 C4: 20.6 N2: 13.9	3.3	27591.5
6	3.7 / 40.0	C1: 21.7 C2: 40.8 C3: 14.6 C4: 13.3 N2: 9.6	3.1	X (Temperature cross)

The procedure starts with initial settings of pressure levels, refrigerant flow rate and compositions. When we check the hot and cold composite curves of the initial setting, a temperature cross occurs inside the heat exchanger. We then keep changing the pressure levels (so that the pressure ratio is decreasing) and reducing the refrigerant flow rate, and use the optimal selection of refrigerant compositions to find the best composition under each condition. The procedure stops at the 6^{th} step when temperature crosses always occur and no further improvement is possible. The final design of the PRICO process is obtained from the 5^{th} stage, the last successful run in the procedure for optimal selection of refrigerant compositions. Figure 4-22 shows the hot and cold composite curves of our final design. If we compare the results with the commercial PRICO process, we achieve an energy saving of 21.3%.

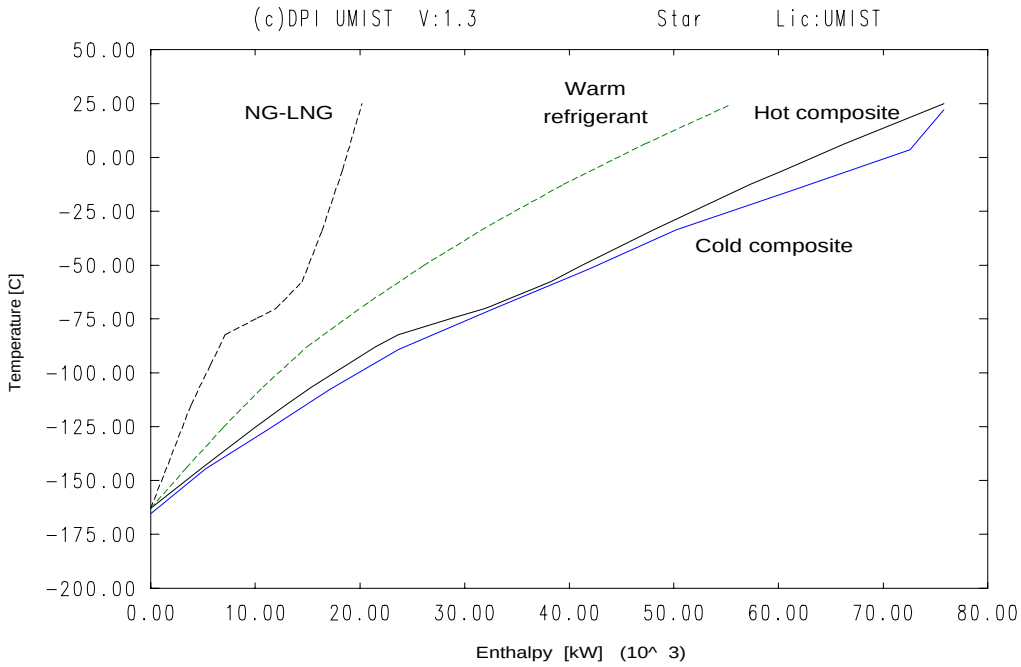

Figure 4-22. The composite curves of the final design.

Case Study 2

In this thesis, three different forms of objective function have been proposed, and each has its own characteristics and strengths. "Minimise shaftwork consumption" usually generates the design of the lowest shaftwork consumption, but can also result in wetness in the inlet stream to a compressor when the refrigerant flow rate is high. Since the refrigerant flow rate in the previous case study has been reduced significantly at the 5^{th} stage, it is safe to try using “Minimise shaftwork requirement” as the objective function in order to achieve further shaftwork saving. As shown in Table 4-4, a further 3.6% saving in shaftwork requirement is achieved at the $\{6'\}^{th}$ stage by switching the objective function form to “Minimise shaftwork requirement” from the $(5')^{th}$ step.

Table 4-4. Changing objective function since step 5.

	Pressure levels (bar)	Composition (wt %)	Refrigerant flow rate (kmol/s)	Shaftwork (kW)
5'	3.7 / 40.0	C1: 25.9 C2: 36.4 C3: 4.49 C4: 22.1 N2: 11.2	3.3	26679.9
6'	3.7 / 40.0	C1: 27.3 C2: 35.6 C3: 5.20 C4: 20.9 N2: 11.0	3.2	26601.5
7'	3.6 / 40.0	C1: 25.8 C2: 36.6 C3: 0.15 C4: 15.9 N2: 21.6	3.1	X (Temperature cross)

It demonstrates that different objective functions perform well under different conditions. The general guidelines are: while the refrigerant flow rate is still high, “Minimise crossover” and “Minimise sum of crossover” give satisfactory and reliable results. “Minimise shaftwork requirement” reaches greater saving when the refrigerant flow rate is reasonably low and thus less possibility for the compressor inlet stream having wetness. Using "Minimise crossover" or "Minimise sum of crossover" first is suggested as the objective function, and when the optimisation terminates, then switch to "Minimise shaftwork" to explore further possibility for shaftwork saving. Table 4-5 summarises the comparison with the commercial PRICO process (*Finn et al*., 1999).

Table 4-5. Comparison among commercial PRICO process and two design results.

	Commercial PRICO	PRICO by optimal selection of composition	PRICO by optimal selection of composition using different obj. functions
Refrigerant coposition	--	C_1~C_4, N_2	C_1~C_4, N_2
Wshaft (kJ/kg LNG)	1485.0	1168.6	1126.7

Case study 3

The default degree of temperature shifting is 5 °C. In this case study, different degrees of temperature shifting are tried to see the impact on the final optimisation results. To maintain consistency, “Minimise sum of crossover” is used as the objective function throughout case study 3. Table 4-6 lists the results by using different degrees of temperature shifting.

Table 4-6. Results by using different degrees of temperature shifting.

Temperature shifting degree (^{o}C)	Shaftwork (kW)
3	26857.9
4	27243.5
5	27591.5
6	29323.5
7	30142.8
8	31115.6

The optimal shaftwork consumption is progressively increased with the increasing degree of temperature shifting. This is in accordance with the fact that a bigger degree of temperature shifting for the pseudo-cold composite curve should generate a design with a wider gap between the hot and cold composite curves, thus more exergy loss within heat exchangers. In other words, a higher shaftwork consumption is required. This adds another dimension of complexity of finding the truly optimal trade-off between energy savings and capital costs.

4.8 Conclusions

Using mixtures as refrigerants in the design of refrigeration systems offers significant opportunities in search for the most energy efficient and compact design. MR systems have a great potential in many aspects. The systematic design of MR systems is extremely challenging but of great economic benefit. The difficulty in design mainly stems from two aspects: one is the expensive and the highly nonlinear nature of computation, and the other is the sensitivity of the systems to the operating changes, especially the change in the composition of refrigerant mixtures. There has been no

systematic synthesis method for the MR systems and as a result the operation of the existing systems can be far from the optimal conditions. In this thesis, a novel method for the selection of refrigerant compositions has been proposed by a combined NLP/thermodynamic approach. Rigorous thermodynamic methods for the VLE calculations, the the ϕ - ϕ approach, has been employed. The results of the search for the optimal composition of refrigerant mixtures are thus accurate. Based on this, a systematic synthesis tool for the complete design of MR systems has been developed. This approach combines the power of thermodynamics and mathematical programming. While the NLP can satisfactorily give the optimal choice of process operating conditions, thermodynamics at the same time gives the user insights and confidence in the solution. Three key design variables, the pressure levels of condensation and evaporation, the refrigerant flow rate, and the refrigerant composition, are also discussed. Refrigerant composition is the most flexible and significant variable among the three. A case study, using PRICO process as the base case, demonstrates that up to 25% saving in shaftwork requirement compared with commercial PRICO process can be achieved by using this method. This study also opens up the further possibility to achieve full automation of the design of MR systems and extend this method to more complex MR systems.

Nomenclature

Parameters and variables

A : a parameter in Peng-Robinson EOS as defined in eq.(4-7).

B : a parameter in Peng-Robinson EOS as defined in eq. (4-8).

C : number of components in Gibbs Phase Rule.

F : degrees of freedom in Gibbs Phase Rule.

$\bar{f}_i^L$: fugacity of component *i* in liquid phase mixture.

$\bar{f}_i^V$: fugacity of component *i* in vapour phase mixture.

G^{EX} : excess Gibbs free energy.

h^{IGM} : enthalpy of an ideal gas mixture.

h_i^L : enthalpy of the liquid phase in the i^{th} interval.

h_i^V : enthalpy of the vapour phase in the i^{th} interval.

h_{ti} : enthalpy of fluid at the inlet of throttling valve.

h_{to} : enthalpy of fluid at the outlet of throttling valve.

L_i : liquid mass flow rate in interval *i*.

J : number of components.

M : number of independent reactions in Gibbs Phase Rule.

N : number of intervals.

P : pressure.

P_c : critical pressure.

Q : number of phases in Gibbs Phase Rule.

R : universal gas constant.

T : temperature.

T_c : critical temperature.

$\overline{T}_i$: temperature of interval *i* on the pseudo-cold composite curve.

$\hat{T}_i$: temperature of interval *i* on the real cold composite curve.

$T_{j,i}^h$: temperature of the *j*th hot stream in interval *i*.

T_{ti} : temperature of a fluid at the inlet of a throttling valve.

T_{to} : temperature of a fluid at the outlet of a throttling valve.

V_i : vapour mass flow rate in interval *i*.

$\overline{V}_i$: specific volumn of component *i* in a mixture.

$\overline{V}_i^{IGM}$: specific volumn of component *i* in an ideal gas mixture.

WS_j : shaftwork requirement of compressor *j*.

Z : compressibility factor.

$X_{j,i}$: mole fraction of component *j* in interval *i* in liquid phase.

$Y_{j,i}$: mole fraction of component *j* in interval *i* in vapour phase.

x : a vector of composition of liquid phase.

y : a vector of composition of vapour phase.

Greek letters

ϕ_i : fugacity coefficient of component *i*.

ω : acentric factor.

γ : activity coefficient.

ξ : a vector of all continuous variables.

ξ' : a subset of ξ, comprising the mole fraction of each component.

ξ' : the upper bound of vector ξ.

ξ'' : the lower bound of vector ξ.

δ : specified minimum temperature approach.

References

Bellow E. J., Ghazal Jr. F. P., Silverman A. J., 1997, Technology advances keeping LNG cost-competitive, *Oil & Gas Journal*, **June 2**, 74-78.

Bensafi A., Haselden G. G., 1994, Wide-boiling refrigerant mixtures for energy saving, *Intl. J. Refrig.*, **17 (7)**, 469-474.

Duvedi A., Achenie L. E. K., 1997, On the design of environmentally benign refrigerant mixtures: a mathematical programming approach, *Computers chem. Engng*, **21 (8)**, 915-923.

Finn A. J., Johnson G. L., Tomlinson T. R., 1999, Developments in natural gas liquefaction, *Hydrocarbon Processing*, April, p. 47-59.

Gaumer L. S., Newton C. L., 1971, *U.S. Patent* 3,593,535.

Haselden G. G., Barber N.R., 1957, *Trans. Inst. Chem. Engrs.*, **35 (2)**, 77.

Kinard G. E., Gaumer L. S., 1973, Mixed refrigerant cascade cycles for LNG, *Chemical Engineering Progress*, **69 (1)**, 56-61.

Lamb R., Foumeny E. A., Haselden G. G., 1996, The use of wide boiling refrigerant mixtures in water chiller units for power saving, *The 1996 IChemE Research Event/Second European Conference for Young Researchers*, 223-225.

Lee M. J., Sun H. C., 1992, Thermodynamic property prediction for refrigerant mixtures, *Ind. Eng. Chem. Res.*, **31**, 1212-1216.

Linnhoff B. Townsend D. W., Boland D., Hewitt, G. F., Thomas B. E. A., Guy A. R., Marsland R. H., 1991, *A User Guide on Porcess Integration for the Efficient Use of Energy*, The Institute of Chemical Engineers.

MacKenzie D. H., Donnelly S. T., 1985, Mixed refrigerants proven efficient in natural-gas liquids recovery process, *Oil & Gas Journal*, **Mar 4** 116-120.

Patel N. C., Teja A. S., 1982, A new cubic equation of state for fluids and fluid mixtures, *Chemical Engng Science*, **37 (3)**, 463-473.

Perret J. C., 1968, *U. S. Patent* 3,364,685.

Podbienlniak W. J., 1936, *U. S. Patent* 2,041,725.

Price B. C., Mortko R. A., 1996, PRICO – A simple, flexible proven approach to natural gas liquefaction, *17th International LNG/LPG Conference*, Gastech '96, Vienna, Vol. 2, Session 7, Part 1, Dec 1996.

Pua L. M., Lee G. C., Zhu X. X., Plate-fin Heat Exchanger Network Synthesis Considering Process Changes, *AIChE 2000 Spring Meeting*, Atlanta, March 5-9, 2000.

Radermacher R., 1989, Thermodynamic and heat transfer implications of working fluid mixtures in Rankine cycles, *Int. J. Heat and Fluid Flow*, **10 (2)**, 90-101.

STAR , Department of Process Integration, UMIST, Manchester, United Kingdom.

Steed J. M., 1989, Present uses of chlorofluorocarbons and effects due to environment regulations. *Intl. J. Thermophys.* **10**, 545.

5 SYNTHESIS OF COMPLEX MIXED-REFRIGERANT SYSTEMS

5.1 Introduction

In the previous chapter, a new systematic synthesis method for the design of single-stage mixed refrigerant systems has been introduced. This method uses thermodynamics to define the objective function, and then applies an NLP model to optimise the composition of refrigerant mixtures. In this chapter, the method will be extended to the design of advanced mixed refrigerant systems. As will be shown, a complex mixed refrigerant system can be more flexible and energy efficient than a single-stage mixed refrigerant system.

In a single-stage mixed refrigerant (MR) system, the whole of the mixed refrigerant is compressed and passes through a main heat exchanger where the refrigerant is condensed and subcooled. The refrigerant flow rate is usually high. For example, in LNG applications, the flow rate of mixed refrigerant can be as high as three times that of natural gas feed flow. This results in large exergy losses in the processes, hence low efficiency. To overcome this problem, several improved MR systems have been proposed.

Paradowski *et al*. (1984) classified complex MR systems, according to their types of condensation, condensing agents and operating temperature ranges, into four different categories:

Type A: systems having *total* condensation by means of an external agent (cooling water or air) and evaporation at several pressure levels. The useful temperature range is from 30°C to -75°C. Typical application is NGL recovery.

Type B: systems having *partial* condensation by means of an external agent (cooling water or air) and evaporation after self-subcooling at a single pressure level. The useful temperature range is from 30°C to -170°C. Typical application is small-scale LNG plant (peak shaving).

Type C: systems having *total* condensation by means of refrigeration, either of the conventional type such as a propane cycle, or an MR systems of type A. Evaporation takes place after self-subcooling at a single pressure level. The useful temperature range is from -30°C down to -110°C. Typical applications include steam cracking.

Type D: systems having *partial* condensation by means of refrigeration, either of the conventional type such as a propane cycle or an MR systems of type A. Evaporation takes place after self-subcooling at a single pressure level. The useful temperature range can extend from -30°C down to -170°C. a typical example is large-scale LNG production (base load).

Therefore, a complex MR system can be a multistage MR system rejecting heat to an external cooling agent, a cascade system comprising a conventional pure refrigerant system and an MR system, or a cascade system comprising two MR systems. The design of a complex MR system requires the ability to deal with both conventional pure refrigerant systems and MR systems, and the ability to find the optimal partition separating two systems.

Alternatively, MR systems can be categorised as two different types of operation: closed systems and open systems. In a closed MR system, refrigerant and feed do not mix, i.e. each circulates in a closed cycle. A typical example of closed MR system is shown in Figure 5-1.

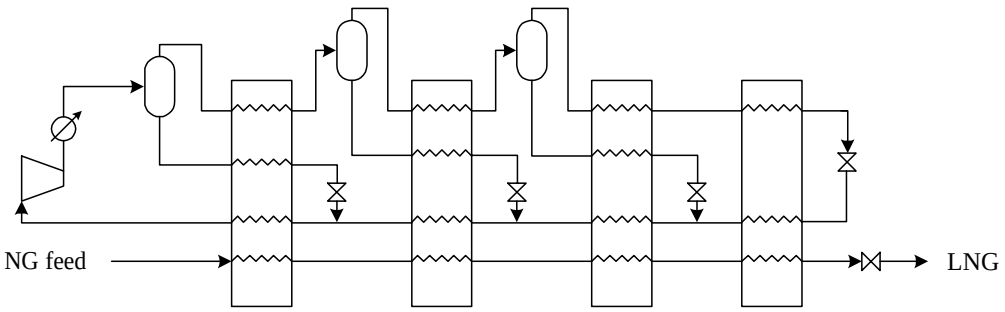

Figure 5-1. A four-stage closed MR system.

On the other hand, an open system uses the components of the feed gas to cool the feed by heat exchange or internal refrigeration. Figure 5-2 shows an open cycle. In

this way, the outside purchase of, and storage facilities for, refrigerants can be minimised.

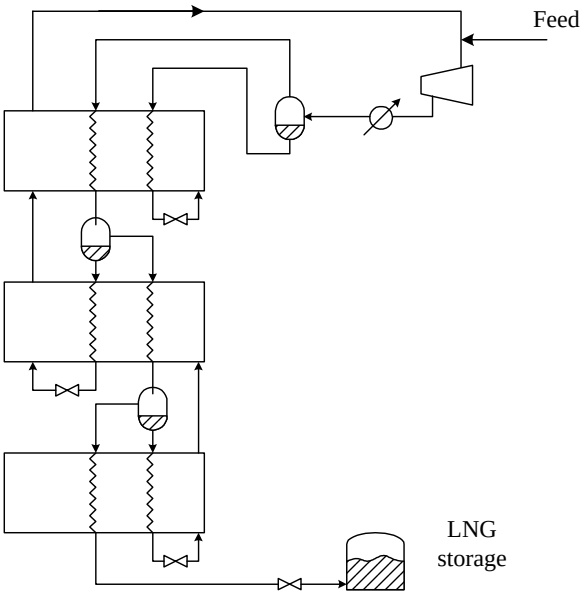

Figure 5-2. A three-stage open MR system.

A complex MR system usually comprises multiple evaporation/condensation stages. The optimum number of stages of partial condensation, separation and expansion is itself a trade-off between energy and capital costs. It depends on the relative importance of energy efficiency, capital investment, flexibility requirements and complexity of operation. Lower shaftwork consumption can be expected if the number of stages is increased, but inevitably results in greater complexity and difficulty in control. Moreover, the effect of reducing shaftwork consumption by increasing the number of stages is progressively diminishing. As an optimal number of stages is reached, any further installed stage will have minimal benefit on energy saving, and only increase the complexity and the overall costs. An evaluation by Costain, acording to Finn *et al*. (1999), shows the effect of increasing number of stages against shaftwork consumption, as shown in Table 5-1.

Table 5-1. The effect of increasing number of stages on shaftwork consumption.

Number of stages	Shaftwork requirement relative to one stage process
1	1

2	0.93
3	0.90
4	0.88
5	0.87

Therefore, in the design of multistage MR systems, the number of stages is a problem of optimisation.

It is generally perceived that MR systems, given that the many advantages compared with conventional cascade refrigeration systems, are very inflexible in operations and the performance of the systems depends entirely on the accuracy of the original designs. This is contradicted by fact that an MR system has more degrees of freedom in control and design than a conventional cascade, thus more flexibility should in theory be expected. Although the close approach between the hot and cold streams and the tight integration among heat exchange, compression and expansion make MR systems difficult to design and control, the major reason for this contradiction is believed to be the lack of thorough understanding and systematic design methods for complex MR systems.

A complete design method for complex MR systems needs to have ways to deal with the design of conventional pure-refrigerant systems, the design of multistage MR systems, and the integration, or "cascade", of the two systems. In Chapter 2, a new design method was presented, by combining shaftwork targeting and MINLP, for the pure-refrigerant multistage or cascade refrigeration systems. This method is equally applicable to the design of pure-refrigerant systems in complex MR systems.

In this chapter, the design method for single-stage MR systems, which was introduced in Chapter 4, is first extended to the design of multistage MR systems. Then, a new and systematic design method for synthesis of complex MR systems is proposed. For type A and B systems, the design method for multistage MR systems is applied. For type C and D systems having a cascade of two multistage MR systems, a modified approach, with considering the partition of the two systems by using the grand composite curve (GCC), is proposed. For type C and D systems having a cascade of a pure-refrigerant cycle and a multistage MR cycle, the design method introduced in

Chapter 2 for pure-refrigerant systems is applied to the pure-refrigerant cycle, and the design method for multistage MR systems is applied to the MR cycle. The optimal partition of the two systems is considered by using the GCC and optimisation.

5.2 Characteristics of Multistage MR Systems

The major difference that distinguishes multistage MR systems from single-stage MR systems is that the whole refrigerant flow does not circulate through the overall heat transfer area. For example, Figure 5-3 illustrates a two-stage MR system for liquefaction of natural gas. The compressed refrigerant mixture from the compressor is first partially condensed by an external heat sink, and then separated in the knock-out drum (S-1) into vapour and liquid flows. The vapour flow is partially condensed in the first heat exchanger (E-1), split into vapour and liquid flows in the knock-our drum (S-2), and passed to the second heat exchanger (E-2). On the other hand, subcooled liquid flow from E-1 is expanded to compressor inlet pressure and mixed with the returning refrigerant flow from E-2. The heat exchanger E-2 serves to further subcool the natural gas feed and the vapour and liquid streams from S-2. The vapour is now totally condensed and mixed with the subcooled liquid stream. The combined stream is expanded to compressor inlet pressure and then flows countercurrently in heat exchangers E-1 and E-2. It cab be seen that the liquid flow after E-1 does not pass through E-2. This has two significant effects on the performance of an MR system. First, only part of refrigerant circulates through the overall heat transfer surface, thus reducing exergy losses within heat exchangers. Second, the amount of refrigerant flow in each heat exchanger is different, adding one more degree of freedom in the design of MR systems. This extra degree of freedom creates opportunities to achieve a more efficient design, but, on the other hand, it also causes more complexities in the modelling of MR systems.

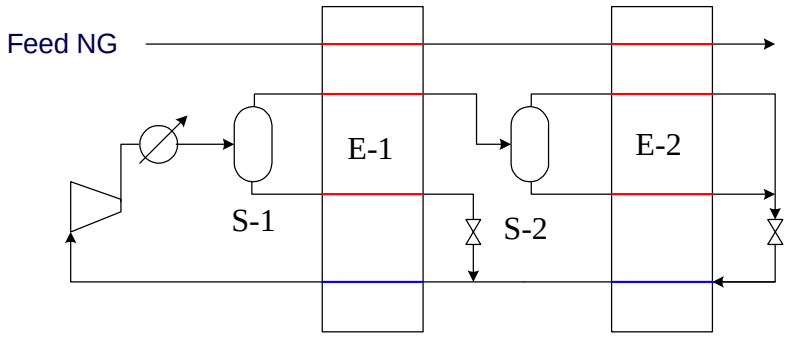

Figure 5-3. A two-stage MR system for LNG

It is reasonable to assume that all outlet streams from the same heat exchanger have equal temperatures. Thus, the natural gas feed, the precooled vapour and the subcooled liquid at the outlet of E-1 are all of the same temperature. The temperature, called "intermediate temperature" of each stage, plays a significant role effecting the performance of MR systems. The following example illustrates the characteristics of the intermediate temperature. As shown in Figure 5-4, the composite curves of a two-stage MR system, having the intermediate temperature at -60°C, exhibit a temperature cross. This means the heat transfer process within the heat exchanger is infeasible. To overcome this problem, the intermediate temperature is changed to -120°C. The temperature cross problem is then avoided, and the shaftwork consumption of this system remains the same. Figure 5-5 shows the results. Changing the intermediate temperatures alone, however, has no effect on the shaftwork consumption. But, because it can alter the shape of the hot and cold composite curves, the design actually has more opportunities to achieve lower shaftwork consumption by reducing the amount of refrigerant flow, changing the refrigerant composition, or changing the evaporation\condensation pressures of refrigerant mixtures. For instance, after the intermediate temperature is changed to -120°C, we can try using a lower refrigerant flow to reduce the shaftwork requirement in the compressor.

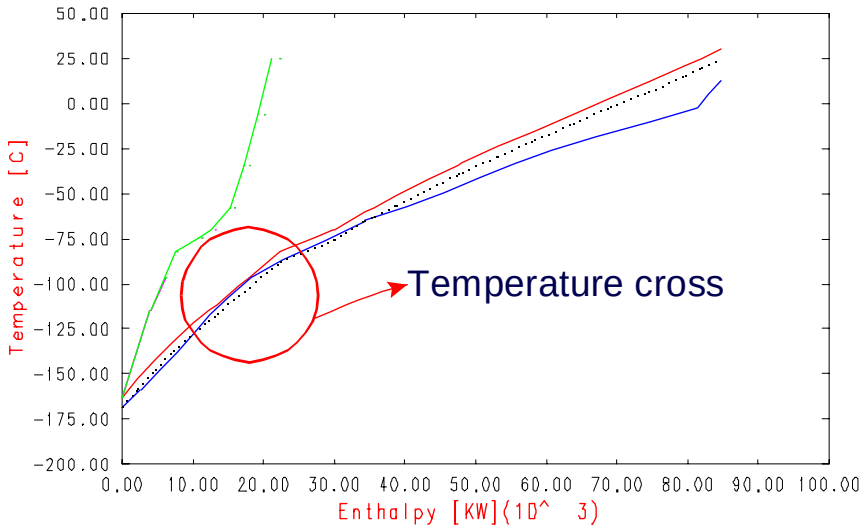

Figure 5-4. The composite curves of a two-stage MR system. Intermediate temperature = -60 °C, shaftwork consumption = 32436.5 kW

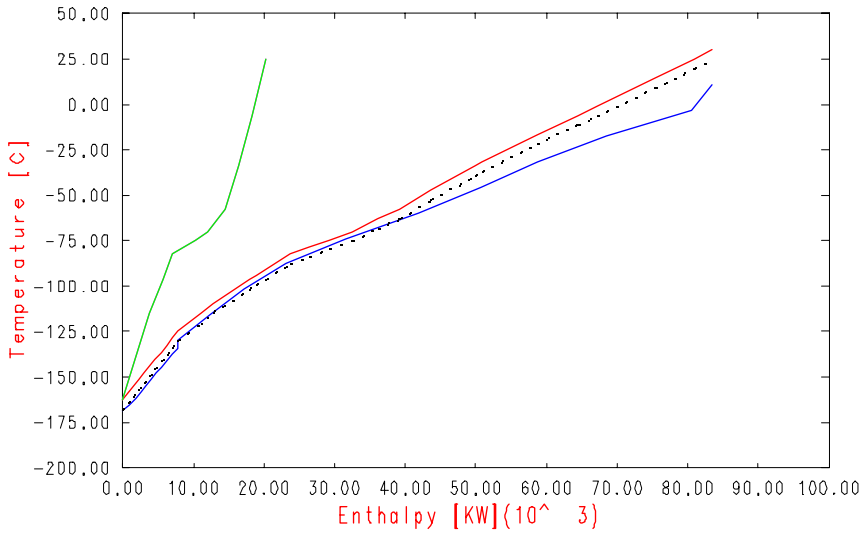

Figure 5-5. The composite curves of a two-stage MR system. Intermediate temperature = -120 °C, shaftwork consumption = 32436.5 kW

In summary, introducing more stages into an existing MR system helps reduce energy consumption indirectly by creating more opportunities for lower refrigerant circulating amount or reducing pressure gap between condensation and evaporation. Changing intermediate temperatures is therefore a way to seek better “distribution” of refrigeration duty throughout MR systems.

5.3 Modelling of Multistage MR Systems

A multistage MR system can be conceptually viewed as a heat exchanger device having serially connected single-stage MR systems. As a result, a multistage MR system can be decomposed into a series of single-stage MR systems, as Figure 5-6 illustrates. The unit of the l^{th} stage is effectively the building element for each stage in a multistage MR system, except for the first stage where the precooled vapour and subcooled liquid refrigerant mix together and return countercurrently back to the main heat exchanger and for the N^{th} stage where a compressor and a partial condenser are attached. So the modelling of a multistage MR system needs first to model the l^{th} stage and repeat it for the rest stages unless some modifications are required.

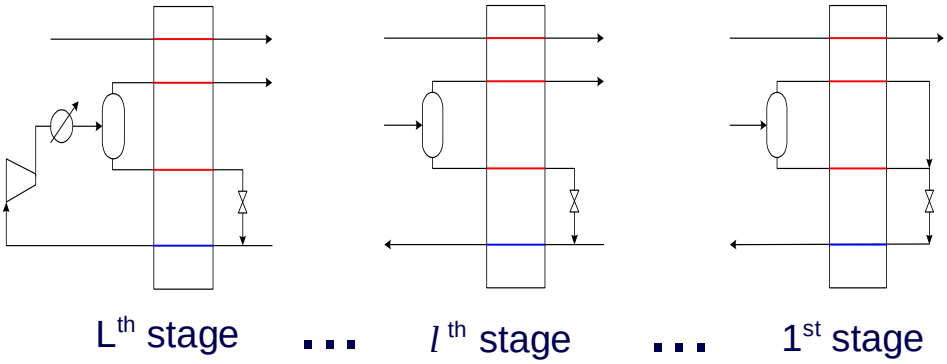

Figure 5-6. The decomposition of a multistage MR system.

The method of the optimal selection of refrigerant composition for single-stage MR systems proposed in Chapter 4 can be applied to each stage in a multistage MR system. The only modification is the objective function should consider the whole system rather than any single stage. For the l^{th} stage, the modelling work starts with building the hot composite curve with given refrigerant flow rate, composition, and evaporation/condensation pressures. The hot composite curve is than shifted down by a certain temperature difference, say 5 °C, to generate the "pseudo-cold composite curve". The pseudo-cold composite curve is the "target" for the objective function. The modelling of the l^{th} stage can be illustrated in Figure 5-7. The whole heat exchanger in this work is divided according to temperature intervals into N segments. Mass, energy and composition balances and phase equilibrium and relevant constraints are calculated and satisfied for each segment therefore build up the

complete temperature profile of each stream. The subscript *i* denotes the number of segments in a stage, the subscript *j* the number of components and the subscript *l* the number of stages.

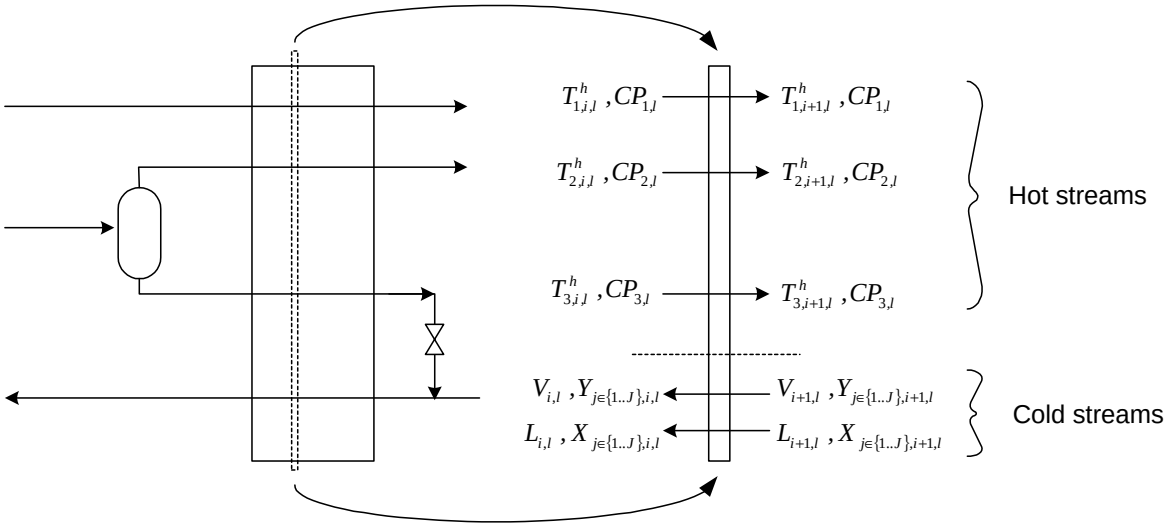

Figure 5-7. System boundary of the l^{th} stage for balance equations.

Here the detailed modelling of cold composite curve, the evaporation line of refrigerant, of the l^{th} stage is listed:

mass and composition balance

$$L_{i,l} + V_{i,l} = L_{i+1,l} + V_{i+1,l} \qquad \forall i \in \{1 \ldots N\}; \forall l \in \{1 \ldots L\} \qquad (5\text{-}1)$$

$$X_{j,i,l} \cdot L_{i,l} + Y_{j,i,l} \cdot V_{i,l} = X_{j,i+1,l} \cdot L_{i+1,l} + Y_{j,i+1,l} \cdot V_{i+1,l} \qquad \forall i \in \{1 \ldots N\}; \forall j \in \{1 \ldots J\}; \forall l \in \{1 \ldots L\} \qquad (5\text{-}2)$$

N is the number of segment we choose to model the l^{th} stage. J is the number of component for the refrigerant mixture. L is the number of stages in the system.

energy balance

$$L_{i,l} \cdot h_{i,l}^{L} + V_{i,l} \cdot h_{i,l}^{V} = L_{i+1,l} \cdot h_{i+1,l}^{L} + V_{i+1,l} \cdot h_{i+1,l}^{V} + \sum_{k} CP_{k,l} \cdot \left(T_{k,i,l}^{h} - T_{k,i+1,l}^{h}\right)$$

$$\forall i \in \{1 \ldots N\} \; ; \forall k \in \{1 \ldots K\}; \forall l \in \{1 \ldots L\} \qquad (5\text{-}3)$$

K is the number of hot streams that undergo temperature change from $T_{k,i,l}^{h}$ to $T_{k,i+1,l}^{h}$. The hot streams are calculated beforehand since this proposed method requires knowing hot composite curve to generate the pseudo-cold composite curve.

phase equilibrium

$$Y_{j,i,l} \cdot \phi_{j}^{V}\left(p, \hat{T}, \overline{Y}\right) = X_{j,i,l} \cdot \phi_{j}^{L}\left(p, \hat{T}, \overline{X}\right) \qquad \forall i \in \{1 \ldots N\} \; ; \forall j \in \{1 \ldots J\}; \forall l \in \{1 \ldots L\} \qquad (5\text{-}4)$$

As discussed in the previous chapter, the phase equilibrium is formulated by the ϕ - ϕ approach. Peng-Robinson EOS is applied to calculate the fugacity coefficients for both vapour and liquid phases. An iterative computation is needed for this constraint.

sum of mole fractions

$$\sum_{j} Y_{j,i,l} = 1 \qquad \forall i \in \{1 \ldots N\} \; ; \forall j \in \{1 \ldots J\}; \forall l \in \{1 \ldots L\} \qquad (5\text{-}5)$$

$$\sum_{j} X_{j,i,l} = 1 \qquad \forall i \in \{1 \ldots N\} \; ; \forall j \in \{1 \ldots J\}; \forall l \in \{1 \ldots L\} \qquad (5\text{-}6)$$

evaporation temperature of a mixture, $\hat{T}$

$$\hat{T}_{i,l} = T\left(P, \overline{X}\right) \qquad \forall i \in \{1 \ldots N\}; \forall l \in \{1 \ldots L\} \qquad (5\text{-}7)$$

$\overline{X}$ is a vector containing the composition of each component in the liquid phase.

generating of $\overline{T}$

$$\overline{T}_{i,l} = \tilde{\tilde{T}}_{i,l} - \delta \qquad \forall i \in \{1 \ldots N\} \; ; \forall l \in \{1 \ldots L\} \qquad (5\text{-}8)$$

$\tilde{\tilde{T}}_{i,l}$ is the temperature on the hot composite curve for the i^{th} segment in the l^{th} stage. Details of construction of composite curves refer to Linnhoff *et al.* (1991) and Biegler *et al.* (1997).

physical property constraints

$$h_{i,l}^{L} = h^{L}\left(P, \hat{T}, \overline{X}\right) \qquad \forall i \in \{1 \ldots N\} \; ; \forall l \in \{1 \ldots L\} \qquad (5\text{-}9)$$

$$h_{i,l}^{V} = h^{V}\left(P, \hat{T}, \overline{Y}\right) \qquad \forall i \in \{1 \ldots N\} \; ; \forall l \in \{1 \ldots L\} \qquad (5\text{-}10)$$

After-throttling and after-mixing refrigerant temperature

$$\begin{aligned} & T_{to} = f\left(T_{ti}, P_{ti}, P_{to}, \overline{X}_{ti}\right) \\ & s.t. \;\; h_{to} = h_{ti} \end{aligned} \qquad (5\text{-}11)$$

The above equation states that after-throttling the refrigerant temperature is a function of temperature, pressure and compositions of throttle inlet liquid and throttle outlet pressure, subject to isenthalpic changes. The after-mixing refrigerant temperature can be calculated as mass-averaged temperature:

$$T_{mx} = \frac{\dot{m}_{to} \cdot T_{to} + \dot{m}_{(l^{th}-1)-(l^{th})} \cdot T_{(l^{th}-1)-(l^{th})}}{\dot{m}_{to} + \dot{m}_{(l^{th}-1)-(l^{th})}} \qquad (5\text{-}12)$$

The subscript $(l^{th}\text{-}1)\text{-}(l^{th})$ indicates refrigerant flowing from $l^{th}\text{-}1$ stage to l^{th}. This relation corresponds to the discontinuity on the cold composite curve at each intermediate temperature. For the first stage, $\dot{m}_{(l^{th}\text{-}1)\text{-}(l^{th})} = 0$ so T_{mx} is equal to T_{to}.

pressure profile constraint

$$P_{i,l} = P_{i+1,l} + \sigma \qquad \forall i \in \{1 \ldots N\}\ ; \forall l \in \{1 \ldots L\} \qquad (5\text{-}13)$$

mole fractions constraints

$$0 \le Y_{j,i,l} \le 1 \qquad \forall i \in \{1 \ldots N\}\ ; \forall j \in \{1 \ldots J\}; \forall l \in \{1 \ldots L\} \qquad (5\text{-}14)$$

$$0 \le X_{j,i,l} \le 1 \qquad \forall i \in \{1 \ldots N\}\ ; \forall j \in \{1 \ldots J\}; \forall l \in \{1 \ldots L\} \qquad (5\text{-}15)$$

temperature approach constraint

$$\hat{T}_{i,l} < \overline{T_{i,l}} + \delta \qquad \forall i \in \{1 \ldots N\}\ ; \forall l \in \{1 \ldots L\} \qquad (5\text{-}16)$$

This constraint states that everywhere the temperature on the cold composite curve should be colder than that on the hot composite curve. In this way, heat transfer validity within a heat exchanger is enforced.

As introduced in the previous chapter, there are three different forms of objective function, namely minimise crossover, minimise sum of crossover, and minimise shaftwork requirement. When considering multistage MR systems, the three different objective functions are modified as follows:

1) Minimise crossover

$$\text{Minimise} \quad \max\left(\left|\overline{T_{i,l}} - \hat{T}_{i,l}\right|\right) \qquad i \in N,\ l \in L \qquad (5\text{-}17)$$

$$\text{Subject to} \quad \hat{T}_{,il} < \overline{T_{i,l}} + \delta \qquad i \in N,\ l \in L$$

2) Minimise sum of crossover

$$\text{Minimise} \quad \sum_{l=1}^{L}\sum_{i=1}^{N} \max\left\{0,\ \left(\overline{T_{i,l}} - \hat{T}_{i,l}\right)\right\} \quad i \in N,\ \ l \in L \qquad (5\text{-}18)$$

$$\text{Subject to} \quad \hat{T}_{i,l} < \overline{T_{i,l}} + \delta \qquad i \in N,\ l \in L$$

The above two forms of objective function are modified with the inclusion of another subscript *l*, which indicates the number of stages from 1 to L. The physical meanings are the same as the ones introduced in previous chapter.

3) Minimise shaftwork requirement

$$\text{Minimise} \qquad \sum_{j=1}^{M} WS_j \tag{5-19}$$

$$\text{Subject to} \qquad \hat{T}_{i,l} < \overline{T_{i,l}} + \delta \qquad i \in N,\ l \in L$$

This objective function is unchanged regardless of the number of stages in the systems. However, care needs to be taken that the temperature approach constraint has another subscript, *l*, included.

5.4 New Method for the Design of Complex MR Systems

A complex MR system, according to Paradowski's classification, can be a multistage MR system, a hybrid cascade of a conventional pure-refrigerant system and an MR system, or a hybrid cascade of two MR systems. To systematically design a complex MR system, therefore, it is essential that the method developed needs to have the ability to deal with a conventional pure-refrigerant system and an MR system, and simultaneously optimise their partition. In this thesis, we shall focus on the complex MR system having a conventional multistage pure-refrigerant system and a multistage MR system. A complex MR system of such type for LNG application is shown in Figure 5-8. A typical example of this kind is the widely used propane-precooled multistage MR systems for base-load LNG plants. The refrigeration system is a complex MR system having a three-stage pure-refrigerant cycle and a two-stage MR cycle. Natural gas at ambient temperature is progressively cooled at three evaporators of the pure-refrigerant (usually propane) cycle, and then goes through two-stage subcooling at the MR cycle until the final desired temperature for LNG is reached. The compressor outlet vapour of a multistage MR system is partially condensed by the conventional pure-refrigerant system. All condensing heat from the pure-

refrigerant system is rejected to an external agent (cooling water or air). This kind of system, a specific kind of Type D, is shown in Figure 5-9. The multistage MR system operates in the lower temperature part, while the conventional pure-refrigerant system operates in the higher temperature part. Their partition temperature is a major parameter to concern.

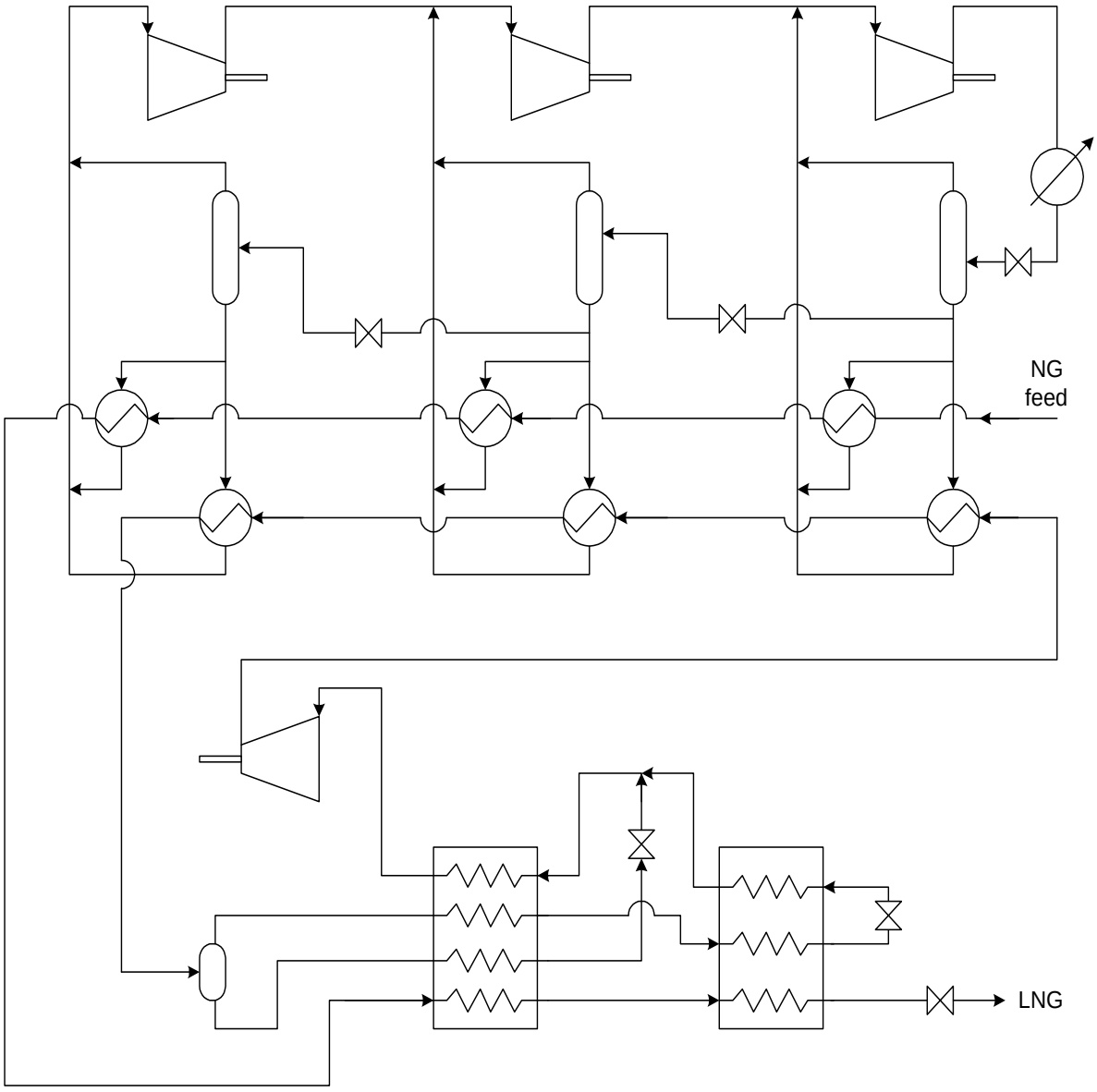

Figure 5-8. A complex MR system comprising of a multistage pure-refrigerant cycle and a multistage MR cycle.

In Chapter 2, an optimal synthesis method for cascade refrigeration systems has been proposed. The method uses shaftwork targeting to optimise major parameters of a refrigeration system, and then employs a disjunctive-programming-enhanced MINLP model to exploit all design options. The partition temperature is also optimised in the shaftwork targeting stage. In the previous chapter, a systematic synthesis method of single-stage MR systems was introduced. Based on the combination of the two, a novel synthesis method for complex MR systems can be developed.

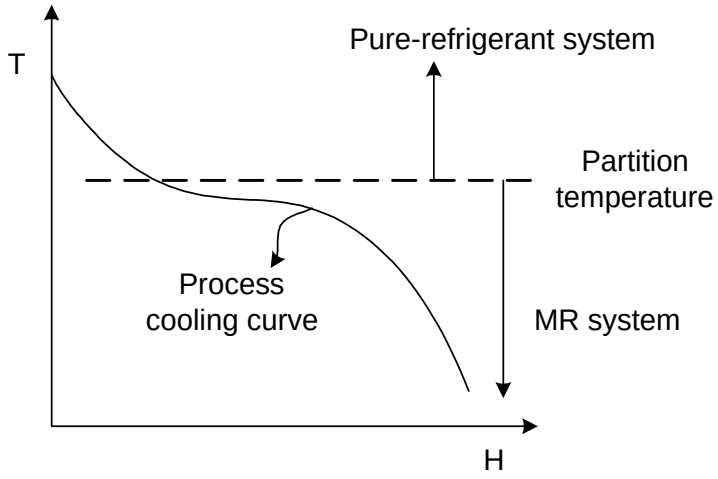

Figure 5-9. A split of process cooling curve.

The method comprises three steps, as illustrated in Figure 5-10. First, as illustrated in Figure 5-10a, process stream data are collected to draw the process cooling curve. An initial partition temperature is set to allow the split of the process cooling curve into two parts: the high-temperature part and the low-temperature part. Then, as Figure 5-10b shows, the optimal synthesis method of multistage MR systems is applied to the low-temperature part of the process cooling curve. Condensing heat from the multistage MR system is rejected to the pure-refrigerant system at the partition temperature. The process cooling curve is modified to include the rejected heat from the multistage MR system. Note that in Figure 5-10b the high-temperature part of the modified process cooling curve starts from a higher temperature, reflecting the fact that the compressor outlet vapour is usually superheated to high temperature, and has a close-to-flat slope, as shown in dashed line. This represents condensation of a major part of the MR refrigerant. Because of the non-constant nature of condensing temperatures of refrigerant mixtures, it is safe to define the partition temperature as

the lowest temperature in the condensing curve. Finally, as in Figure 5-10c, the modified high-temperature part of the process cooling curve is used to design the multistage pure-refrigerant system, by applying the method developed in Chapter 2. Often the modified process cooling curve has the highest temperature, as a result of the compressor outlet temperature of the MR system, start well above ambient temperature. Instead of using refrigeration systems, ambient heat sink, air or cooling water, is used to absorb this part of heat from the process. This situation will be demonstrated later in case study 2 in detail.

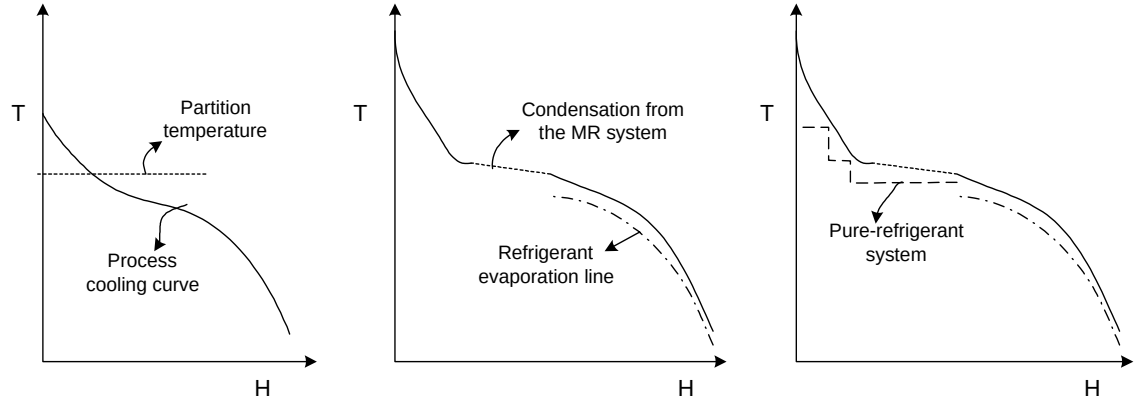

Figure 5-10. Procedures of design of a complex MR system.

Figure 5-11 summarises the flow of the new approach. The whole procedure iterates to try different values of partition temperature until the optimisation criteria is met or the optimal value of the objective function.

The full synthesis procedures have been implemented in the latest version of STAR. Figure 5-12 shows the interface of the function of the design of MR systems in STAR.

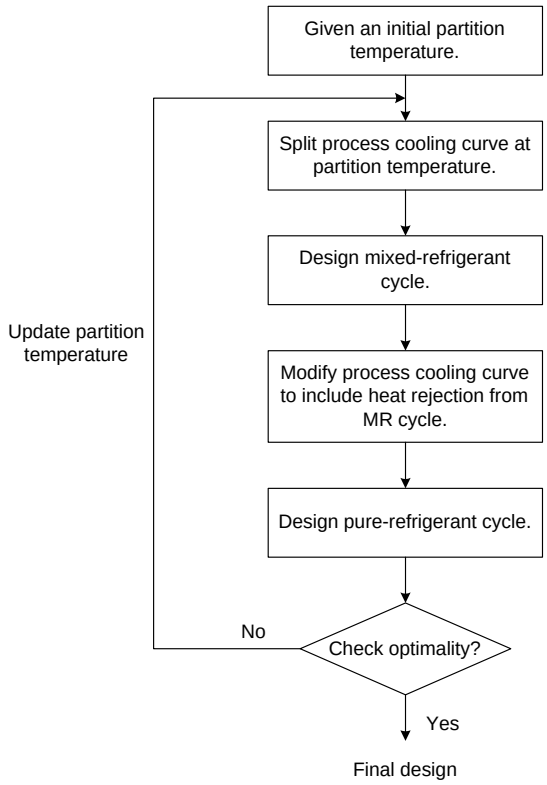

Figure 5-11. The proposed strategy for synthesis of complex MR system.

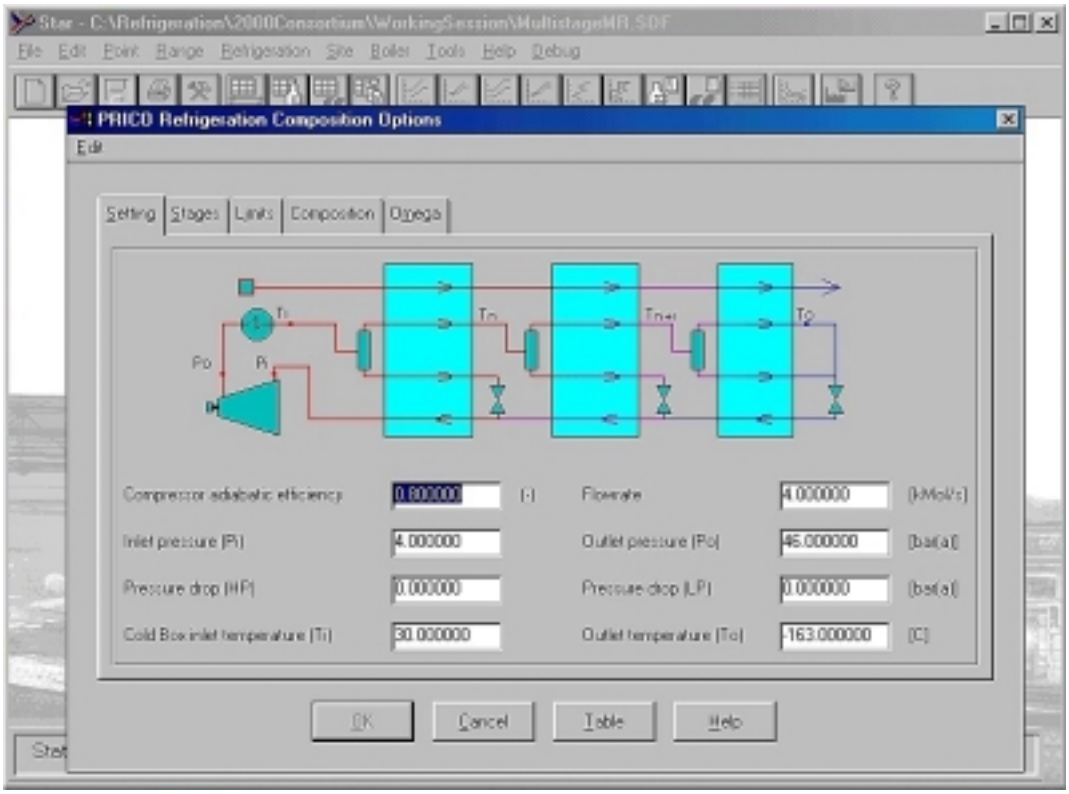

Figure 5-12. A snapshop of the user interface in STAR for design of complex MR systems.

5.5 Case Study

Case study I – design of a multistage MR system

In this case study the features and practicality of the proposed method for multistage MR systems is demonstrated. Given the natural gas feed conditions and the LNG product conditions, as illustrated in Figure 5-13, the proposed method is applied to design a two-stage MR system to satisfy the process cooling demand. For the purpose of comparison, the process conditions are set the same as in the case study in the previous chapter.

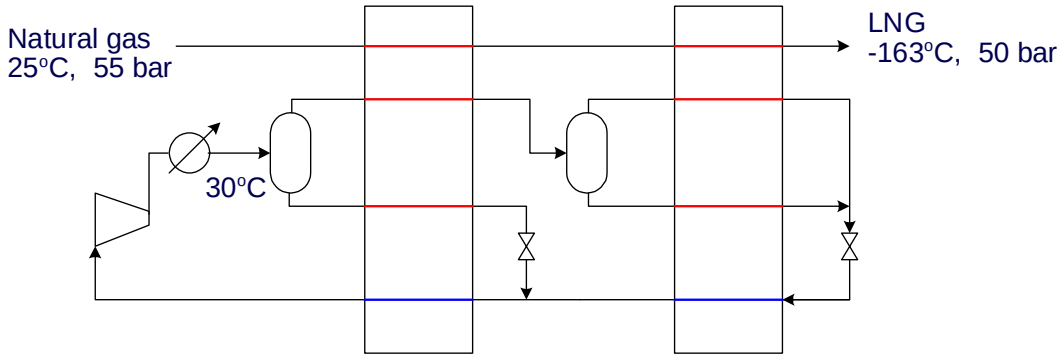

Figure 5-13. The design task – a two-stage MR system.

The first step is to establish the GCC of the natural gas cooling curve, as shown in Figure 5-14.

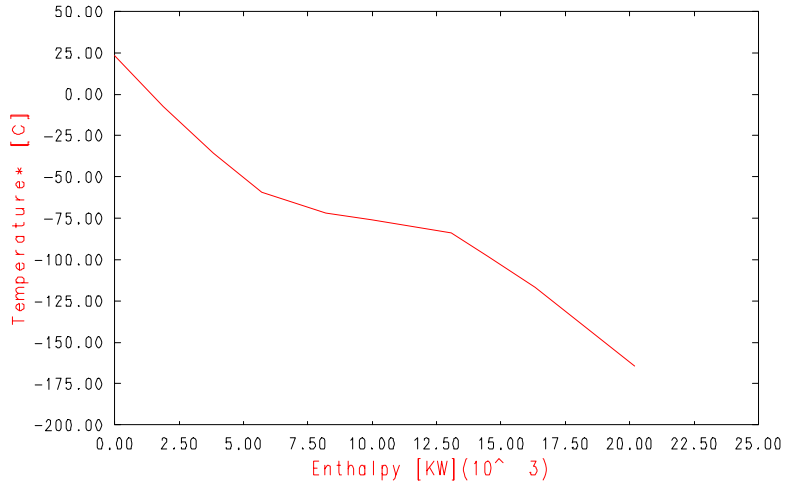

Figure 5-14. The GCC of the natural gas cooling curve.

The initial intermediate temperature is set as –100 ^{o}C. Under the initial conditions, the design is invalid since temperature crosses occur within the heat exchanger. The first step uses the proposed approach for the optimal selection of mixed refrigerant compositions and generates a feasible design. However, when the process composite curves of the first design, as shown in Figure 5-15, is checked, we can see the temperature difference above the intermediate temperature is wide while that below the intermediate temperature is very small. The discontinuity at an intermediate temperature reflects the fact that two streams of different temperatures mix together, one is the expanded refrigerant from the first exchanger and the other is the evaporated refrigerant from the second exchanger. To help reduce refrigeration duty below the intermediate temperature, the intermediate temperature is updated to –120 ^{o}C.

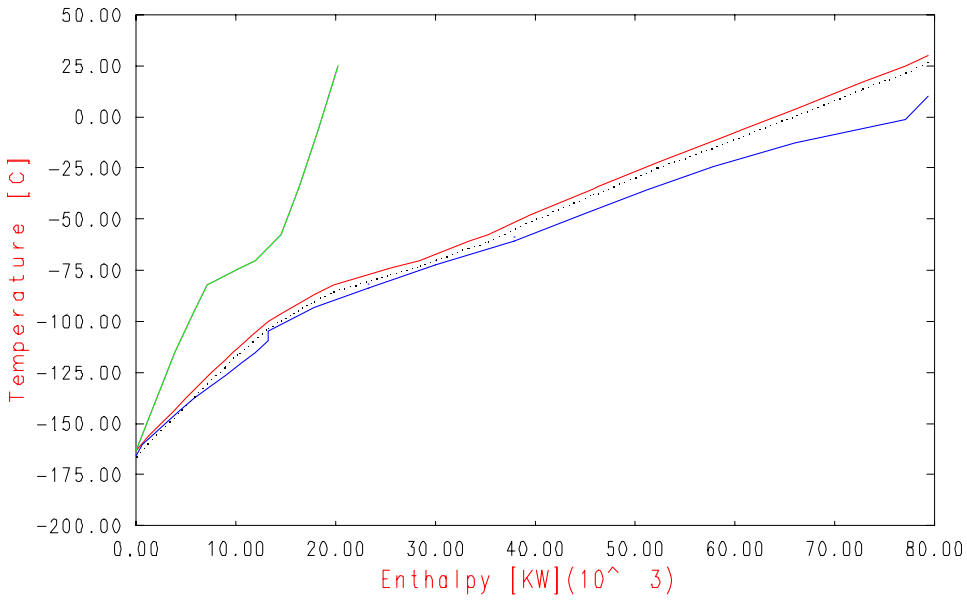

Figure 5-15. The GCC of the results from the first step optimisation.

In the second step, not only the intermediate temperature is lowered but also the refrigerant flow rate is reduced. In this way, there is a 6.6% reduction in shaftwork from the first step. Step three to six continue the same philosophy to reduce the shaftwork consumption. The overall optimisation stops at the 6th step, where a permanent temperature cross problem occurs. The results from the 5th step are then picked as the final design, which has the intermediate temperature at –125 ^{o}C and

refrigerant flow rate reduced to 3.1 kmol/s. The shaftwork consumption of the final design is reduced by more than 21% compared with the results from the first step. Overall optimisation procedures are summarised in Table 5-2. The GCC of the final design is shown in Figure 5-16, in which it can be seen the match between the hot and cold composite curves is much improved compared with the initial case in Figure 5-15. The horizontal length of composite curves of the final design is also shorter than that of the initial case, which reflects the reduction in refrigeration duty. In the previous chapter, the optimal design of a single-stage MR system for the same process conditions has a shaftwork consumption of 27591.5 kW. As a consequence, by using a two-stage MR system the energy consumption can be further reduced by 8.3% from that of a single-stage MR system. This is in accordance with Costain's evaluation as in Table 1, in which a two-stage MR system has 7% lower shaftwork consumption than a single-stage MR system.

Table 5-2. Optimisation procedures of case study 1.

	Intermediate Temperature (^{o}C)	Pressure levels (bar)	Composition (wt %)	Refrigerant flow rate (kmol/s)	Shaftwork (kW)
Initial	-100	4.0 / 46.0	C1: 28.9 C2: 37.5 C3: 16.5 C4: 4.8 N2: 12.3	4.00	X (Temperature cross)
1	-100	4.0 / 46.0	C1: 27.5 C2: 32.1 C3: 10.0 C4: 8.9 N2: 21.5	3.80	32135.2
2	-120	4.0 / 46.0	C1: 31.3 C2: 25.4 C3: 6.5 C4: 16.8 N2: 19.9	3.60	30016.8
3	-120	4.5 / 46.5	C1: 28.9 C2: 30.3 C3: 2.1 C4: 20.5 N2: 18.2	3.40	28561.4
4	-125	4.5 / 46.0	C1: 27.4 C2: 35.6 C3: 4.8 C4: 20.8 N2: 11.4	3.20	26126.5
5	-125	4.5 / 46.0	C1: 27.0 C2: 43.1 C3: 0.5 C4: 21.2 N2: 8.2	3.10	25295.7
6	-125	4.5 / 46.0	C1: 33.1 C2: 29.8 C3: 6.6 C4: 20.1 N2: 10.4	3.00	X (Temperature cross)

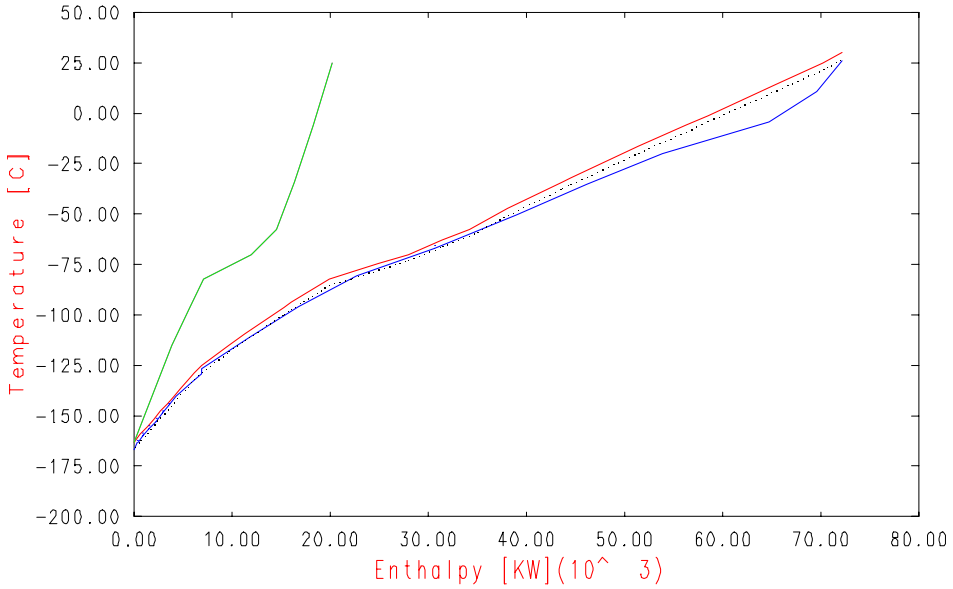

Figure 5-16. The GCC of the final design when the intermediate temperature is set as –125 ^{o}C.

In this case study, the changes to the intermediate temperatures, pressure levels, and refrigerant flow rate were done manually, following observations and heuristics. Although this helps understand the nature of the proposed method, updating variables also can be done automatically by optimisers, which is more systematic.

Case study II – design of a complex MR system

In this case study, a refrigerant-precooled complex MR system is to be designed for the same LNG process requirements in case study 1. The proposed method for the design of complex MR systems combines shaftwork targeting, synthesis of MR systems, thermodynamics and optimisation. The shaftwork consumption will be compared with the previous case study results of single-stage or two-stage MR systems.

To start with the method, an initial partition temperature needs to be set to split the whole process cooling requirements into an upper part and a lower part. As shown in Figure 5-17, the initial partition temperature is set as –40 ^{o}C. The lower part will first be dealt with by the method of optimal synthesis of MR systems. A two-stage MR system is to be designed.

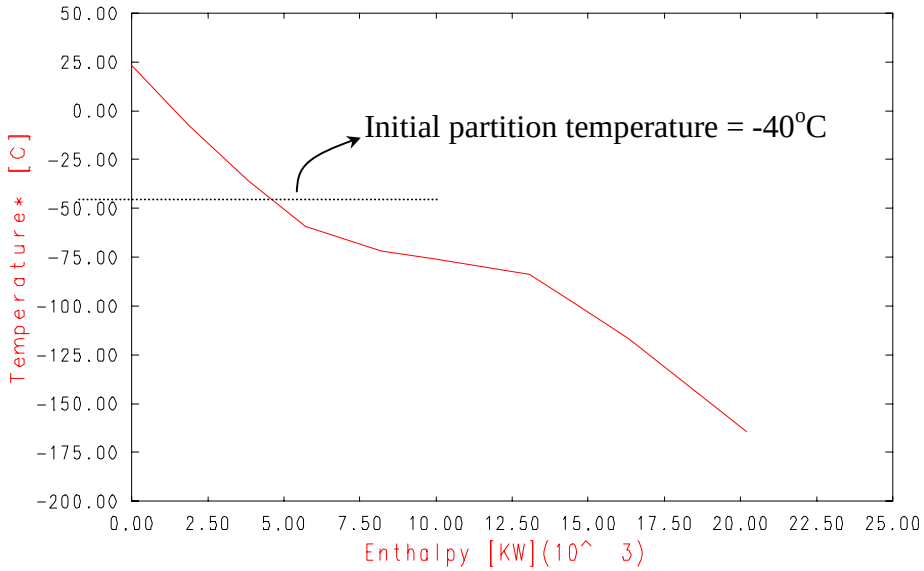

Figure 5-17. Setting of the initial partition temperature at –40 °C.

Note that by setting the partition temperature at –40 °C, the temperature of the lowest level in the pure-refrigerant cycle is automatically set at -45 °C, to allow a 5 °C temperature difference for heat transfer. The mixed refrigerant outlet temperature from the partition temperature is assigned to be –40 °C, also having a 5 °C temperature difference to the lowest temperature level of the pure-refrigerant cycle. The same philosophy will be applied later when the partition temperature is further changed.

Following the procedure in case study 1, a two-stage MR system, having the intermediate temperature at –125 °C, is achieved within 6 steps, as summarised in Table 5-3. The initial refrigerant flow rate is set as 3.0 kmol/s, smaller than the initial value in case study 1. The reason is because the refrigeration duty in this case study is smaller than that in case study 1, in which a two-stage MR system has to satisfy the overall LNG process cooling demands. The final design of the two-stage MR system has the refrigerant flow rate reduced to only 2.3 kmol/s.

Table 5-3. Optimisation procedures of case study 2.

	Intermediate Temperature (°C)	Pressure levels (bar)	Composition (wt %)	Refrigerant flow rate (kmol/s)	Shaftwork (kW)
Initial	-100	4.5 / 46.0	C1: 28.9 C2: 37.5 C3: 16.5 C4: 4.8 N2: 12.3	3.00	X (Temperature cross)
1	-100	4.5 / 46.0	C1: 31.2 C2: 33.4 C3: 5.8 C4: 10.2 N2: 19.4	3.00	22316.5
2	-115	4.5 / 44.0	C1: 28.9 C2: 45.4 C3: 13.2 C4: 8.7 N2: 3.8	2.80	20158.9
3	-120	4.5 / 42	C1: 33.5 C2: 40.3 C3: 7.3 C4: 14.7 N2: 4.2	2.60	17665.4
4	-125	4.5 / 40	C1: 36.0 C2: 45.5 C3: 4.9 C4: 2.1 N2: 11.5	2.30	13509.8
6	-125	4.5 / 40	C1: 27.0 C2: 43.1 C3: 0.5 C4: 21.2 N2: 8.2	2.10	X (Temperature cross)

Figure 5-18 shows the composite curves of the final design of the two-stage MR system. The hot and cold composite curves are well matched, and no wetness appears at the end of the cold composite curve. Also noted is that a temperature discontinuity occurs at an intermediate temperature, which reflects the fact that two refrigerant flows mix together before entering next stage heat exchanger.

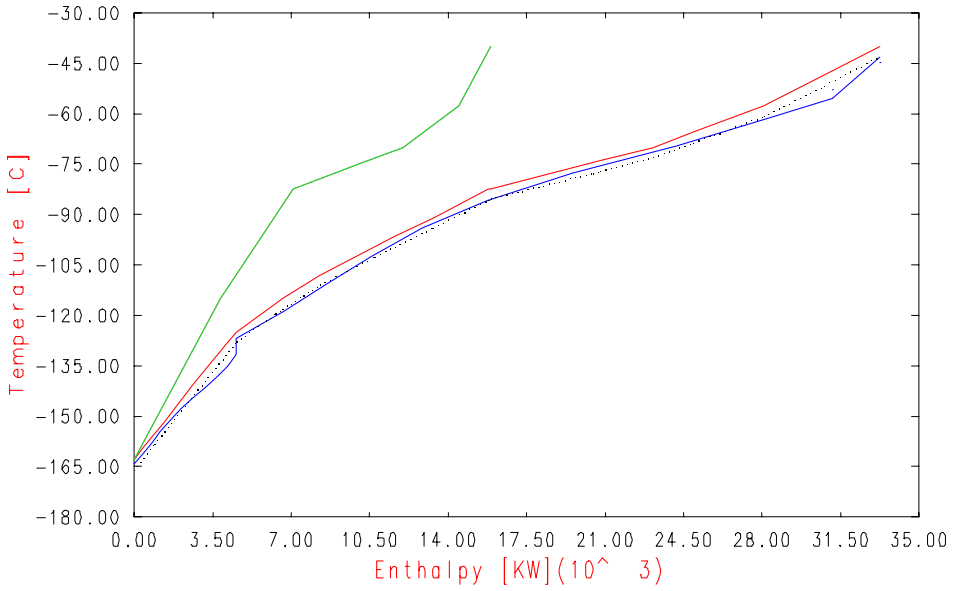

Figure 5-18. Composite curves of the final design of the two-stage MR system.

In the next step, the condensing heat from the partial condenser in the two-stage MR system is included into the GCC. The modified GCC is shown in Figure 5-19. Note that the major change of shape of the GCC above the partition temperature.

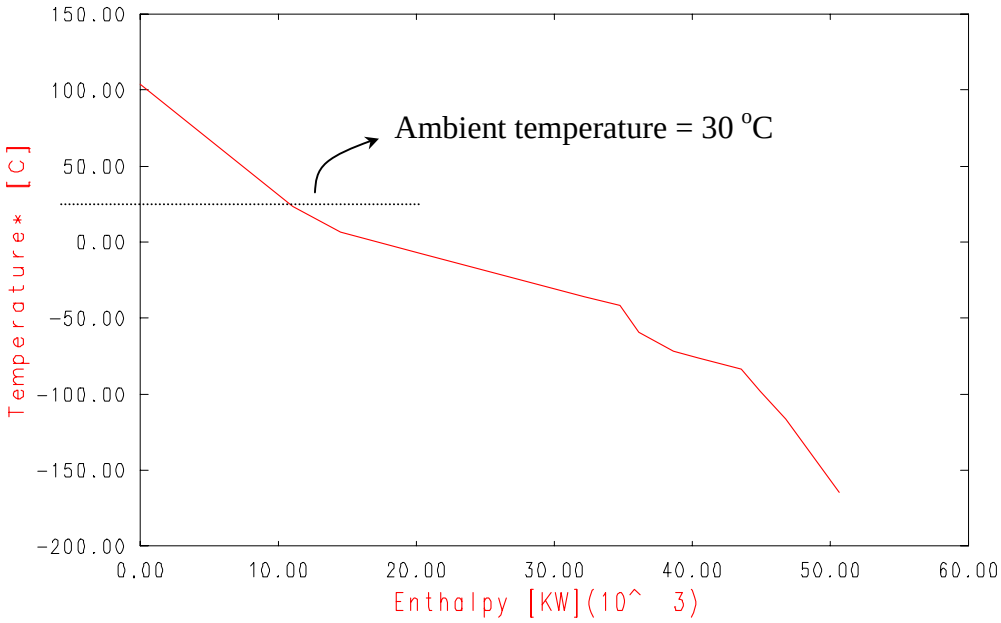

Figure 5-19. The modified process cooling curve which includes rejected condensing heat from the two-stage MR system.

The modified process cooling curve has the highest temperature starting at 105 °C, which is the compressor outlet temperature of the two-stage MR system. Ambient air or cooling water can be used to absorb heat from the part above ambient temperature, and also absorb condensing heat rejected from the condenser in the pure-refrigerant system. The design of the pure-refrigerant system, using propane as the refrigerant, is done by the shaftwork targeting method, as proposed in Chapter 2. A three-stage system is found to be the most favourable considering the trade-off of energy saving and capital costs. The design is summarised in Table 5-4. Therefore, the overall shaftwork requirement of the complex MR system is 23053.5 kW.

Table 5-4. The design of the propane refrigeration system.

No. of stages	Temperature/Load/Shaftwork of each level						Total shaftwork [kW]
3	-45	(°C)	-22.5	(°C)	-2.3	(°C)	9543.7
	10131	(kW)	8568	(kW)	6286.1	(kW)	
	1358.3	(kW)	2239.8	(kW)	5945.6	(kW)	

Drawing the GCC for the propane refrigeration system, as shown in Figure 5-19, we can see clearly the arrangements of each temperature level and heat rejection operations. Three refrigeration levels touch against the GCC. Condensing heat is rejected to the ambient. The sloping line in the condensing curve represents the superheat part of condensation. The part of process cooling curve above ambient temperature is balanced with ambient (air or cooling water) to minimise the cooling demand for the refrigeration system.

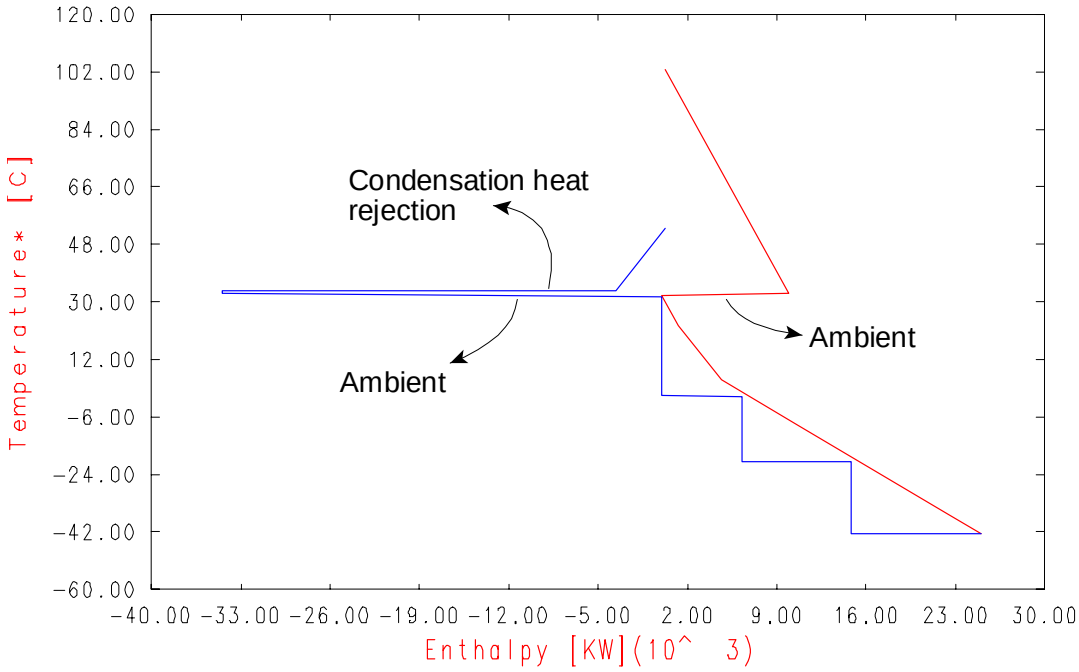

Figure 5-19. The balanced GCC of the propane refrigeration system.

The overall procedure then runs iteratively for different values of partition temperatures. However, it is found that at –40 °C, the overall shaftwork requirement is the lowest. Because –40 °C is the allowable lowest operating temperature for propane as a refrigerant, referring to Figure 1-5 in Chapter 1, the optimal partition temperature thus reaches the lower bound of the temperature ranges, and we conclude no further

improvement for the partition temperature is possible. Table 5-5 lists the details of the iteration procedures.

Table 5-5. Partition temperature vs. overall shaftwork requirement.

Partition temperature (^{o}C)	Individual shaftwork (kW)		Overall shaftwork (kW)
	Pure-refrigerant cycle	Mixed-refrigerant cycle	
-40.0	9543.7	13509.8	23053.5
-38.0	9479.9	13754.8	23234.7
-36.0	9504.4	14012.3	23516.7
-34.0	9518.5	14487.1	24005.6

Comparing with the previous design results of the single-stage MR system, consuming 27291.5 kW, the complex MR system saves shaftwork of 16.4 %. Comparing with the previous design results of the two-stage MR system, the complex system saves shaftwork of 8.9 %. However, it is noted that the design of the complex MR system is more complicated than that of the two-stage system as in case study 1. The complex MR system needs at least two compression trains, while the two-stage MR system requires only one. Also, the complex MR system requires more heat exchangers than the two-stage MR system does. Further economic investigations are required to justify the optimal trade-off.

5.6 Final points on LNG and MR systems

LNG is attracting great interest because it is clean, easy to transport, and has high heating value. It can be used to generate electricity, used as a feedstock for petrochemical and refining, domestic uses, etc. It can even be used directly as fuel in vehicles. LNG projects are always capital-intensive, with the liquefier making up around 25-50% of the total cost (Finn *et al.* 1999). Therefore, the liquefier is where the greatest cost saving can emerge, and even affect the overall viability of the projects. Despite the common perception, “Considering that liquefaction technology

is mature, future technological advancements in LNG manufacturing would most likely be focused on increasing the single-unit capacity of the major equipment to reduce the number of such units, that is, gaining from economy of scale" (Bellow *et al.* 1997), a survey of historical liquefaction plant costs carried out in 1993 (Jamieson *et al.* 1998) reveals some interesting and unexpected points. The unit cost of LNG plants, after adjusted for size to estimate the equivalent cost for a 3 million tonne per annum facility, has actually been increasing from year to year. Figure 5-20 illustrates the trend.

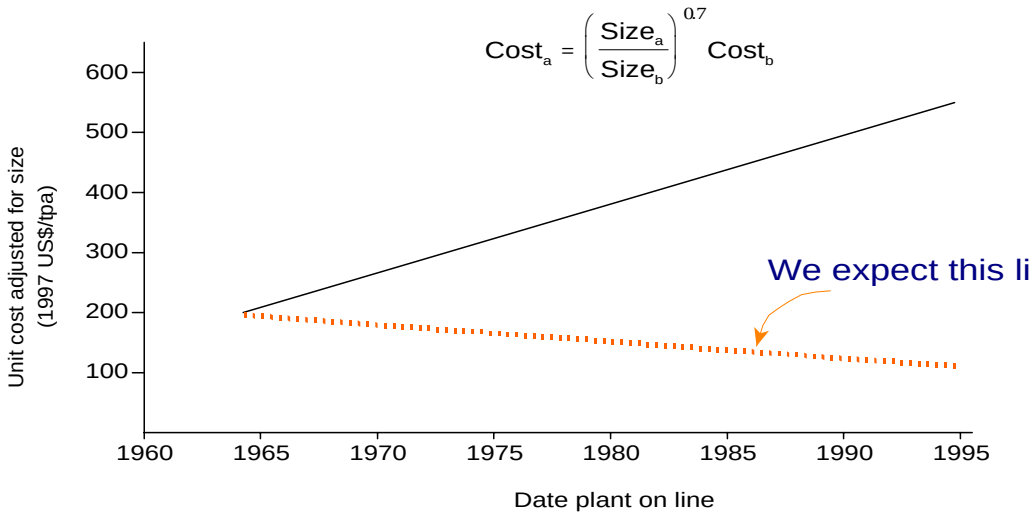

Figure 5-20. Unit cost trend of LNG plant.

The general increase in costs contradicts the normal trend that would be expected as a technology advances. There is no obvious reason why LNG shouldn't follow the common trend and become cheaper as the technology matures. The most possible causes are:

1. The market of LNG is monopolised.
2. The design of mixed refrigerant systems is still largely manipulated by trial-and-error.
3. There has been no systematic method for design and optimising the operating variables.

Therefore, "gaining from economy of scale" instead of "gaining from real technological advancement" leads to the problem that the sheer size of the overall investment might swell to such a point that makes the LNG projects very difficult to carry out.

Here, with the success of the novel systematic synthesis of MR systems, we can rightly doubt that the “liquefaction technology is mature” and foresee a considerable scope for total cost reduction of LNG plants.

5.7 Conclusions

In this chapter, the design method of MR systems has been extended to deal with complex MR systems. A multistage MR system can be decomposed into several serially connected single-stage MR systems, so the modelling approach used in Chapter 4 can be applied with minor changes. Besides the major variables for the design of single-stage MR systems, intermediate temperatures are the additional degrees of freedom. Although it doesn’t affect the shaftwork requirement directly, it creates more opportunities for the systems to have lower refrigerant flow rate or pressure levels, hence saving shaftwork. There are three different forms of objective function, minimise crossover, minimise sum of crossover and minimise shaftwork that can be used to suit different process design needs. The pure-refrigerant precooled multistage MR system is the major subject of study in this thesis. Heat rejected from the MR system is absorbed by the pure-refrigerant system. Overall condensing heat is rejected to ambient heat sinks (air or cooling water). Partition temperature, defined as the lowest temperature of the MR system condensing curve, separates the two systems and has an impact on the overall shaftwork requirement. The proposed method starts with an initial partition temperature that splits the process cooling curve into upper and lower parts. A MR system is optimally designed to satisfy the cooling demand from the lower part. Condensing heat rejected from the MR system is included into the original process cooling curve. Then, the pure-refrigerant system is designed by the method proposed in Chapter 2. The whole procedure iterates to optimise the partition temperature. Case studies demonstrate the practicality of the proposed method. A propane-precooled MR system is designed in case study 2, which demonstrates a more energy-efficient system can be achieved compared with standalone single-stage or two-stage MR systems. However, it is also emphasised that detailed economic analysis is required to justify the saving in shaftwork and the additional complexity in system design.

Nomenclature

Parameters and variables

$h_{i,l}^{L}$: enthalpy of the liquid phase in the i^{th} interval of the l^{th} stage.

$h_{i,l}^{V}$: enthalpy of the vapour phase in the i^{th} interval of the l^{th} stage.

h_{ti} : enthalpy of fluid at the inlet of the throttling valve.

h_{to} : enthalpy of fluid at the outlet of the throttling valve.

$L_{i,l}$: liquid mass flow rate in the i^{th} interval of the l^{th} stage.

J : number of components.

$\dot{m}_{to}$: flow rate at the outlet of the throttling valve.

N : number of intervals.

P : pressure.

P_{ti} : inlet pressure of the throttling valve.

P_{to} : outlet pressure of the throttling valve.

T : temperature.

T_c : critical temperature.

$\overline{T}_{i,l}$: temperature of interval *i* on the pseudo-cold composite curve in the l^{th} stage.

$\hat{T}_{i,l}$: temperature of interval *i* on the real cold composite curve in the l^{th} stage.

$T_{k,i,l}^{h}$: temperature of the k^{th} hot stream in the i^{th} interval of the l^{th} stage.

T_{mx} : after-mixing refrigerant temperature.

T_{ti} : temperature of a fluid at the inlet of a throttling valve.

T_{to} : temperature of a fluid at the outlet of a throttling valve.

$V_{i,l}$: vapour mass flow rate in the i^{th} interval of the l^{th} stage.

WS_j : shaftwork requirement of compressor *j*.

$X_{j,i,l}$: mole fraction of component *j* in liquid phase in the i^{th} interval of the l^{th} stage.

$Y_{j,i,l}$: mole fraction of component *j* in vapour phase in the i^{th} interval of the l^{th} stage.

Greek letters

ϕ_i : fugacity coefficient of component *i*.

δ : specified minimum temperature approach.

Reference

Bellow E. J., Ghazal Jr. F. P., Silverman A. J., 1997, Technology advances keeping LNG cost-competitive, *Oil & Gas Journal*, **June 2**, 74-78.

Biegler L. T., Grossmann E. I., Westerberg A. W., *Systematic Method of Chemical Process Design*, 1997, Prentice Hall International Ltd.

Finn A. J., Johnson G. L., Tomlinson T. R., 1999, Developments in natural gas liquefaction, *Hydrocarbon Processing*, April, p. 47-59.

Jamieson D., Johnson P., Redding P., 1998, Targeting and achieving lower cost liquefaction plants, *12th International Conference and Exhibition on Liquefied Natural Gas*, Perth, Australia, May 1998, p. 7.1.

Linnhoff B. Townsend D. W., Boland D., Hewitt, G. F., Thomas B. E. A., Guy A. R., Marsland R. H., 1991, *A User Guide on Porcess Integration for the Efficient Use of Energy*, The Institute of Chemical Engineers.

Paradowski H., Kaiser V., Gourguechon F., 1984, Use Mixed Cycle for Gas Cooling, *Hydrocarbon Processing*, March, 73-75.

Part 3.

The Ω – H Diagram: a Graphical Exergy Analysis Tool

6 Graphical Exergy Analysis of Refrigeration Systems

6.1 Introduction

There are many different forms of energy in processes. To make the best use of these different forms of energy, we need to know clearly not only their “quantity”, but also their “quality”. A conventional process analysis is usually performed as mass and energy balances. However, this type of analysis can only show the energy flows of processes and does not give insights into how the inefficiencies occur and why the quality of energy degrades throughout processes. A more thorough analysis of processes is often performed based on two different approaches: pinch analysis or exergy analysis.

Pinch analysis has the power to illustrate the main features of a system on simple diagrams. By investigating these diagrams, e.g. the composite curves and the grand composite curve (GCC), the energy targets can be set swiftly and conceptual analysis can be done to identify promising modifications. The weakness of pinch analysis is that it cannot deal with processes involving pressure and composition changes. However, these processes are often of principal importance and have significant impact towards overall performance and costs. As a result, possibilities to achieve significant modifications can be missed.

Exergy is a simultaneous measure of the quantity and quality of energy. It is derived from a combination of the first and second law of thermodynamics, and can be defined as the maximum work potential of a system or of a particular form of energy in relation to the environment. It helps us to identify inefficiencies in processes, so engineers can identify the cause and magnitude of exergy loss in each operation unit and therefore generate ideas for debottlenecking or retrofit. Moreover, exergy analysis makes it possible to compare different processes or alternative process routes on a universal thermodynamic basis. By describing the consumption of energy and material in terms of exergy loss, engineers are able to gain important understanding. As a

result, areas where large improvements are promising can be found, and more efficient technologies and retrofit tools are therefore employed for more efficient resources conversion. But the weakness of exergy analysis is the lack of an overall picture of a system as clearly and concisely as pinch analysis does.

To overcome this problem, several graphical representation tools to assist exergy analysis have been proposed. The Grassmann diagram and the pie diagram (Kotas, 1995) show the exergy balance of overall processes in a pictorial way. However, they cannot represent the information of exergetic quality of each stream in a process and therefore lack of sufficient physical meaning. Another group of graphical representation tools use the exergetic temperature τ, also called the Carnot factor η_C, as the vertical axis and enthalpy change as the horizontal axis. The definition of the exergetic temperature or the Carnot factor is:

$$\tau \,(or\ \eta_C) = 1 - \frac{T_0}{T} \tag{6-1}$$

Brodyanskii and Ishkin (1963) used the τ-ΔH diagram to analyse the distribution of inefficiencies in both the simple Linde air liquefaction plant and in one with auxiliary refrigeration. Niida et al. (1981) proposed the same type of diagram, called heat availability diagram, to study heat integration and characteristics of cryogenic processes. Linnhoff and Dhole (1992) proposed using the Exergy Grand Composite Curve (EGCC) to quickly predict shaftwork requirement of refrigeration systems. The EGCC uses the Carnot factor as the vertical axis. Since the area on the EGCC represents exergy, changes in the area reflect changes in the exergy loss, and is proportional to the shaftwork consumption change. However, because these proposed graphical representations all use the exergetic temperature as the vertical axis, which is only a function of temperature, they cannot reflect the exergy loss from pressure and composition changes. This limitation may miss promising process improvement opportunities, since these core process units (e.g. compressors, expanders, throttling valves, etc.) usually have significant impacts on the overall performance and costs.

Ishida and Ohno (1982) proposed a graphical exergy analysis tool called the energy-

utilisation diagram (EUD), using a more generic factor, the energy level A:

$$A = 1 - \frac{T_0 \cdot \Delta S}{\Delta H} \tag{6-2}$$

It assumes that every process must have energy transformed between energy donors and acceptors. Therefore, it can represent mechanical exergy loss from process units such as turbines and compressors. However, it still cannot deal with mechanical exergy loss from adiabatic or isenthalpic processes, e.g. the Joule-Thomson (J-T) throttling valve, which usually causes large part of exergy loss especially in subambient processes.

Feng and Zhu (1997) introduced a graphical representation method, called the Ω - H diagram, for power plant. It combines the pinch and exergy analysis on a rational basis for assessing process modifications. Ω indicates the energy level and H indicates the amount of energy, and both thermal and mechanical exergy losses can be represented on the same diagram. Since Ω has a general definition as exergy/enthalpy, it can cope with temperature, pressure or composition changes in processes and all types of process units can be represented and studied.

Refrigeration systems are employed in the process industries to supply low temperature cooling. In subambient processes, such as ethylene plants or natural gas liquefaction plants, the design of refrigeration systems is usually the major concern for energy consumption and capital investment. However, due to its intrinsic complexity of structure and interaction with processes, both new design and retrofit are challenging. The existing analysis methods do not serve subambient processes and refrigeration systems well, since irreversibility due to heat transfer over a finite temperature difference is not the dominant factor, as is usually the case in above-ambient processes. An analysis tool for the front-end conceptual design or for retrofit would be very valuable.

In this chapter, the Ω - H diagram is extended to the analysis of complex refrigeration systems. A new concept, the exergy donor and exergy acceptor pair, is introduced to

rationalise the Ω - H diagram and allow direct calculation of exergy loss from the diagram. In case studies, both multistage refrigeration systems and mixed-refrigerant (MR) systems will be examined. The results show that the Ω - H diagram can effectively identify the inefficiencies in refrigeration systems and give insights into the problems. Particularly important, it successfully represents the distribution of inefficiencies and the associated exergy flow among the various units of a steady operating process, that can be of great value in the analysis or retrofit of a process.

6.2 The theory of exergy analysis

While the first law of thermodynamics states the conservation of energy, the second law of thermodynamics says that the quality of the energy always decreases during a natural process. Entropy is a thermodynamic property generated from the second law. However, entropy alone cannot characterise the quality of different forms of energy, as the example in Figure 6-1 shows. High pressure steam at 650^{o}C and 100 bar on the T-S diagram reads the same value of entropy as the steam from the kettle at ambient conditions.

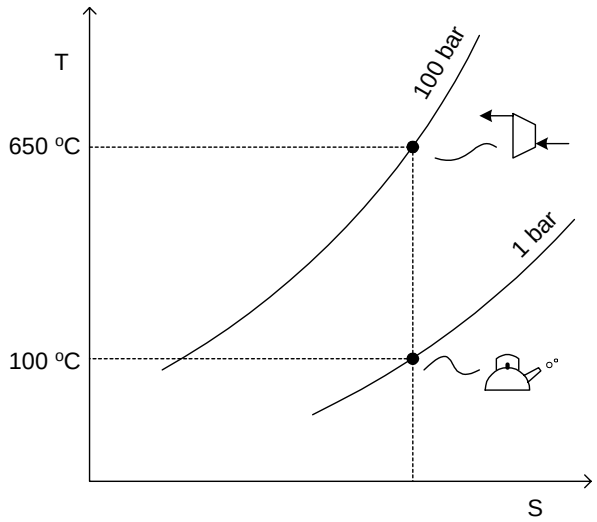

Figure 6-1. The limitation of using entropy.

Szargut (1998) defines the exergy as

Exergy is the amount of work obtainable when some matter is brought to a state of thermodynamic equilibrium with the common components of the natural surroundings by means of reversible processes, involving interaction only with the above mentioned components of nature.

The definition can be further explained. Whenever two systems at different states interact, an opportunity to generate useful work occurs, as in theory a reversible Carnot engine can be placed between to generate work as the two are allowed to come into a perfect state of equilibrium, i.e. absence of any gradients of pressure, temperature, chemical potential, kinetic energy and potential energy. When one of the systems is the *environment* and the other is some system of interest, *exergy* is the maximum theoretically obtainable work when the two reach equilibrium. Alternatively, exergy is the minimum work required when a quantity of matter from the environment is brought to a specified state of interest. Equally, exergy is a measure of the departure of the state of the system from that of the environment. Changing the status from the system of interest to equilibrium with the environment involves the following steps:

1. Change temperature and pressure from system of interest at (T, P) to environmental conditions at (T_0, P_0) by means of a reversible process. This is the state when the system is in thermal and mechanical equilibrium with the environment. Conceptually, the system is kept separate from the environment by a physical boundary to prevent mixing and chemical interaction with the environment. The amount of useful work obtainable from the step is called the physical exergy.

2. Separate the substances that make up the system into those commonly present in the environment. These environmental substances are then brought about to be in equilibrium with the environment. This is the state when the system is also in chemical equilibrium with the environment and said to be in the *dead state*. The amount of useful work obtainable from this step is called the chemical exergy.

In many cases of practical applications, the physical exergy suffices for the purpose of exergy analysis. When processes being considered do not involve chemical reactions or there is no exchange of substances with the environment, the chemical exergy part will cancel out when exergy flows of the incoming and outgoing streams are subtracted in an exergy balance. Other forms of exergy of streams in a steady state are kinetic exergy and potential exergy. Kinetic exergy is associated with the bulk velocity of a fluid, and potential exergy is evaluated with respect to sea level.

We can use the conceptual system, as shown in Figure 6-2, to derive the exergy content of a stream. The stream at T1 and P1 enters the system boundary and leaves the system boundary at environment conditions T_0 and P_0. W amount of work is delivered from the system boundary to the environment and Q amount of heat is transferred across the boundary at T_0.

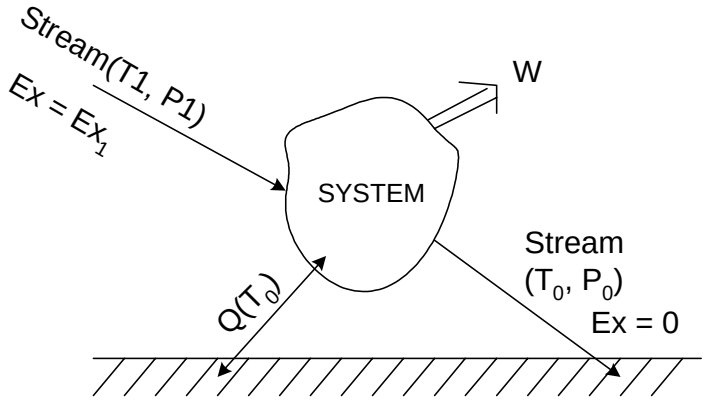

Figure 6-2. The definition of stream exergy.

The exergy of a stream is calculated in the following way:

Energy Balance

$$W = H_1 - H_0 + Q(T_0) \tag{6-3}$$

Entropy Balance

$$S_1 + \frac{Q(T_0)}{T_0} = S_0 \tag{6-4}$$

$$Q(T_0) = T_0 \cdot (S_0 - S_1) \tag{6-5}$$

$$\therefore \quad W = (H_1 - H_0) - T_0 \cdot (S_1 - S_0) \tag{6-6}$$

Results:

$$Ex = (H_1 - H_0) - T_0 \cdot (S_1 - S_0) \tag{6-7}$$

Exergy, as enthalpy and entropy, is a state function and is independent of the path. Therefore the change of exergy from one state to another is simply the difference between the exergy values of the two. Figure 6-3 explains the situation.

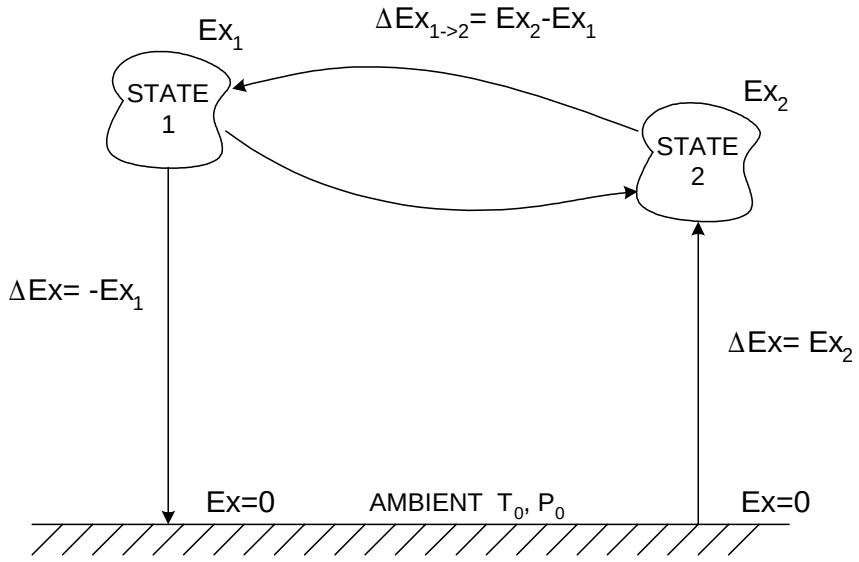

Figure 6-3. Exergy as a state function.

The change of exergy between two states thus can be derived as:

$$\begin{aligned}\Delta Ex_{1\to 2} &= Ex_2 - Ex_1 \\ &= (H_2 - H_0) - T_0 \cdot (S_2 - S_0) \\ &\quad - \left[(H_1 - H_0) - T_0 \cdot (S_1 - S_0)\right]\end{aligned}$$

$$\therefore \quad \Delta Ex_{1\to 2} = \Delta H - T_0 \cdot \Delta S \tag{6-8}$$

When only heat is transferred between the system of interest and the environment, the calculation of thermal exergy of a stream depends on the temperature associated with itself. If the temperature is higher than that of the environment, as Figure 6-4 shows, the exergy is calculated as:

$$Q1 = Q2 + W \tag{6-9}$$

$$\frac{Q1}{T} = \frac{Q2}{T_0} \quad (reversible\ engine) \tag{6-10}$$

$$\Rightarrow \quad Q2 = Q1\frac{T_0}{T} \tag{6-11}$$

$$\therefore \quad W = Q1(1 - \frac{T_0}{T}) \tag{6-12}$$

Result:

$$Ex_{Q1} = Q1(1 - \frac{T_0}{T}) \tag{6-13}$$

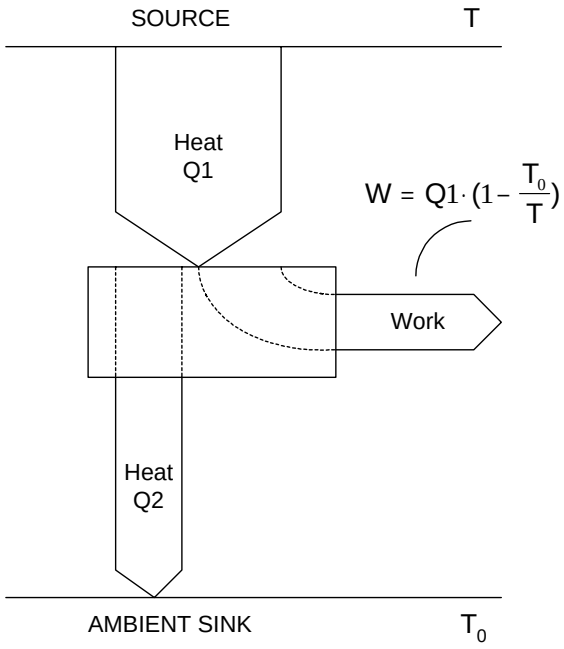

Figure 6-4. Calculation of exergy, above ambient temperature.

If the temperature is lower than that of the environment, as Figure 6-5 shows, the exergy is calculated in the following way:

$$W = Q1 \cdot \left(1 - \frac{T}{T_0}\right) \tag{6-14}$$

$$Q1 = Q2 + W \tag{6-15}$$

$$\therefore \quad W = Q2 \cdot \left(\frac{T_0}{T} - 1\right) \tag{6-16}$$

Result:

$$Ex_{Q2} = Q2 \cdot \left(\frac{T_0}{T} - 1\right) \tag{6-17}$$

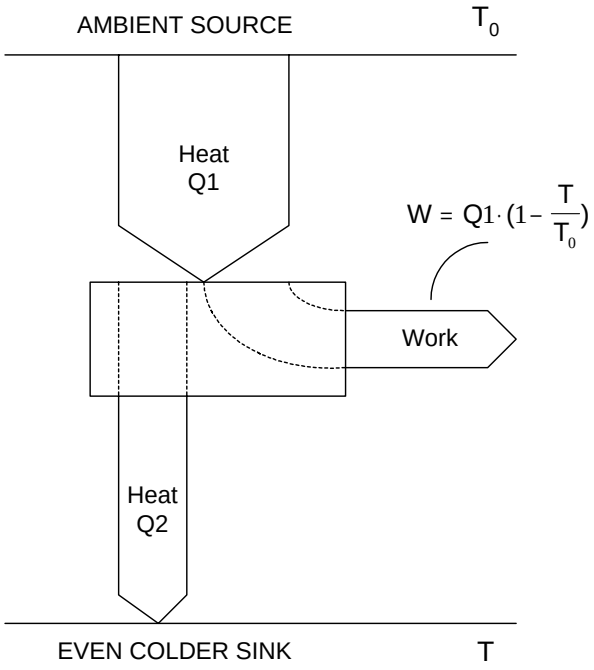

Figure 6-5. Calculation of exergy, below ambient temperature.

Table 6-1 summarises the calculation of exergy in different conditions.

Table 6-1. Summary of the calculation of exergy.

W units of shaftwork	$Ex = W$
Q units of heat at T_0 *	$Ex = 0$
Q units of heat at T	$T > T_0$ $E_X = Q\left(1 - \frac{T_0}{T}\right)$ $T < T_0$ $E_X = Q\left(\frac{T_0}{T} - 1\right)$
Stream exergy	$E_X = (H_1 - H_0) - T_0(S_1 - S_0)$
Stream exergy change	$\Delta E_X = \Delta H - T_0 \Delta S$ At constant T : $\Delta E_X = \Delta H\left(1 - \frac{T_0}{T}\right)$

Exergy balance is performed in the same way as the material or the energy balances. To start the exergy balance, a *control region* of the system of interest needs to be defined as shown in Figure 6-6.

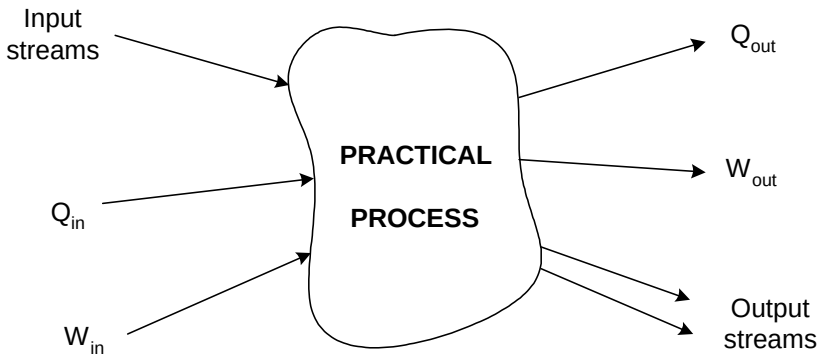

Figure 6-6. A control region for exergy balance.

Material streams, work exchange and heat transfer are carried out through the defined boundary of the control region. A balance equation of each exergy term is written as such:

$$\sum_{\text{streams}} Ex_{in} + \sum \left(Ex_Q\right)_{in} + \sum W_{in} = \sum_{\text{streams}} Ex_{out} + \sum \left(Ex_Q\right)_{in} + \sum W_{out} + Ex_{loss} \qquad (6\text{-}18)$$

The last term represents the deficit or surplus of the total exergy between the inlet and outlet conditions. This is termed the “exergy loss” of the process. By suitably selecting the control region, the exergy balance can be written for either the overall process, parts of the whole process, or an operation unit within the process. In this way, the cause and distribution of inefficiencies within a process can be identified.

We shall use an example to illustrate the application of exergy balance. A gas turbine cogeneration system is required to be analysed, as illustrated in Figure 6-7. To carry out exergy analysis, the exergy flow rate of each stream is first calculated. Table 6-2 summarises the results.

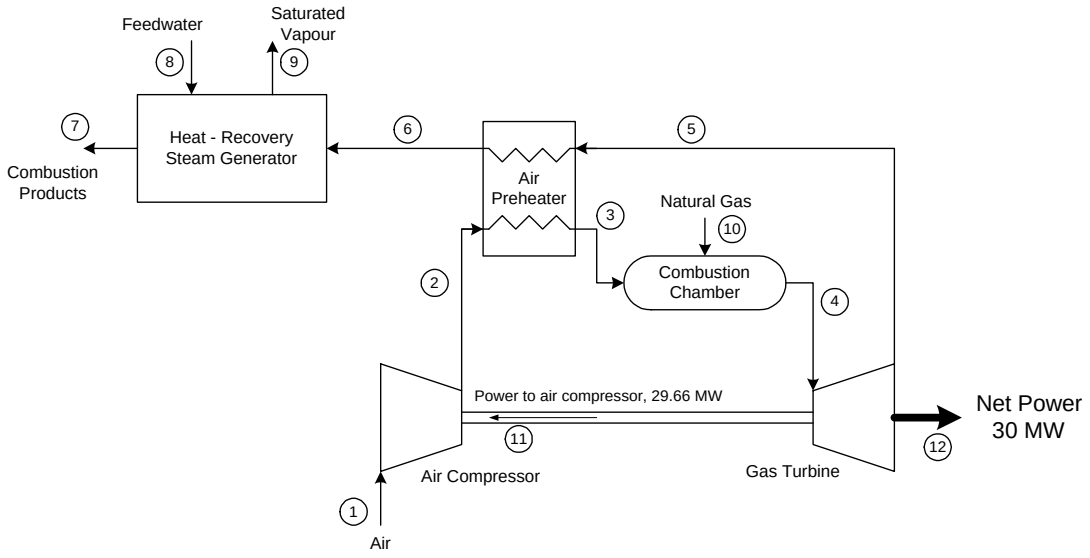

Figure 6-7. A cogeneration system.

Table 6-2. Energy rate data of the cogeneration system.

State	Substance	Exergy rate (MW)
1	Air (environmental substance)	0.00
2	Air	27.54
3	Air	41.94
4	Combustion products	101.45
5	Combustion products	38.78
6	Combustion products	21.75
7	Combustion products	2.77
8	Water	0.06
9	Water	12.81
10	Natural Gas	84.99

For each unit, the exergy loss rate is obtained from the exergy balance. Calculations of some of the units are listed:

(1) For the combustion chamber

As the chamber is under adiabatic conditions and no work is exchanged, the relevant terms in the exergy balance cancel out.

$$\sum_{\text{streams}} Ex_{in} + \sum \left(Ex_Q\right)_{in} + \sum W_{in} = \sum_{\text{streams}} Ex_{out} + \sum \left(Ex_Q\right)_{in} + \sum W_{out} + Ex_{loss} \tag{6-19}$$

So, the exergy loss rate can be calculated as:

$$Ex_{loss} = Ex^3 + Ex^{10} - Ex^4 = (4194 + 84.99 - 10145) = 25.48 \text{ MW}$$

(2) For the air preheater

The exergy balance and data from Table 6-3 gives:

$$Ex_{loss} = Ex^2 + Ex^5 - Ex^3 - Ex^6 = 27.54 + 38.78 - 4194 - 2175$$
$$= 2.63 \text{ MW}$$

(3) For the air compressor

$$Ex_{loss} = Ex^1 + W_{shaft} - Ex^2 = 0.0 + 29.66 - 27.54 = 2.12 \text{ MW}$$

The exergy loss rate for the other units is calculated in the same way. To summarise, Table 6-3 provides a rank-ordered list of the exergy loss rate for principal units. From the analysis, it is clear that the combustion chamber is the major site of thermodynamic inefficiency. The next most significant is the heat-recovery steam generator (HRSG). Gas turbine, air preheater and air compressor cause approximately the same magnitude of exergy loss rate. This agrees with the common fact that combustion is intrinsically a very significant source of irreversibility.

Table 6-3. Exergy loss percentage of each unit.

Unit	Ex_{loss} rate (MW)	Percantage of total Ex_{loss} (%) *	Percantage of exergy input with fuel (%) **
Combustion chamber	25.48	64.56	29.98
Heat-ercovery steam generator	6.23	15.78	7.33
Gas turbine	3.01	7.63	3.54
Air preheater	2.63	6.66	3.09
Air compressor	2.12	5.37	2.49
Total	39.47	100.00	46.44

* : calculated by Ex_{loss} rate / 39.47 * 100%
** : calculated by Ex_{loss} rate / NG exergy rate(84.99) * 100%

6.3 The Concept of Ω

Especially in subambient processes, a major part of the inefficiencies in processes comes from compressors, turbines and J-T valves. While previous graphical representation tools fail to analyse mechanical exergy loss within processes, Feng and Zhu (1997) proposed a new graphical representation, called the Ω-H diagram, to overcome this limitation. Using this diagram, the advantages of the pinch and exergy analysis are integrated, since the diagram can represent the main features of a process concisely, pinpoint the distribution of inefficiencies within the process accurately and set targets for improvement. Both energy and exergy balances for a whole process can be represented simultaneously on the Ω-H diagram. It also visually aids the comparative studies among different designs.

The general definition of Ω is exergy divided by enthalpy:

$$\Omega = \frac{\text{Exergy}}{\text{Enthalpy}} \tag{6-20}$$

With this generic definition, the Ω concept can accommodate all forms of energy. For

steady-state non-isenthalpic process streams, the Ω becomes:

$$\Omega = 1 - \frac{T_0 \cdot \Delta S}{\Delta H} \tag{6-21}$$

The above definition of Ω is the same as Ishida (1982) used for the energy level *A*. Instead of using the energy donor/energy acceptor concept as in Ishida's work, we propose using the concept of exergy donor/exergy acceptor for each process unit. As in the case of J-T valves, although there is no enthalpy change (isenthalpic) between inlet and outlet, there is exergy loss due to entropy generation after throttling. The exergy difference between the exergy donor and the exergy acceptor is the exergy loss.

For the case of processes involving only temperature change, such as heat exchangers, the Ω is equal to the Carnot Factor:

$$\Omega = 1 - \frac{T_0}{T} \tag{6-22}$$

Figure 6-8 shows the Ω-H diagram of a heat exchanger. The upper curve represents the hot stream and the lower curve represents the cold stream. The area enclosed by the two curves is the exergy loss due to finite temperature difference heat transfer in the heat exchanger. The exergy donor is the hot stream and the exergy acceptor is the cold stream. Since the exergy delivered by the hot stream is not completely received by the cold stream, the difference is the exergy loss in the heat exchanger. It can be seen intuitively that decreasing the temperature difference between the hot and cold streams can reduce the exergy loss.

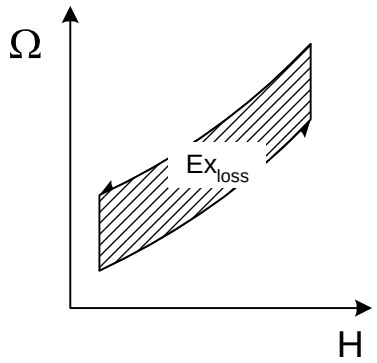

Figure 6-8. The Ω-H diagram of a heat exchanger.

An adiabatic throttling process is characterised by the isenthalpic operation, *h*=constant. If a cooling effect is to be obtained in the throttling process, the Joule-Thomson coefficient $\mu_h \equiv (\partial T/\partial P)_h$ must be positive in the range of properties under consideration. Clearly, an isenthalpic process cannot be represented by the previous exergetic temperature-enthalpy diagram, since there is no heat transfer and the enthalpy change is zero. Using its general definition, the Ω for the inlet stream of a throttling valve is:

$$\Omega_{ti} = \frac{(H_{ti} - H_0) - T_0(S_{ti} - S_0)}{H_{ti}} \tag{6-23}$$

The Ω for the outlet stream of a throttling valve is:

$$\Omega_{to} = \frac{(H_{to} - H_0) - T_0(S_{to} - S_0)}{H_{to}} \tag{6-24}$$

Since $H_{ti} = H_{to}$, the exergy loss due to an adiabatic throttling process can be represented on the Ω-H diagram as a square having $\Omega_{ti} - \Omega_{to}$ in height and H_{ti} in length. This is equal to an area of $T_0(S_{to} - S_{ti})$, which is the exergy loss from the adiabatic throttling process. The exergy donor is the inlet stream, and the exergy acceptor is the outlet stream. Across the throttling valve, H_{ti} amount of enthalpy is degraded from Ω_{ti} to Ω_{to}, therefore causing exergy loss. Figure 6-9 shows the Ω-H

diagram of an adiabatic throttling valve.

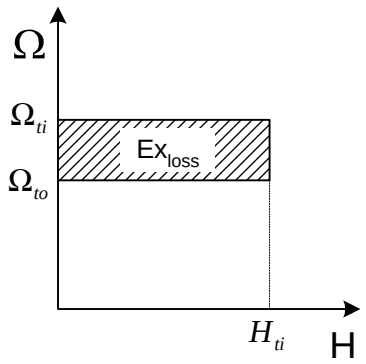

Figure 6-9. The Ω-H diagram of an adiabatic throttling valve.

A simple exergy balance can derive the exergy loss in a compressor is:

$$\Delta Ex, comp = T_0 \left(S_{co} - S_{ci} \right) \tag{6-25}$$

The Ω of a compressor is written as:

$$\begin{aligned} \Omega_{comp} &= 1 - \frac{T_0 \cdot \Delta S}{\Delta H} \quad \left(< 1, \because \Delta S > 0, \Delta H > 0 \right) \\ &= 1 - \frac{T_0 \left(S_{co} - S_{ci} \right)}{W} \end{aligned} \tag{6-26}$$

When represented on the Ω-H diagram, the exergy loss of a compressor is a rectangular area, as shown in Figure 6-10. The exergy donor is the input of electricity, with Ω equal to 1. The exergy acceptor is the fluid though the compressor. The difference between the electricity input (the area below Ω=1) and the actual amount of exergy received by the fluid (the area below Ω_{comp}) is the exergy loss in the compressor. Although the horizontal position of the area is arbitrary, the vertical position has a physical meaning and should be fixed. It can be interpreted as though the external shaftwork input to the compressor is W, the compressor in fact accepts only $W \cdot \Omega_{comp}$ amount of shaftwork. The difference, $W - W \cdot \Omega_{comp}$, is the exergy loss in the compressor.

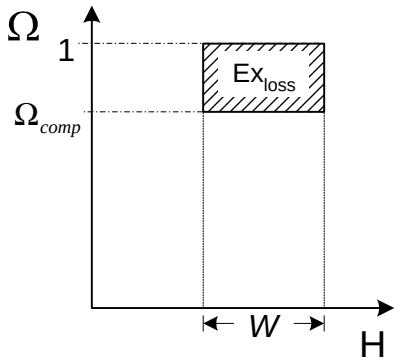

Figure 6-10. The Ω-H diagram of a compressor.

For an adiabatic expander or turbine, the exergy loss is:

$$\Delta Ex_{expd} = T_0\left(S_{eo} - S_{ei}\right) \tag{6-27}$$

The Ω of an expander can be written as:

$$\begin{aligned}\Omega_{expd} &= 1 - \frac{T_0 \cdot \Delta S}{\Delta H} \quad (>1,\ \because \Delta S > 0, \Delta H < 0) \\ &= 1 - \frac{T_0\left(S_{eo} - S_{ei}\right)}{W}\end{aligned} \tag{6-28}$$

Note the difference between a compressor and an expander. In an expander, the exergy donor is the fluid and the exergy acceptor is the electricity generated. Therefore, when represented on the Ω-H diagram, the exergy loss in an expander is a rectangular area above the Ω=1 line. The exergy delivered by the fluid passing through the expander is the area below Ω_{expd}. The actual exergy generated as electricity is the area below Ω=1. The difference is the exergy loss in the expander. Figure 6-11 shows the situation.

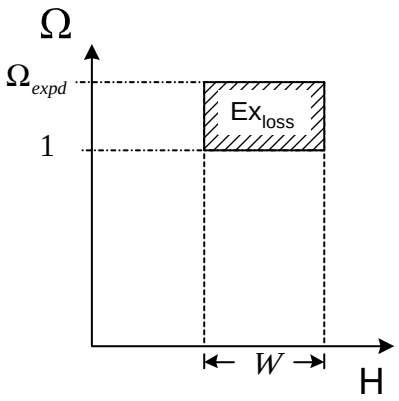

Figure 6-11. The Ω-H diagram of an expander.

In a multistage refrigeration operation, the mixing of a saturated vapour with a superheated compressor outlet from the lower level can be treated as co-current heat transfer between two streams with the final temperature as the after-mixing temperature. Therefore, the Ω-H diagram of a mixer can be represented as in Figure 6-12.

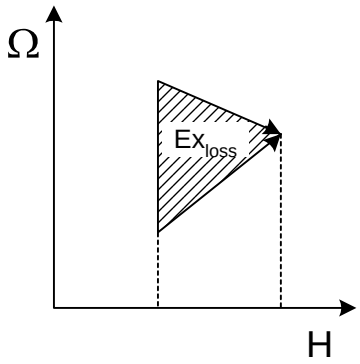

Figure 6-12. The Ω-H diagram of a mixer.

The exergy loss due to a mixing process is calculated by an exergy balance:

$$\Delta Ex_{mixing} = T_0\left[(\dot{m}_1 + \dot{m}_2)\cdot \hat{S}_{after-mixing} - \dot{m}_1\hat{S}_1 - \dot{m}_2\hat{S}_2\right] \tag{6-27}$$

$\hat{S}$ means the specific entropy. Subscripts 1 and 2 indicate two inlet streams to the mixer. In the case, the exergy donor is the initially hotter stream and the exergy acceptor is the initially colder stream.

In addition, to represent the exergy loss of each unit in a process, the Ω-H diagram can also embody the exergy loss of the overall process by using pinch analysis. The construction of the Ω-H diagram from composite curves is exactly the same as for the Exergy Grand Composite Curves (EGCC) (Linnhoff and Dhole, 1992), as illustrated in Figure 6-13. For thermal changes only, Ω is equal to the Carnot Factor. The straight lines of the composite curves become curved in the Ω-H diagram. The area between the Ω-H diagram curve and utilities is equal to exergy loss in the heat exchanger network.

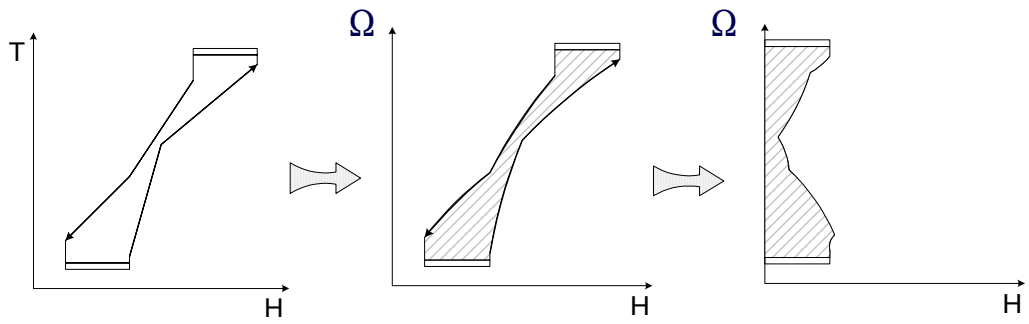

Figure 6-13. Construction of the Ω-H diagram of process.

The area on the Ω-H diagram illustrates the corresponding exergy loss from the process.

The practicability of the Ω-H diagram for the analysis and design of industrial refrigeration systems will be examined by two case studies. The first case study is an ammonia refrigeration system. We can see how each exergy loss on the Ω-H diagram changes as we introduce more stages into the existing single stage refrigeration cycle. The second case study is a mixed refrigerant system for an LNG plant, and demonstrates that the Ω-H diagram can identify the exergy loss in each unit, and direct the modification to achieve better performance. Together with the optimal design methods for refrigeration cycles, we can achieve considerable improvement and significant shaftwork saving.

6.4 Integrated design and retrofit method

The Ω-H diagram is a powerful and visual tool for getting insights of the processes, since it can illustrate all kinds of exergy loss; thermal, mechanical or chemical. Therefore, we can integrate it with other design methods, such as the shaftwork targeting method in Chapter 2 for multistage or cascade refrigeration cycles and the systematic synthesis method for mixed refrigerant (MR) systems in Chapter 4. Two case studies will be used to demonstrate the integrate design or retrofit approach.

Graveland and Gisolf (1998) discussed the use of exergy analysis together with optimisation to reduce process exergy losses by the following points:

1. Optimisation of the utility generation process.
2. Optimisation of the process itself, thus reducing the utility consumption.
3. Co-production.
4. Select more exergy-efficient process routes.
5. Reducing the required process steps.
6. Heat integration.

Once an exergy analysis is done, these points can guide the direction that process improvements or revamps should follow.

Case I. Multistage Refrigeration Cycle

Suppose we have a process whose Grand Composite Curve (GCC) is shown in Figure 6-14, and we want to design a refrigeration cycle to satisfy its cooling demand and achieve minimal shaftwork consumption. Ammonia is selected as the refrigerant.

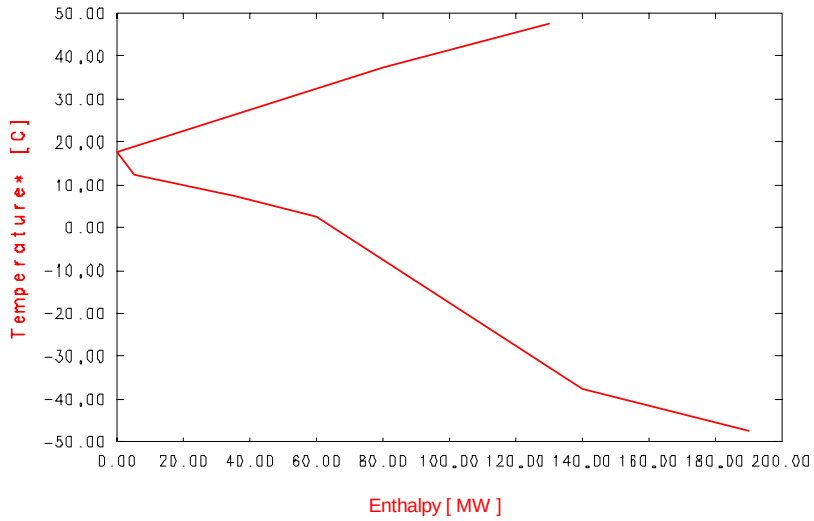

Figure 6-14. Process GCC, in which we want to design the refrigeration cycle.

Firstly, a single-stage ammonia refrigeration cycle is installed to accommodate the cooling demand from the process. The Ω-H diagram is shown in Figure 6-15, in which ①: exergy loss in the compressor; ②: exergy loss in the evaporator; ③: exergy loss in the condenser due to latent heat transfer; ④: exergy loss in the condenser sue to sensible heat transfer; ⑤: exergy loss in the throttling valves. It can be observed that the biggest exergy loss comes from the evaporator and condenser, area ② and ④. We can use the Ω-H details to calculate exergy loss in each unit directly. Table 6-4 lists the details of the Ω-H diagram. The inlet Ω denotes the Ω value of the exergy donor in a unit, and the outlet Ω denotes the exergy acceptor in the same unit. To calculate exergy loss of a unit, we multiply the difference between inlet and outlet Ω by the associated enthalpy change.

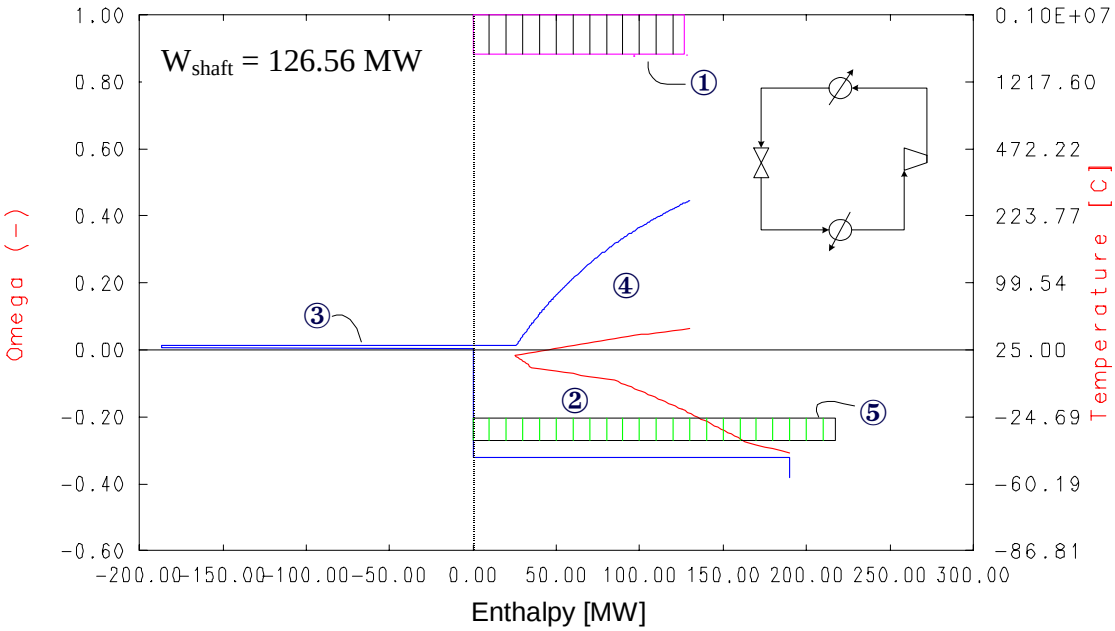

Figure 6-15. The Ω-H diagram of the single-stage ammonia refrigeration cycle.

Table 6-4. The Ω-H details of the single-stage ammonia refrigeration cycle.

Evaporator: -50 °C / 190 MW; Condenser: 35 °C / 316.6 MW		
	Compressor Ω-H details	Throttle valve Ω-H details
Inlet Ω	1.000	-0.270
Outlet Ω	0.884	-0.205
ΔH (MW)	126.60	217.40
Exergy loss (MW)	14.69	14.13

To reduce the shaftwork requirement, we introduce more stages and optimise the evaporating temperature level and load of each stage by shaftwork targeting method. The results show significant reduction in shaftwork requirement. The Ω-H diagram of the three-stage ammonia system in Figure 6-16 reflects the reduction of exergy loss. Exergy loss in compressors and throttling valves, shown as area ① and ⑤, splits into three blocks. Due to two additional levels, exergy loss in evaporators, shown as area ②, is significantly reduced. It can also be seen that the Ω-H profile of the sensible heat transfer part of the condenser, area ④, includes a new horizontal line. It reflects the fact that heat rejected by the sensible heat transfer is not sufficient to satisfy the process heating demand, and therefore another hot utility, such as low pressure steam at 100 °C, needs to be employed. The resulting shaftwork requirement of the new

three-stage design is significantly (45%) lower than that of the single-stage design.

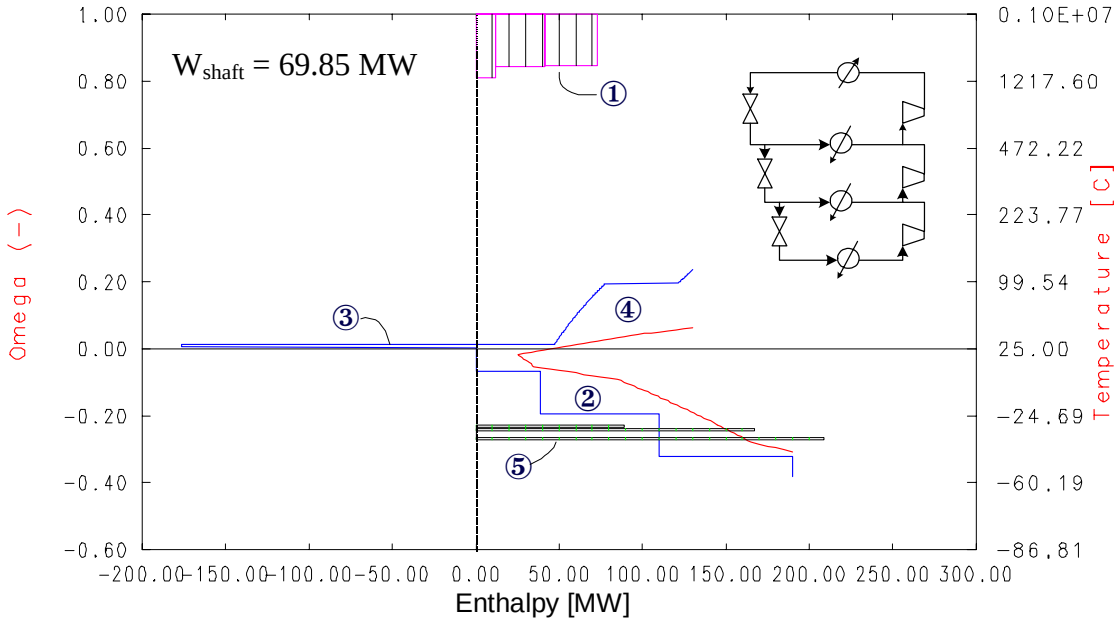

Figure 6-16. The Ω-H diagram of the 3-stage ammonia refrigeration cycle.

The Ω-H details of the 3-stage ammonia refrigeration cycle are listed in Table 6-5. The exergy loss of each unit is calculated as previously discussed.

Table 6-5. The Ω-H details of the 3-stage ammonia refrigeration cycle.

Level 1: evaporator: -50 °C / 80 MW		
	Compressor Ω-H details	Throttle valve Ω-H details
Inlet Ω	1.000	-0.234
Outlet Ω	0.812	-0.229
ΔH (MW)	12.73	89.17
Exergy loss (MW)	2.40	0.48
Level 2: evaporator: -25 °C / 50 MW		
	Compressor Ω-H details	Throttle valve Ω-H details
Inlet Ω	1.000	-0.242
Outlet Ω	0.833	-0.237
ΔH (MW)	22.05	154.86
Exergy loss (MW)	3.67	0.80
Level 3: evaporator: 0.5 °C / 60 MW		

	Compressor Ω-H details	Throttle valve Ω-H details
Inlet Ω	1.000	-0.270
Outlet Ω	0.850	-0.262
ΔH (MW)	36.67	208.78
Exergy loss (MW)	5.50	1.85
Σ Exergy loss	11.57	3.13

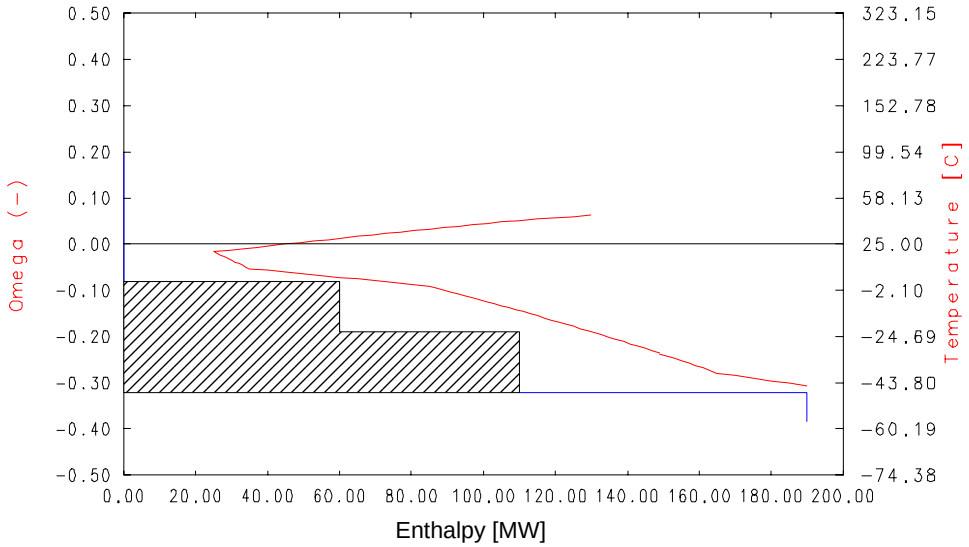

Figure 6-17. The hatched area shows the reduction of exergy loss in evaporators.

The hatched area in Figure 6-17 represents the reduction of the exergy loss due to use of three evaporation levels. By calculating the area, the reduction of exergy loss is 21.52 MW. Following the same calculation, the reduction of exergy loss in the condenser (area ③ and ④) is estimated as 15.44 MW. As a result, the overall reduction of exergy loss in compressors, throttling valves, evaporators and condenser can be found to be 51.26 MW. This is very close to the reduction of shaftwork requirement, which is 56.71 MW. Table 6-6 summarises the results.

Table 6-6. Comparison between exergy loss reduction and shaftwork reduction.

	Exergy loss reduction (MW)		Shaftwork requirement (MW)
Compressor	3.13	Single-stage HN_3 cycle	126.56
Throttle valve	11.17		
Evaporator	21.52	Three-stage HN_3 cycle	69.85
Condenser	15.44		
Overall	51.26	Shaftwork reduction	56.71

Case II. Mixed Refrigerant Cycle

In this case study, an existing single-stage MR system for LNG, whose Ω-H diagram is shown in Figure 6-16, needs revamping. We need to retrofit energy performance and enhance the performance. From Figure 6-18, the Ω-H diagram reveals that the biggest exergy loss is in the heat exchanger, caused by the mismatch between hot and cold composite curves. It is calculated that 12.48 MW of exergy is lost in the main heat exchanger. The throttling valve also contributes a significant exergy loss. The exergy loss in the compressor results from the large amount of refrigerant circulation through it.

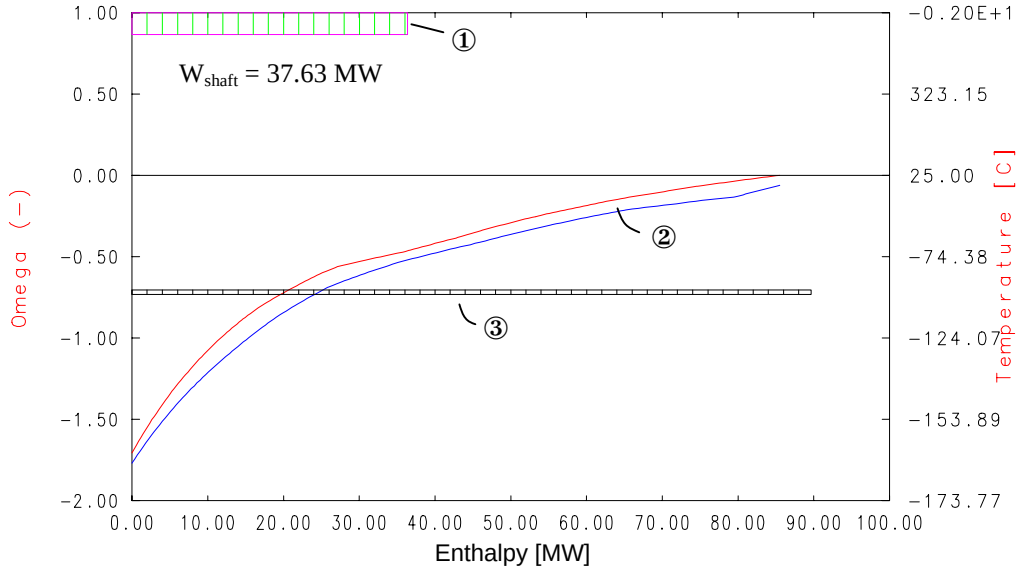

Figure 6-18. The Ω-H diagram of the existing PRICO process.

Table 6-7 summarises the Ω-H details and exergy loss results. To improve the efficiency of this process, we should focus on reducing exergy loss by better selection of refrigerant compositions and reducing the refrigerant flow rate.

Table 6-7. The Ω-H details of the single-stage MR system.

	Compressor Ω-H details	Throttle valve Ω-H details
Inlet Ω	1.000	-0.645
Outlet Ω	0.821	-0.537
ΔH (MW)	37.63	90.50
Exergy loss (MW)	6.74	9.77

By applying the optimal selection method of refrigerant composition introduced in Chapter 4, an improved PRICO process is obtained with a better set of refrigerant compositions, flow rate and pressure levels of evaporation and condensation. This results in 21.4% lower shaftwork consumption. Figure 6-18 shows the optimised PRICO process.

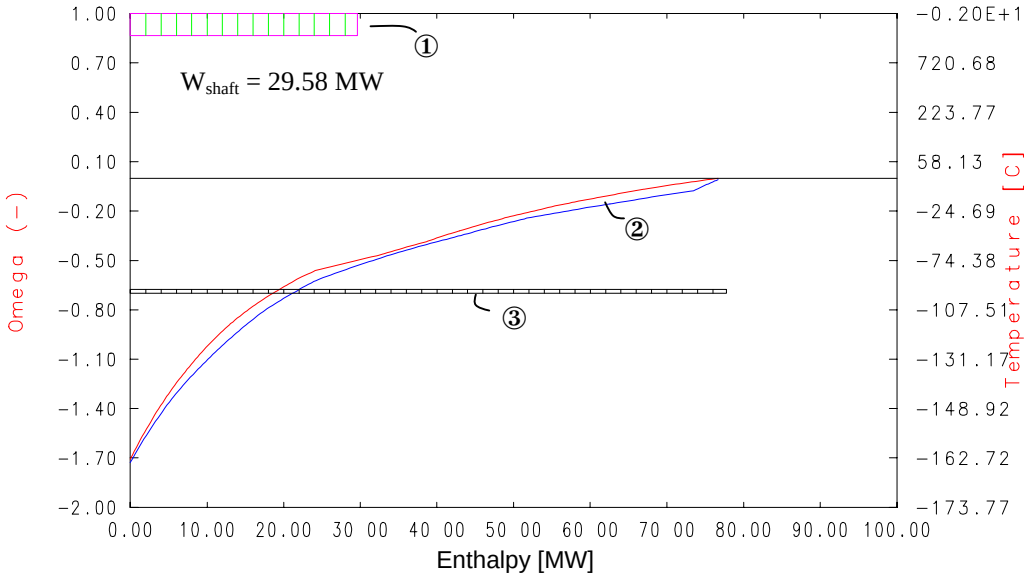

Figure 6-19. The Ω-H diagram of the optimised PRICO process.

The calculated exergy loss in the main heat exchanger is 9.65 MW, a reduction of 2.83

MW exergy loss compared with the existing design. The overall exergy loss reduction is 6.84 MW. Comparing to the shaftwork reduction, 8.05 MW, this figure is close. The Ω-H and exergy loss details is summarised in Table 6-8.

Table 6-8. The Ω-H details of the optimised single-stage MR system.

	Compressor Ω-H details	Throttle valve Ω-H details
Inlet Ω	1.000	-0.715
Outlet Ω	0.824	-0.622
ΔH (MW)	29.58	78.43
Exergy loss (MW)	5.21	7.29

Since the main heat exchanger still contributes a major exergy loss, it is reasonable to try to improve its efficiency to save more energy. The insights from the Ω-H diagram indicate that a large amount of refrigerant circulated through the heat exchanger causes the major exergy loss. Structural modifications might help to further save the shaftwork consumption. We try a two-stage MR system with optimised refrigerant compositions. The results, as shown in Figure 6-19, achieve further 8.0 % saving in shaftwork from the previous optimised single-stage MR system. In Figure 6-20, we can see the exergy loss of throttling valves now splits into two parts, each corresponding to exergy loss in one throttling valve.

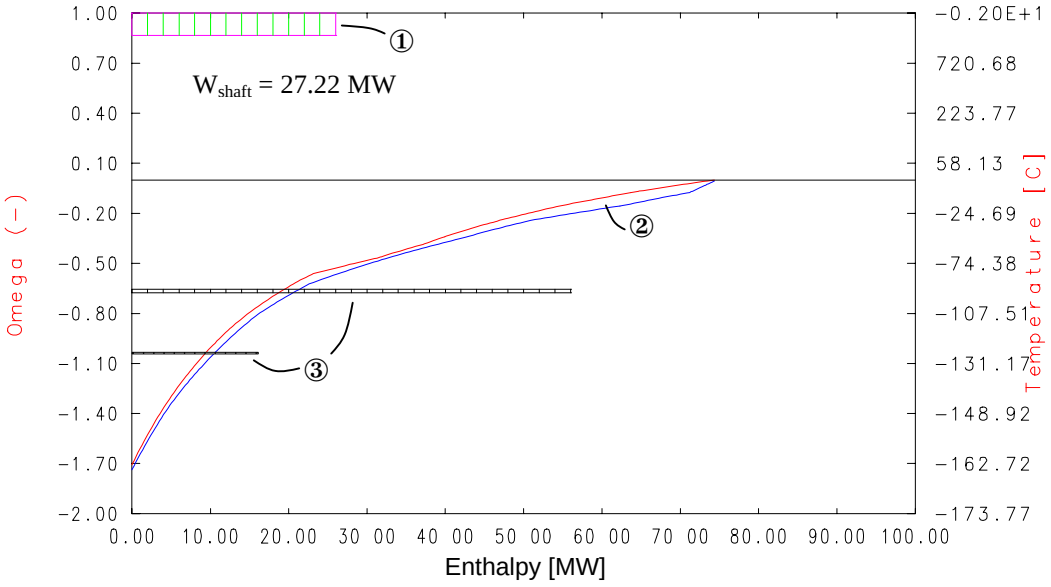

Figure 6-20. The Ω-H diagram of the optimised two-stage MRC process.

The exergy loss in the main heat exchanger is calculated to be 8.74 MW, a reduction of 0.91 MW from the previous optimised single-stage MR system. The overall reduction of exergy loss is 2.14 MW. The shaftwork reduction is 2.36 MW.

Table 6-9. The Ω-H details of the optimised two-stage MR system.

	Compressor Ω-H details	Throttle valve 1 Ω-H details	Throttle valve 2 Ω-H details
Inlet Ω	1.000	-0.621	-1.056
Outlet Ω	0.833	-0.696	-1.204
ΔH (MW)	27.22	57.43	16.29
Exergy loss (MW)	4.55	4.31	2.41

It can be seen from these two case studies that the overall exergy loss reduction is very close to the shaftwork reduction. In theory, they should be identical. More accurate and thorough exergy loss calculation for each component should minimise the deviation between the two values.

6.5 Conclusions

The Ω-H diagram is a powerful tool for giving engineers the insights of the problems. The essence of this method is the proper combination of pinch and exergy analysis in a visual way. It can represent all kinds of exergy loss, thermal, mechanical or chemical, on the same diagram. Exergy loss of each unit can be calculated directly from the Ω-H diagram. The causes of inefficiency in processes can be quickly identified. Based on the insights, engineers can confidently evolves better design and introduce ideas for improving performance. In this chapter, we show two cases to demonstrate how the Ω-H diagram can be applied to achieve significant improvement in energy saving.

Nomenclature

Parameters and variables

A : The energy level.

Ex : Exergy.

H : Enthalpy.

H_0 : Enthalpy at the specified ambient conditions.

H_{ti} : Enthalpy of a throttling valve inlet.

H_{to} : Enthalpy of a throttling valve outlet.

P_0 : Specified ambient pressure.

Q : Heat.

S : Entropy.

S_0 : Entropy at the specified ambient conditions.

S_{ci} : Entropy of a compressor inlet.

S_{co} : Entropy of a compressor outlet.

S_{ti} : Entropy of a throttling valve inlet.

S_{to} : Entropy of a throttling valve outlet.

T : Temperature.

T_0 : Specified ambient temperature.

W : Work

Greek letters

Ω : as defined in eq.(6-20).

τ : The exergetic temperature.

η_C : The Carnot factor.

Reference

Bejan A., Tsatsaronics G., Moran M., 1996, *Thermal Design and Optimization*, John Wiley & Sons, Inc.

Brodyanskii, V. M., Ishkin I. P., 1963. *Inzhenerno-fizicheskii zhurnal*, October, 6, 19-26 (English translation: J of Engineering Physics).

Feng X., Zhu X. X., 1997, Combined pinch and exergy analysis for process modifications, *App. Thermal Engng*. **17**, 249-261.

Graveland A. J. G. G., Gisolf E., 1998, Exergy Analysis: An Efficient Tool for Process Optimization and Understanding, *Computers chem.. Engng*. **22**, S545-S552.

Ishida M., Ohno T., 1982, Application of energy-direction factor diagram for exergy analysis of a distillation column, *J. Chem. Engng Jpn*. **15**, 105-116.

Kotas T. J., 1986, Exergy Method of Thermal and Chemical Plant Analysis, *Chem Eng Res Des*, **64**, May, 212-229.

Kotas T. J., 1980, Exergy Concepts for Thermal Plant, *Int J. Heat & Fluid Flow*, **2 (3)**, 105-114.

Lee G. C., Zhu X. X., Smith R., 1998, Shaftwork targeting method for refrigeration systems, *Process Integration Research Consortium 98'*, UMIST, Manchester, United Kingdom.

Lee G. C., Zhu X. X., 2000, Systematic Design of Mixed Refrigerant Cycle for Subambient Process, *AIChE Spring Meeting 2000*, Atlanta, March 2000.

Linnhoff B., Dhole V., 1992, Shaftwork Targets for Low Temperature Process Design. *Chem. Engng Sci*. **4 (8),** 2081-2091

Niida, K., Shiroko, K., Umeda, T., 1981, A Thermodynamic Analysis for Heat Integration In Cryogenic Process Systems, *Proceedings 2nd World Congress of Chem. Engng*., *Montreal, Canada*, Vol. II, p. 381.

STAR, Department of Process Integration, UMIST, Manchester, Untied Kingdom.

Szargut J., Morris D. R., Steward F. R., 1988, *Exergy Analysis of Thermal, Chemical and Metallurgical Processes. Hemisphere*, New York.